Analysis of the bidirectional VSR-mediated transport in the plant endomembrane system

Dissertation

der Mathematisch-Naturwissenschaftlichen Fakultät

der Eberhard Karls Universität Tübingen

zur Erlangung des Grades eines

Doktors der Naturwissenschaften

(Dr. rer. nat.)

vorgelegt von

Simone Früholz

aus Ulm

Tübingen

2017

Gedruckt mit Genehmigung der Mathematisch-Naturwissenschaftlichen Fakultät der Eberhard Karls Universität Tübingen.

Tag der mündlichen Qualifikation:	18.01.2018
Dekan:	Prof. Dr. Wolfgang Rosenstiel
1. Berichterstatter:	Prof. Dr. Peter Pimpl
2. Berichterstatter:	Prof. Dr. Gerd Jürgens
3. Berichterstatter:	Prof. Dr. Jean-Marc Neuhaus

Danksagung

An dieser Stelle möchte ich mich bei allen bedanken, die zum Gelingen dieser Arbeit beigetragen haben.

Mein besonderer Dank geht dabei an Prof. Dr. Peter Pimpl für die Überlassung des spannenden Themas und für die hervorragende wissenschaftliche Betreuung sowie für die vielen sehr wertvollen Diskussionen. Des Weiteren möchte ich mich bei ihm für die Möglichkeit der Teilnahme an mehreren internationalen Konferenzen sowie die Möglichkeit für Forschungsaufenthalte in Hongkong bedanken.

Herrn Prof. Dr. Gerd Jürgens möchte ich für die Übernahme des Zweitgutachtens sowie den Anregungen zu dieser Arbeit danken.

Danke auch an Dr. Üner Kolukisaoglu für die Bereitstellung des SYN nanobodies.

Außerdem möchte ich mich bei den derzeitigen sowie ehemaligen Kolleginnen und Kollegen der AG Pimpl für die gute Zusammenarbeit und die tolle Arbeitsatmosphäre danken: Florian Fäßler, Fabian Künzl, Beibei Li und Richard Gavidia. Ein großes Dankeschön geht an Diana Vranjkovic für die hervorragende und zuverlässige technische Unterstützung im Labor.

Bedanken möchte ich mich auch bei allen Kolleginnen und Kollegen der Entwicklungsgenetik für das gute Arbeitsklima, die große Hilfsbereitschaft und die vielen tollen Momente.

Danke auch an, Sabine Brumm, Kerstin Huhn, Arvid Herrmann, Elisabeth Lipka, Dorothee Stöckle, Anna Wunderling, Azahara Barra-Jimenez und Dietmar Mehlhorn für die vielen tollen gemeinsamen Aktivitäten und die schöne Zeit in Tübingen.

Mein herzlichster Dank geht an meine Eltern, meine Schwester und Freunde, die mich jeder Zeit unterstützt und ständig motiviert haben. Danke, dass ihr an mich glaubt!

Table of contents

1. Summary

Post-translational regulation of membrane proteins is pivotal for all eukaryotic cells. In particular, the regulation of transporter proteins at the plasma membrane. They are post-translationally regulated by vacuolar degradation after their endocytic removal. For this to occur, the vacuole needs a constant supply of soluble hydrolyzing enzymes. At the heart of this process operate vacuolar sorting receptors (VSRs) mediating the transport of these enzymes towards the lytic vacuole. Based on the research on mammalian cells, it is assumed that VSR transport occurs bidirectional and follows the common principle of receptor-mediated transport: Receptors bind ligands in the donor compartment, thereby forming a receptor-ligand complex that is transported to the acceptor compartment. Upon arrival, ligands are released and receptors recycle back to the donor compartment to reload ligands. It is presumed that this transport occurs between the *trans*-Golgi network/early endosome (TGN/EE) and the multivesicular bodies/late endosomes (MVBs/LEs) in plants. It now became clear that VSR bind ligand in the early secretory pathway and transport them to the TGN/EE were they are released (Künzl et al., 2016).
To analyze the post TGN/EE transport of soluble proteins, we generated a nanobody-based system to follow the fate of soluble proteins lacking vacuolar sorting signals that were placed in the TGN/EE via the endocytic pathway. This enabled us to demonstrated that post TGN/EE transport of ligands to the vacuole occurs independently of VSRs (Künzl et al., 2016). Usage of this system, however, required testing that nanobody-triggered protein-protein interactions between two soluble proteins can occur in the endomembrane system (Früholz and Pimpl, 2017).
With the demonstration that VSRs release ligands in the TGN/EE (Künzl et al., 2016) it became clear that if VSRs do recycle, then the TGN/EE would be the starting point for such a recycling. To identify the target compartment of the VSR recycling route, we devised an approach where we employ simultaneously two different nanobody-epitope pairs. One to label VSRs fluorescently in the TGN/EE and a second to trigger the lockdown of recycled VSRs via an endocytosed dual epitope linker to block their further anterograde transport. Using this approach, we demonstrate that VSRs recycle from the TGN/EE to the *cis*-Golgi and show that recycled VSRs reload ligands there (Früholz et al., in press).
Together, we proof that the bidirectional VSR-mediated transport exists and occurs between the TGN/EE and the *cis*-Golgi.

2. Zusammenfassung

Die post-translationale Regulation von Membranproteinen ist für alle eukaryotischen Zellen von zentraler Bedeutung, vor allem die Regulation von Transporterproteinen an der Plasmamembran. Diese werden nach ihrem endozytischen Abbau durch vakuoläre Degradation reguliert. Dazu benötigt die Vakuole eine dauerhafte Versorgung mit löslichen hydrolytischen Enzymen. Um dies zu gewährleisten, werden vakuoläre Sortierungsrezeptoren (VSRs), die den Transport dieser Enzyme vermitteln, benötigt. Basierend auf der Forschung in Säugetierzellen wird vermutet, dass der Transport von VSRs bidirektional ist und nach dem allgemeinen Prinzip des Rezeptor vermittelten Transportes abläuft: Rezeptoren binden Liganden in einem Donor Kompartiment und bilden einen Rezeptor-Liganden Komplex, der zum Akzeptor Kompartiment transportiert wird. Dort dissoziieren die Liganden vom Rezeptor und die Rezeptoren rezyklieren zurück zum Donor Kompartiment um neue Liganden zu binden. Bisher wurde vermutet, dass dieser Transportschritt in Pflanzen zwischen dem *trans*-Golgi Netzwerk/frühen Endosom (TGN/EE) und den multivesikulären Körpern/späte Endosomen (MVBs/LEs) stattfindet. Jetzt konnte erstmals gezeigt werden, dass VSRs Liganden bereits im frühen sekretorischen Weg binden und diese nur bis zum TGN/EE transportieren, wo sie dissozieren (Künzl et al., 2016).

Um den post TGN/EE Transport von löslichen Proteinen analysieren zu können, haben wir ein System entwickelt, das auf Nanobody-Epitop Interaktionen basiert. Hierfür haben wir eine Strategie entwickelt um den Transport von löslichen Proteinen ohne Sortierungssignale, die durch den endozytischen Weg im TGN/EE platziert wurden, zu analysieren. Dadurch konnten wir zeigen, dass der post TGN/EE Transport von Liganden hin zur lytischen Vakuole unabhängig von VSRs ist (Künzl et al., 2016). Um dieses System anwenden zu können, musste im Vorfeld jedoch erst bestätigt werden, dass Nanobody-Epitop Interaktionen zwischen zwei löslichen Proteinen im Endomembransystem auch tatsächlich erfolgen (Früholz and Pimpl, 2017).

Der Beweis, dass Liganden im TGN/EE von VSRs dissoziieren, konnte daher auch als ein weiteres Indiz für die Vermutung, dass es sich bei dem TGN/EE auch um das Kompartiment handelt, von dem aus VSRs rezyklieren, herangezogen werden (Künzl et al., 2016).

Um das Zielkompartiment des VSR Rezyklierungsweges zu identifizieren, haben wir einen Ansatz entwickelt, bei dem wir gleichzeitig zwei Nanobody-Epitop Paare einsetzen. Ein Paar um den VSR im TGN/EE fluoreszent sichtbar zu machen und das Zweite um den rezyklierten VSR im Zielkompartiment festzuhalten und den weiteren Transport des VSRs zu blockieren. Mit diesem Ansatz konnten wir zeigen, dass VSRs vom TGN/EE zum *cis*-Golgi rezyklieren und dass rezyklierte Rezeptoren im *cis*-Golgi neue Liganden binden können (Früholz et al., in press). Zusammengefasst konnten wir beweisen, dass der bidirektionale VSR-vermittelte Transport existiert und zwischen dem TGN/EE und dem *cis*-Golgi stattfindet.

3. List of publications

Published articles:

3.1 Receptor-mediated sorting of soluble vacuolar proteins ends at the *trans*-Golgi network/early endosome

Fabian Künzl, **Simone Früholz**, Florian Fäßler, Beibei Li and Peter Pimpl
Nature Plants **2**, Article number: 16017 (2016), doi:10.1038/nplants.2016.17

3.2 Analysis of nanobody-epitope interactions in living cells via quantitative protein transport assays

Simone Früholz and Peter Pimpl
Methods in Molecular Biology, 1662, 171-182

Accepted article:

3.3 Nanobody mediated lockdown of VSRs reveals ligand reloading in the Golgi

Simone Früholz, Florian Fäßler, Üner Kolukisaoglu and Peter Pimpl
Nature Communications

4. Personal contribution

4.1 Receptor-mediated sorting of soluble vacuolar proteins ends at the *trans*-Golgi network/early endosome (Künzl et al., 2016)

For this research article, I contributed the result which shows that VSRs are not involved in the post TGN/EE transport of soluble vacuolar proteins. Further, I showed that the vacuole is the default location of endocytosed soluble proteins. For this, I developed the strategy for the endocytic uptake assay, performed all required experiments and generated the reported genetic constructs. Results are summarized in Figure 6 in Künzl et al. (2016).

4.2 Analysis of nanobody-epitope interactions in living cells via quantitative protein transport assays (Früholz and Pimpl, 2017)

This article illustrates the strategy that was established to test for an occurring interaction between two soluble proteins in the endomembrane system triggered by a nanobody-epitope interaction. The nanobody-epitope interaction was verified with a quantitative protein transport assay. Therefore, I performed all experiments, analyzed the data and generated the reported genetic constructs. The article was written together with Peter Pimpl.

4.3 Nanobody mediated lockdown of VSRs reveals ligand reloading in the Golgi (Früholz et al., in press)

In this research article, we identified the *cis*-Golgi as the target compartment of the VSR recycling route and finally proof the concept of recycling and ligand reloading of the bidirectional VSR-mediated transport. For this achievement, I have developed a strategy that employs simultaneously two different nanobody-epitope pairs. One pair to post-translationally label a VSR in the TGN/EE and the second to lock it after recycling in the target compartment to block its further anterograde transport. Therefore, I performed all experiments, did the statistical analysis and generated the reported genetic constructs. The experiments were designed together with FF, ÜK and PP, the article was written together with PP.

5. Introduction

5.1 The plant endomembrane system

The plant endomembrane system is an interconnected system of different compartments comprised of the endoplasmic reticulum (ER), the Golgi apparatus, the *trans*-Golgi network (TGN), the multivesicular bodies (MVBs), the vacuoles and the plasma membrane (PM). Each of the compartments is characterized by a different set of lipids, enzymes and metabolites linked by dynamic and complex transport routes that are essential for cell growth and cell function as well as the response to environmental stimuli. Three main transport routes exist within the endomembrane system: (1) The secretory route that mediates the transport of proteins from the ER to the PM or the extracellular space. (2) The vacuolar route that passes proteins from the ER to the vacuole and (3) the endocytic route, mediating the transport of PM-localizing proteins and solutes from the exterior to the *trans*-Golgi network/early endosome (TGN/EE). From there, endocytosed proteins are transported via the multivesicular bodies/late endosomes (MVBs/LEs) to the vacuole or might recycle back to the PM (Inada and Ueda, 2014).

5.1.1 Transport routes in the plant endomembrane system

Proteins, lipids and polysaccharides are synthesized, folded and glycosylated in the ER. Proteins that pass the quality control exit the ER. They are packed at ER exit sites (ERES) into coat protein complex II (COPII)-coated vesicles (Barlowe, 1998; daSilva et al., 2004; Yang et al., 2005). Formation of COPII-coated vesicles is induced by the activation of the cytosolic GTPase secretion activated Ras-related protein 1 (Sar1) through the guanine nucleotide exchange factor Sec12. Sar1 is recruited to the ER membrane and binds then the Sec23-24 and the Sec13-31 dimers to form COPII-coated vesicles. (Barlowe et al., 1994; Miller and Barlowe, 2010; Jensen and Schekman, 2011). These vesicles mediate the anterograde transport of proteins to the Golgi where they fuse with the target membrane after uncoating (Takeuchi et al., 2000; Brandizzi and Barlowe, 2013). ER export of soluble proteins occurs by default. They enter passively COPII-coated vesicles (Phillipson et al., 2001) whilst membrane proteins carry specific sorting signals, for example a diacidic (DXE; sorting signal consisting of the two acidic amino acids aspartic acid and glutamic acid that are separated by a random amino acid) or a

diaromatic (FF, YF; sorting signal consisting of the aromatic amino acids phenylalanine-phenylalanine or tyrosine-phenylalanine) motif which interact with the Sec23-24 dimer (Contreras et al., 2004; Hanton et al., 2005). COPI-coated vesicles mediate the retrograde transport between the Golgi and the ER. The ADP-ribosylation factor 1 (ARF1) GTPase recruits the coatomer, a complex that consists of the seven subunits α, β, β′, γ, δ, ε, and ζ, *en bloc* to the Golgi membrane to form COPI-coated vesicles (Hara-Kuge et al., 1994; Contreras et al., 2000; Pimpl et al., 2000). They recycle ER-resident proteins back to the ER that escaped the ER by bulk flow. For this sorting process, different sorting signals are known. Soluble proteins that carry the C-terminal tetrapeptide HDEL or KDEL are recognized by the ENDOPLASMIC RETICULUM RETENTION DEFECTIVE 2 (ERD2) receptor protein in the Golgi (Denecke et al., 1992; Boevink et al., 1998). The cargo ERD2 complex then interacts with p24 proteins of the delta subfamily at acidic pH (Montesinos et al., 2014). Dilysine motifs (KKXX or KXKXX) in the cytosolic tails of ERD2 and p24 interact with ARF1 leading to the formation of COPI-coated vesicles. After vesicles bud off the membrane, the coat falls off and the uncoated vesicles fuse with the ER membrane where HDEL/KDEL ligands are released into the compartmental lumen due to the neutral pH (Montesinos et al., 2014; Pastor-Cantizano et al., 2016). Other ER-resident membrane proteins carrying a dilysine motif in their C-terminal cytosolic domain that have reached the Golgi are also transported to the ER in a COPI dependent manner (Letourneur et al., 1994; Gao et al., 2014). However, COPI is not only responsible for the ER retrieval, it further mediates the retrograde transport from the *trans*-Golgi cisternae to the *cis*-Golgi cisternae (Orci et al., 1997; Pelham and Rothman, 2000). It was further suggested that COPI, at least the β subunit, is involved in the formation of endosomal carrier vesicles (ECVs) which mediate transport between the early and late endosomes (Aniento et al., 1996).

The plant Golgi has a stacked morphology and consists of different cisternae (Staehelin and Moore, 1995; Dupree and Sherrier, 1998). The cisternae of the Golgi are defined as *cis*, *medial* and *trans* whereby the *cis*-cisternae faces the ER and the *trans*-cisternae the TGN (Schoberer and Strasser, 2011). Whilst trafficking through the Golgi, proteins are glycosylated in the *trans*-Golgi (Strasser, 2014) and afterwards reach the TGN. The TGN is a tubular-vesicular structure (Dettmer et al., 2006; Viotti et al., 2010; Kang et al., 2011). Based on the findings that super-

resolution confocal live imaging microscopy (SCLIM) identified Golgi-associated TGNs (GA-TGNs) that locate at the *trans*-side of the Golgi and Golgi-released independent TGNs (GI-TGNs) that do not locate in close proximity to the Golgi and behave independently (Uemura et al., 2014), it is suggested that two different TGNs exist. Further, it is assumed that the secretory and the vacuolar pathway separate in the TGN (Dettmer et al., 2006). Secretory proteins are transported with secretory vesicles (SVs) to the PM or the extracellular space (Dettmer et al., 2006) whilst vacuolar proteins are transported towards the vacuole. Multivesicular bodies (MVBs) mediate the vacuolar pathway: they bud off the TGN by maturation and deliver cargo to the lytic vacuole by fusion (Scheuring et al., 2011). The secretory and vacuolar pathway is described schematically in **Figure 1**.

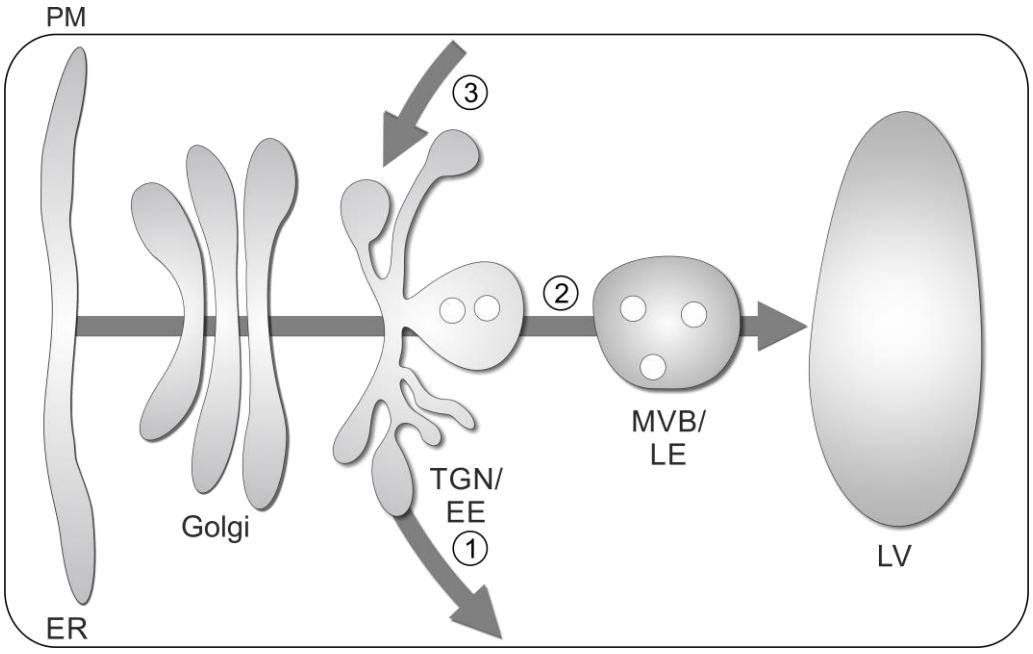

Figure 1: Schematic description of the main transport routs in the plant endomembrane system. (1) The secretory pathway mediates the transport of proteins from the ER to the PM. (2) The vacuolar route passes proteins from the ER to the vacuole and (3) the endocytic route mediates the transport of PM-localizing proteins and solutes from the exterior to the TGN/EE.

The endocytic uptake of proteins, lipids and extracellular proteins from the PM is important for growth and development of cells, the cell-cell communication, hormone signaling and for the response to environmental stimuli such as pathogen defense and nutrient delivery (Chen et al., 2011; Fan et al., 2015). The endocytic pathway starts at the PM were PM-localizing proteins present endocytic sorting signals that are located in their cytosolic tails. Three different endocytic sorting signals are described: (1) linear amino acid motifs (Chen et al., 1990; Collawn et al.,

1990; Letourneur and Klausner, 1992), (2) conformational motifs (Pryor et al., 2008; Yu et al., 2010; Miller et al., 2011) and (3) posttranslational modifications like ubiquitination or phosphorylation (Ferguson et al., 1996; Hicke and Riezman, 1996). As linear amino acid motif, the tyrosine-based motif YXXΦ (where Φ is a bulky hydrophobic amino acid and X is any amino acid) is described. This sorting motif, located in the cytosolic tail of PM proteins is recognized by clathrin adaptors and PM proteins are packed into clathrin-coated vesicles (CCVs) for internalization (Traub, 2009). For example the ETHYLENE INDUCING XYLANASE (LeEIX2) receptor from tomato (*Solanum lycopersicum*) has a tyrosine motif in the cytosolic domain (Ron and Avni, 2004). Upon binding of the fungal elicitor Ethylene-inducing xylanase (EIX) to LeEIX2, the defense response is induced, clathrin adaptors bind to the tyrosine-based motif and the EIX-LeEIX2 complex is internalized into CCVs (Bar and Avni, 2009; Bar and Avni, 2012). For ubiquitination as endocytic sorting signal, two variants are known; either one ubiquitin (monoubiquitination) or more ubiquitin molecules (polyubiquitination) are attached to lysine residues (Paez Valencia et al., 2016). After binding of the bacterial flagellin (flg22) to the flagellin receptor FLAGELLIN SENSING 2 (FLS2) (Robatzek et al., 2006), ubiquitin ligases are recruited. After their BRI1-ASSOCIATED KINASE 1 (BAK1)-mediated phosphorylation, they polyubiquitinate FLS2 (Lu et al., 2011). The polyubiquitinated complex is then endocytosed with CCVs and degraded. Other receptors that are endocytosed after polyubiquitination are the brassinosteroid (BR) receptor BRASSINOSTEROID INSENSITIVE1 (BRI1) (Russinova et al., 2004; Martins et al., 2015) and the auxin efflux carriers PIN-PERFORMED (PIN) (Dhonukshe et al., 2007). The IRON-REGULATED TRANSPORTER 1 (IRT1) cycles between the TGN/EE and the PM or is send to the vacuole for degradation when it is monoubiquitinated (Barberon et al., 2011). IRT1 binds divalent metals at the PM and transports them to the TGN. A transporter that combines different endocytic sorting signals is the BORON TRANSPORTER 1 (BOR1) (Takano et al., 2010). At high boron conditions, BOR1 is mono- and diubiquitinated and the three tyrosine-based sorting motifs in the cytosolic tail recruit clathrin adaptors to be packed into CCVs. BOR1 is then transported to the vacuole for degradation and further transport of boron is avoided (Takano et al., 2005; Kasai et al., 2011).
If the ubiquitin sorting signal is mutated by removing the two C-terminal glycines (UbΔGG), PM proteins are no longer internalized and stay at the PM. The reason

is that UbΔGG can then only be monoubiquitinated and it is speculated that this might not be sufficient to trigger internalization (Scheuring et al., 2012).
After the formation of CCVs, the internalized vesicles are detached from the membrane by the activity of dynamin and dynamin-related proteins (Fujimoto et al., 2010). However, it was also noted that a pathway exists which endocytoses proteins in a clathrin-independent manner (Bandmann and Homann, 2012; Bandmann et al., 2012; Li et al., 2012), but coat proteins that mediate this pathway still have to be identified.
Detached endocytic vesicles uncoat and fuse with the early endosome (EE). The TGN-localizing proteins VHA-a1 and SCAMP1 colocalized with the endocytic tracer FM4-64, indicating that the TGN is the EE in plants (Dettmer et al., 2006; Lam et al., 2007). This also suggests that the TGN/EE is the intersect of the biosynthetic and the endocytic pathway. Spinning disc confocal microscopy revealed that a TGN/EE and a Golgi marker move independently, but the TGN marker can closely associate with the Golgi marker or with other TGNs (Viotti et al., 2010). Accordingly, the TGN/EE has to be considered as an independent compartment, even though it is derived from the Golgi (Viotti et al., 2010; Kang et al., 2011; Uemura et al., 2014).
PM-localizing proteins that are endocytosed to the TGN/EE are either recycled back to the PM or transported via the late endosomes (LEs) to the vacuole for degradation (Paez Valencia et al., 2016). Recycling of endocytosed PM-proteins was reported to occur for PINs, BOR1 or IRT1 (Geldner et al., 2003; Takano et al., 2010; Barberon et al., 2011). Cargo that is destined for vacuolar degradation passes the LE before it is delivered to the vacuole (Tse et al., 2004; Dettmer et al., 2006; Viotti et al., 2010). LEs consist of intraluminal vesicles (ILV) and are thus named multivesicular bodies (MVBs) (Tse et al., 2004). Scheuring et al. (2011) identified that the transport from the TGN/EE to the MVB/LE occurs via maturation. MVBs/LEs bud off the TGN/EE and finally fuse with the vacuole to deliver cargo. The endocytic pathway is described schematically in **Figure 1**.

5.2 Receptor-mediated sorting of soluble vacuolar proteins

Receptor-mediated sorting of soluble proteins exists in all eukaryotic cells. It is suggested that the receptor-mediated transport of soluble proteins follows the

common principle of the bidirectional receptor mediated transport: Receptors bind ligands in a donor compartment and form a receptor-ligand complex. This complex is then transported to the acceptor compartment where the receptor-ligand complex dissociates and the receptors recycle back to the donor compartment for further rounds of ligand transport. The first identified cycling receptor was the low-density lipoprotein (LDL) receptor (Brown et al., 1983). The LDL receptor binds LDL at the cell surface of cultured human fibroblasts (Goldstein and Brown, 1974). After forming a receptor-ligand complex, it is endocytosed in coated vesicles, which fuse with each other to larger vesicles, called endosomes (Anderson et al., 1982; Brown et al., 1983). There, the receptor-ligand complex dissociates and the receptors recycle back to the PM to reload ligands whilst released ligands are transported to the lysosome for degradation (Brown et al., 1983).

Receptors that mediate the transport of soluble vacuolar or lysosomal proteins are the cation-independent (CI)-mannosyl 6-phosphate receptor (MPR) and the cation-dependent (CD)-MPR in mammals (Sahagian et al., 1981; Hoflack and Kornfeld, 1985), the vacuolar protein sorting 10 (VPS10) receptor in yeast (Marcusson et al., 1994) and the vacuolar sorting receptor in plants (Kirsch et al., 1994).

In mammals, soluble lysosomal proteins are glycosylated in the ER and transported to the Golgi. There, oligosaccharide chains are modified by the GlcNac-1-phosphotransferase (Braulke and Bonifacino, 2009). Soluble lysosomal proteins are then transported to the TGN were the uncovering enzyme (UCE) exposes the mannose 6-phosphate (M6P) residues and the sorting signal becomes accessible (Rohrer and Kornfeld, 2001). The M6P residues are then recognized by the MPRs and form a receptor-ligand complex. This complex leaves the TGN in CCVs and fuses with the membrane of the early endosome. There, the MPR-ligand complex dissociates due to the low pH (< 5.5) (Olson et al., 2008) and MPRs recycles back to the TGN. This retrograde transport occurs in a retromer-dependent manner (Arighi et al., 2004; Seaman, 2004), a protein complex consisting of five subunits that bind the unoccupied receptor (Bonifacino and Hurley, 2008). Further transport of ligands occurs with the fluid phase in a receptor-independent manner from the early endosome to the lysosome via maturation (Kornfeld and Mellman, 1989; Huotari and Helenius, 2011).

Deciphering of vacuolar sorting in plants started with the discovery that vacuolar sorting signals (VSS) are not encoded in post-translational modifications but are encoded in the primary amino acid sequence, instead.
Three different classes of VSSs have been described: (1) sequence-specific VSSs (ssVSS), (2) C-terminal VSSs (ctVSS) and (3) protein structure-dependent VSSs (psVSS) (Xiang et al., 2013). The N-terminal ssVSS with the amino acid sequence NPIR was described for barley (*Hordeum vulgare*) aleurain (Holwerda et al., 1992), potato (*Ipomoea batatas*) sporamin (Nakamura and Matsuoka, 1993; Koide et al., 1997) and castor bean (*Ricinus communis*) 2S albumin (Brown et al., 2003) and ricin (Frigerio et al., 2001; Jolliffe et al., 2004). The C-terminal ssVSS AFVY was described for phaseolin from *Phaseolus vulgaris* (Frigerio et al., 1998) whilst FAEAI and LVAE for barley lectin (Bednarek et al., 1990; Bednarek and Raikhel, 1991) and GLLVDTM for tobacco (*Nicotiana tabacum*) chitinase (Neuhaus et al., 1991) act as ctVSS. After the description of the different VSS, VSRs were discovered by the extraction of CCVs from Golgi membranes of developing pea (*Pisum sativum* L.) cotyledons (Kirsch et al., 1994). The extract was applied to a proaleurain coated affinity column and a type I integral transmembrane protein of 80 kDa, named 80 kDa binding protein (BP80), was bound to the column. Analysis of topology revealed that BP80 contains a luminal N-terminus and a cytosolic C-terminus which contains the NPIR binding domain for proaleurain (Kirsch et al., 1994).
Later, the ligand specificity of BP80 was further analyzed. It was shown that BP80 also binds to prosporamin and pro-2S albumin, the C-terminal VSS from Brazil nut (*Bertholletia excels*), *in vitro* (Kirsch et al., 1996).
Soon thereafter, several homologues of BP80 were identified by molecular cloning and homology searches in *Arabidopsis*, maize (*Zea mays*) and pumpkin (*Cucurbita sp.*) (Ahmed et al., 1997; Paris et al., 1997; Shimada et al., 1997) revealing that vacuolar sorting receptors are a conserved family that is unique to plants (De Marcos Lousa et al., 2012). Localization studies of all seven VSRs (AtVSR1-7) from *Arabidopsis* (Shimada et al., 2003) show that VSRs localize at the *trans*-Golgi face and the prevacuolar compartment (PVC) (Paris et al., 1997; Sanderfoot et al., 1998; Li et al., 2002). Moreover, it was demonstrated that VSR bind the ligand Aleurain which carries the ssVSS NPIR *in vitro* in a pH dependent manner: VSRs bind ligands at neutral pH and release them at a lower pH (Kirsch et al., 1994;

Ahmed et al., 2000). The luminal part of the VSR, involved in the VSR-ligand interaction, consists of a protease-associated (PA) domain, a central domain and three epidermal growth factor (EGF) repeats. It is suggested that the PA and the central domain recognize the NPIR motif from the ligand and built a receptor-ligand complex. The EGF repeats, however, might function as calcium binding domains, which induce a conformational change of the PA and the central domain that stabilizes the VSR-ligand complex (Cao et al., 2000; Watanabe et al., 2002; Watanabe et al., 2004). To get more insights into the VSR-ligand interaction, the PA domain of VSR1 was crystalized alone and in complex with a NPIR-containing peptide. Results show, that the PA domain binds the amino acid sequence Alanine-Aspartic acid-Serine (ADS) from the NPIR-containing peptide and induces thereby a conformational change. This change might relocate the central domain, which is then suggested to recognize the NPIR motif of the ligand (Luo et al., 2014).
Another factor that seems to be crucial for the transport of VSRs is their homodimerization. Kim et al. (2010) suggest that VSR1 mutants which lack the tyrosine motif YMPL in the cytosolic domain (C2A mutant) cannot homodimerize and are thus not transported. They were able to show that this mutant localizes to the Golgi and TGN and that vacuolar cargo was secreted into the culture medium when coexpressed with the C2A mutant in *Arabidopsis* protoplasts.
The same tyrosine motif YXXΦ (YMPL) that is conserved among all *Arabidopsis* VSRs (Paris et al., 1997; Hadlington and Denecke, 2000) might also be important for the clathrin-mediated anterograde transport in the endomembrane system. This tyrosine-based motif interacts *in vitro* with the *Arabidopsis* μA-subunit of the clathrin adaptor protein (AP) complex which localizes at the TGN (Happel et al., 2004). If the tyrosine motif is mutated in a truncated receptor, where the N-terminal luminal-binding domain (LBD) was replaced by the green fluorescent protein (GFP; GFP-BP80), it was not targeted correctly (daSilva et al., 2006). For this, the tyrosine was replaced with an alanine (Y612A). After overexpression of the mutated VRS in tobacco protoplasts, the receptor partially retained in the Golgi or was mistargeted to the PM, resulting in a delayed transport of the mutated VSRs to the PVC. The sorting motif for the retrograde transport of VSRs also appears to be in the C-terminal cytosolic tail. If the IM motif of GFP-BP80 is mutated by exchanging it for two alanins, the receptor is mistargeted to the vacuole (Saint-Jean et al.,

2010). Due to the vacuolar delivery of the mutated receptors, the authors concluded that the IM motif might be important for the recycling of VSRs.
It was suggested that the recycling of VSRs is retromer-mediated (Oliviusson et al., 2006; Shimada et al., 2006; Jaillais et al., 2007). The cytosolic retromer is recruited to the membrane of endosomes to recycle VSRs after ligand release back to the donor compartment. The retromer complex is made up of two subunits, a large one, consisting of vacuolar sorting protein (VPS)26, VPS29 and VSP35 that functions as cargo recognition complex (Oliviusson et al., 2006; Jaillais et al., 2007). The small subunit consists of sorting nexin (SNX)1 and SNX2 and induce the membrane curvature (Jaillais et al., 2006; Niemes et al., 2010b). The interaction between the VSR and the retromer complex is suggested to occur via VPS35. *In vitro* interaction analysis showed that antibodies, directed against VPS35, immunoprecipitate VSRs (Oliviusson et al., 2006).
Together, the data from the localization studies of VSRs and *in vitro* receptor-ligand interaction analysis suggests that VSRs mediate the transport of soluble vacuolar proteins between the *trans*-Golgi cisternae or the *trans*-Golgi network, which is the early endosome in plants (TGN/EE) (Dettmer et al., 2006) and the PVC, identified to be the MVB/LE (Tse et al., 2004). It is speculated that VSRs bind ligands in the TGN/EE and transport them with CCVs to the MVB/LE (Kirsch et al., 1994; Happel et al., 2004) where they are released due to the low pH (Kirsch et al., 1994; Paris et al., 1997). It is suggested that the pH drops en route to the vacuole similar as in mammals, where the late endosomes are the most acidic compartment en route to the lysosome (Casey et al., 2010). The unoccupied receptors recycle then in a retromer-dependent manner back to the TGN/EE (Oliviusson et al., 2006; Shimada et al., 2006; Jaillais et al., 2007) for further rounds of ligand transport (see **Figure 2**). However, *in vivo* there is no molecular evidence for ligand binding and release in the TGN/EE and the MVB/LE, respectively.

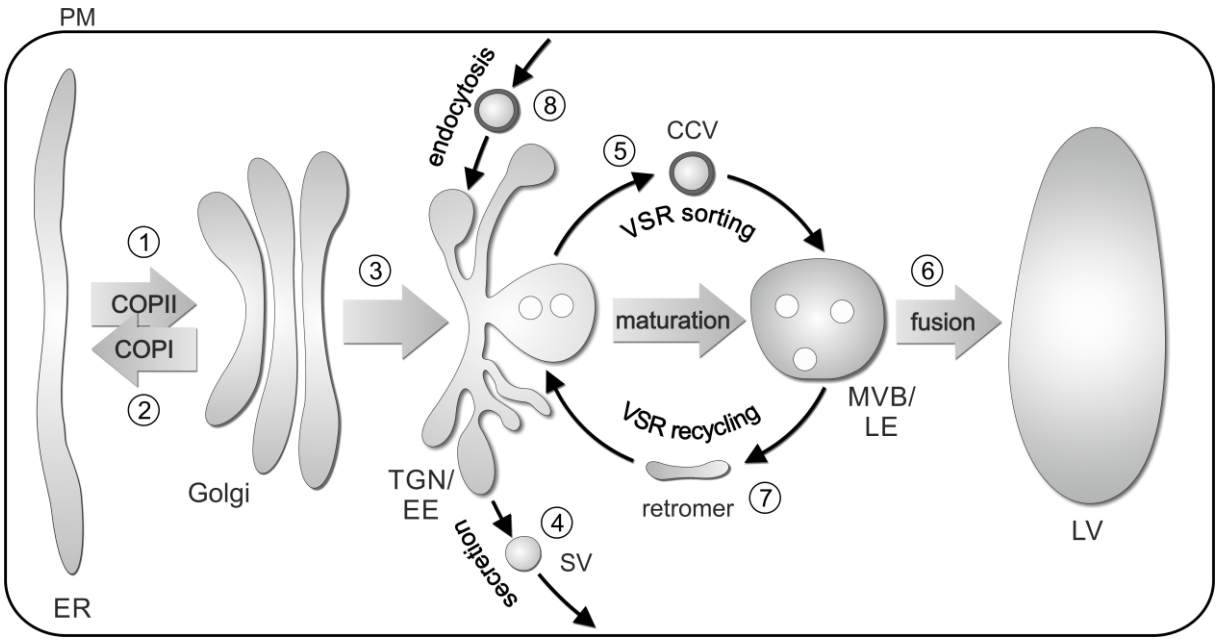

Figure 2: Schematic description of transport processes in the plant endomembrane system. Protein transport starts at the ER. (1) There, proteins are packed into COPII-coated vesicles and transported anterograde to the Golgi apparatus. (2) The retrograde protein transport from the Golgi back to the ER occurs via COPI-coated vesicles. (3) After passing the Golgi, proteins are transported to the *trans*-Golgi network/early endosome (TGN/EE). (4) From there, secretory proteins are transported with secretory vesicles (SVs) to the plasma membrane (PM). (5) Soluble vacuolar proteins are bound to vacuolar sorting receptors (VSRs) in the TGN/EE and transported with CCV to the multivesicular bodies/late endosomes (MVBs/LEs). (6) In the MVBs/LEs, vacuolar proteins dissociate from the receptors and their vacuolar delivery occurs by the fusion with the lytic vacuole (LV). (7) VSRs recycle from the MVB/LE back to the TGN/EE with the retromer complex, were they can go for further rounds of ligand transport. (8) Starting from the PM, proteins are endocytosed in CCVs to the TGN/EE. From there, they recycle back to the PM or they are transported towards the LV. (Adapted and modified from (Früholz et al., in press).

5.2.1 Open questions

Recently, evidence was provided that VSRs might recycle between the TGN/EE and an upstream compartment (Niemes et al., 2010b; Robinson and Pimpl, 2014). VSRs were localized by immunogold labeling in *Arabidopsis* root cells at the TGN/EE and the MVB/LE (Niemes et al., 2010b; Stierhof and El Kasmi, 2010; Viotti et al., 2010). Further, the retromer components SNX1, SNX2a and VPS29 were localized at the TGN/EE suggesting that retromer-mediated recycling of VSRs starts at the TGN/EE (Niemes et al., 2010b; Stierhof et al., 2012) and not at the MVB/LE as proposed earlier. This assumption, however, implies that VSRs release their ligands already in the TGN/EE and subsequently, that VSRs bind cargo in a compartment of the vacuolar transport route that is upstream of the TGN/EE. It was shown that chimeric VSRs where the LDB was fused to the ER-retention signal HDEL were able to accumulate ligands in the early secretory pathway

(Watanabe et al., 2004; daSilva et al., 2005). When the LDB was fused to the ER-resident protein Calnexin and coexpressed with a soluble vacuolar ligand in tobacco protoplasts, the ligand retained in the ER (Niemes et al., 2010a). These results show that VSR-ligand interaction can occur in compartments upstream of the TGN/EE.

At the time, it was reported that a pH between 6.0 and 7.5 triggers the VSR-ligand interaction, whereas ligands dissociate from the receptors at a pH lower than 5.0 *in vitro* (Kirsch et al., 1994; Cao et al., 2000). Just recently, the intraluminal pH values were identified (Martiniere et al., 2013; Shen et al., 2013). pH in the ER is around 7.1 - 7.5 and in the Golgi between 6.8 and 6.9. The TGN/EE is with a pH of 6.1 - 6.3 the most acidic compartment, or slightly more alkaline as the MVB/LE (6.2 - 6.7), en route to the vacuole. These pH values further support the suggestion that VSRs might recycle from the TGN/EE and indicate that VSR-ligand interaction occurs in the early secretory pathway and ligand dissociation in the TGN/EE. However, there is no experimental evidence for this suggestion so far. This proposed mechanism is also supported by the fact that the transport between the TGN/EE and the MVB/LE occurs via maturation of the MVBs/LEs, which finally fuse with the vacuole (Scheuring et al., 2011). The authors could show furthermore that the inhibition of the clathrin-mediated transport does not block the vacuolar delivery of soluble vacuolar proteins. Hence, the maturation of MVBs/LEs provide an alternative explanation that transport between the TGN/EE and the MVBs/LEs can occur independently of VSRs.

A compartment specific VSR-ligand interaction analysis demonstrated that VSRs release ligands in the TGN/EE (Künzl et al., 2016). This suggests that the post TGN/EE transport of soluble vacuolar proteins does not require VSRs. Proving this suggestion would, however, require the dissection of the vacuolar transport route in VSR-dependent and VSR-independent transport steps. Therefore, the post TGN/EE transport of soluble proteins lacking vacuolar sorting signal has to be analyzed because these cargos are transported independently of VSRs. Moreover, the retrograde transport of VSRs has to be examined. If VSRs release ligands in the TGN/EE and the VSR-mediated transport occurs bidirectional, VSRs might be recycled from the TGN/EE to an upstream target compartment to reload ligands for further rounds of ligand transport.

6. Objectives

The post-translational regulation of plasma membrane localizing proteins such as receptors or translocators is of great importance for plant cells. They are transported to the lytic vacuole for degradation, requiring a constant supply of the vacuole with these enzymes. This transport strictly depends on vacuolar sorting receptors (VSRs). VSR-mediated protein transport is suggested to be a bidirectional process and was initially supposed to occur between the TGN/EE and the MVB/LE, according to the estimated similarities between plant and mammalian cells. However, the suggested model is only based on VSR localization studies and *in vitro* VSR-ligand binding analyses that do not reflect the *in vivo* situation.
One objective of this work is the identification of VSR-dependent and VSR-independent transport steps. To determine whether VSRs are required for the transport of ligands between the TGN/EE and the MVB/LE, we wanted to analyze the post TGN/EE transport of soluble proteins. To this end, we placed soluble proteins that lack vacuolar sorting signals via the endocytic route in the TGN/EE and followed their fate. Together with results from a compartment-specific VSR-ligand interaction analysis, it became clear that VSRs release their ligands in the TGN/EE and that VSRs might recycle from this compartment. Therefore, another aim was to demonstrate that VSRs recycle and to identify the elusive target compartment of the VSR recycling route. This first necessitates a differentiation of VSRs on the anterograde and VSRs on the retrograde route. Hence, we post-translationally labeled a VSR, based on nanobody epitope interactions, with an endocytosed GFP in the TGN/EE, the compartment where ligands release occurs. Upon recycling of the post-translationally labeled VSR to the upstream target compartment, we wanted to lock the recycled receptors there by the interaction of a second nanobody-epitope pair to prevent its further anterograde transport. Finally, we aimed to show whether VSRs reload ligands after recycling for subsequent rounds of ligand transport and release.
Together, the analysis for the post TGN/EE transport of soluble vacuolar proteins as well as the analysis of the anterograde and retrograde transport was proof of concept for the bidirectional receptor-mediated transport.

7. Results and Discussion

7.1 The post TGN/EE transport of soluble vacuolar cargo occurs independent of VSRs

To better understand the mechanisms of the VSR-mediated transport of ligands in the plant endomembrane system, a determination of compartments in which VSR-ligand interaction can occur is necessary. To date, receptor-ligand interaction analysis were performed only *in vitro*. This, however, does not allow to establish a model for VSR-mediated sorting of soluble vacuolar proteins in the plant endomembrane system, since it cannot be assumed where these interactions do occur. In the research article “Receptor-mediated sorting of soluble vacuolar proteins ends at the *trans*-Golgi network/early endosome” (Künzl et al., 2016), we have analyzed all compartments of the vacuolar transport route for VSR-ligand interactions. Since full length VSRs (Sanderfoot et al., 1998; Hillmer et al., 2001; Tse et al., 2004; Hinz et al., 2007; Niemes et al., 2010b; Saint-Jean et al., 2010; Stierhof and El Kasmi, 2010; Viotti et al., 2010; Wang et al., 2011), but also trafficking mutants of VSRs (daSilva et al., 2006; Foresti et al., 2010; Saint-Jean et al., 2010) exhibit pleiotropic localizations, we had to develop a system that allows for precise targeting of VSRs to specific compartments. For this, we chose to use the soluble luminal ligand-binding domain (LDB) of *At*VSR4, since it was shown that the LBD is sufficient to bind ligands *in vivo* (Watanabe et al., 2004; daSilva et al., 2005). Therefore, we targeted the LDB selectively to specific compartments to test for LDB ligand interactions. VSRs are type I transmembrane proteins and therefor can only be fused to other type I transmembrane proteins because the LBD has to face the compartmental lumen for ligand interaction analysis (Niemes et al., 2010a). Based on topology restrictions, however, it was not possible to place the LBD as translational fusion protein to different compartments along the vacuolar route. Type I transmembrane proteins are only known for the ER and the MVB/LE and not for the Golgi and the TGN/EE. To overcome these topology restrictions, we assembled genetically encoded VSR sensors *in vivo*. For this purpose, we used the variable domain of an alpaca (*Lama paco*) heavy chain antibody (V_HH) that was raised against GFP (Kubala et al., 2010). Heavy chain antibodies from *Camelidae* sp. have no light chain and consist only of a heavy chain (Hamers-Casterman et

al., 1993; Muyldermans, 2013). The variable domain of these heavy chain antibodies is termed nanobody (Nb) and forms the smallest functional antigen-binding fragments with a size of 13 kDa (Muyldermans, 2001). In living cells, GFP-nanobody-tagged proteins specifically bind GFP-tagged proteins after coexpression (Rothbauer et al., 2006; Rothbauer et al., 2008; Schornack et al., 2009). Therefore, we translationally fused the GFP-Nb to the soluble LBD (LBD-Nb).

To target the LBD to specific compartments, we assembled genetically encoded VSR sensors. Therefore, we coexpressed the nanobody-tagged LBD (LBD-Nb) with different established GFP-tagged membrane marker proteins, GFP-Calnexin (CNX) for the ER, α-mannosidase 1 (Man1)-GFP for the *cis*-Golgi cisternae, sialyltransferase (ST)-GFP for the *trans*-Golgi cisternae, SYP61-GFP for the TGN/EE and GFP-BP80 for the MVB/LE. After coexpression, the GFP-nanobody epitope interaction between the GFP from the marker protein and the Nb from the LBD occurs to assemble the compartment specific membrane bound VSR sensors (LBD-Nb:GFP-CNX, LBD-Nb:Man1-GFP, LBD-Nb:SYP61-GFP and LBD-Nb:GFP-BP80).

Usage of these VSR sensors allowed for a compartment-specific VSR-ligand interaction analysis and identified that the ER and the Golgi provide an environment that fosters VSR-ligand interaction whereas the TGN/EE and the MVB/LE do not. This suggests that the VSR-mediated transport occurs towards the TGN/EE were ligands are released from the receptors and that the post TGN/EE transport of soluble vacuolar proteins might occur independently of VSRs.

To test this assumption, we envisaged a system allowing us to generally analyze the post TGN/EE transport of soluble proteins, and the general requirement of VSSs for post TGN/EE transport. These signals, however, are a mandatory requirement for the VSR-mediated transport. To analyze the post TGN/EE transport we took advantage of the TGN being the early endosome in plants (Dettmer et al., 2006; Lam et al., 2007). To test the requirement of VSSs in the post TGN/EE transport, we placed soluble proteins that lack VSS via the endocytic pathway in the TGN/EE and followed their fate. For this, culture medium of triple (3x)RFP expressing protoplasts was used as fluorescent reporter for the endocytic uptake. 3xRFP was expressed as a secretory protein in tobacco mesophyll protoplasts and was recovered from the culture medium after expression. Usage of this proto-

plast secreted 3xRFP ensures that the proteins do not carry intrinsic vacuolar sorting signals and that they have passed the quality control mechanisms of the cell (Pimpl et al., 2006; Scheuring et al., 2012). To analyze protein transport, we supplemented a second population of protoplasts with the protoplast secreted 3xRFP. This population expressed cytosolic (Cyt)-GFP as internal control. 3xRFP was endocytosed and transported to the vacuole, demonstrating that the endocytosed 3xRFP is delivered to the vacuole independent of VSRs. After cell fractionation by centrifugation of these cells, 3xRFP was only present in the soluble and not in the membrane fraction, whereas in controls, the PM-localizing protein RFP-TMD23 fractionated with the membranes, showing that the endocytosed reporter 3xRFP did not bind unspecifically to membranes. To rule out that the 3xRFP molecules reached the vacuole via an alternative route rather than via the endocytic route, we mapped the route of the endocytosed 3xRFP. For this, we fused the GFP-nanobody to the 3xRFP, resulting in 3xRFP-Nb. After having verified that 3xRFP-Nb is endocytosed and transported to the vacuole in Cyt-GFP expressing protoplasts, we mapped its transport route. Cells expressing the PM marker SYNTAXIN OF PLANTS 132 (SYP132)-GFP, the TGN/EE marker SYP61-GFP or the MVB/LE marker GFP-BP80 were supplemented with 3xRFP-Nb for the endocytic uptake. A requirement for this was that the GFP from the compartment specific membrane marker faces the compartmental lumen so that the GFP nanobody-epitope interaction can occur to bind the endocytosed 3xRFP-Nb. Confocal laser scanning microscopy (CLSM) revealed that endocytosed 3xRFP-Nb was anchored due to nanobody-epitope interaction in all cases, showing that the 3xRFP followed the endocytic pathway via the TGN/EE and the MVB/LE to the vacuole. These results clearly show that vacuolar sorting signals and thus VSRs are not required for the post TGN/EE transport of soluble proteins. Together with previous observations that endocytosed polystyrene beads reach the vacuole (Etxeberria et al., 2006), we demonstrated that the vacuole is the default location of the endocytic pathway. Taken together, results from the analysis of the post TGN/EE transport of soluble vacuolar proteins and the results from the compartment specific VSR-ligand interaction analysis, performed by Fabian Künzl, provide evidence that the transport of soluble vacuolar proteins occurs in a two-stage process: the first one is VSR-dependent and the second VSR-independent. VSRs bind ligands in the ER or Golgi, compartments of the early secretory pathway, and transport them to the TGN/EE

were ligands are released. Further transport of ligands occurs independently of VSRs and leads per default to the vacuole. This is in agreement with the localization of retromer subunits at the TGN/EE (Niemes et al., 2010b; Stierhof et al., 2012), since retromer is suggested to mediate the retrograde transport of VSRs back to the donor compartment after ligand release. Moreover, the finding that transport from the TGN/EE to the MVB/LE occurs via maturation of the MVBs/LEs, which fuse with the vacuole (Scheuring et al., 2011) support our result even further that VSRs are not necessary for this transport step.

In vitro VSR ligand analysis identified that ligand binding occurs at neutral pH (6.0 -7.5) and ligand release at a pH lower than 5 (Kirsch et al., 1994; Cao et al., 2000). However, at this time compartmental pH values were not known. Together with localization data for VSRs, the prevacuoles were suggested to be the compartment for ligand release (Ahmed et al., 1997). Recently, experimental data on pH values for all compartments became available (Martiniere et al., 2013; Shen et al., 2013; Luo et al., 2015). Measurements revealed that the pH in the ER is neutral (7.1 – 7.5). Strikingly, *in vitro* ligand-binding studies were also performed at neutral pH (Watanabe et al., 2002; Watanabe et al., 2004; Shen et al., 2014). Together with our data, these results demonstrate that ligand binding occurs at neutral pH *in vitro* and *in vivo*. pH measurements further reveal that the pH values decrease from the ER towards the vacuole. The TGN/EE, however, is the most acidic compartment (6.1 – 6.3) en route to the vacuole. pH values for the MVB/LE are with an value of 6.2 either similar (Shen et al., 2013) or with an value of 6.7 more alkaline (Martiniere et al., 2013) than the TGN/EE. An explanation therefore might be that the V-ATPases which are mainly responsible for the acidification localize at the TGN/EE (Dettmer et al., 2006) and are absent from MVBs/LEs (Viotti et al., 2013). The acidification between the TGN/EE and the MVB/LE promotes our suggestion that VSR-mediated sorting occurs towards the TGN/EE and that the post TGN/EE transport of ligands occurs by default.

Another factor that seems to be important for the VSR-mediated transport of ligands is the concentration of calcium ions (Ca^{2+}) (Watanabe et al., 2002). Ca^{2+} was shown to bind to the EGF repeats in the LBD and thereby induce conformational changes of the LBD that stabilize the receptor ligand complex (Cao et al., 2000; Watanabe et al., 2002). Ca^{2+} even promotes ligand binding at pH 4 and otherwise triggers ligand release at neutral pH and a low Ca^{2+} concentration (Watanabe et

al., 2002). It is assumed that the ER is with an concentration of 50 - 500 µM free Ca^{2+} the compartment with the highest calcium concentration (Stael et al., 2012). It drops in the compartments along the vacuolar route and was shown to be in a nanomolar range in the Golgi (Ordenes et al., 2012). These data suggest that the luminal pH and the calcium concentration might be the two key components for occurring VSR-ligand interactions. However, there might be more influencing factors that are crucial for this interaction which are still unknown.

7.2 Analysis of nanobody-epitope interactions in living cells via quantitative protein transport assays (Früholz and Pimpl, 2017)

To analyze protein-protein interactions between soluble proteins in the lumen of the compartments of the endomembrane system, we have developed a system using nanobody-epitope interactions. To test for occurring nanobody-epitope interactions, we apply quantitative protein transport assay.

For the quantitative protein transport assays, we used the secretory protein α-amylase from barley (Rogers, 1985). α-amylase is synthesized and folded in the ER of the aleurone layer during seed germination and is transported to the endosperm along the secretory pathway. There, starch is hydrolyzed by the α-amylase into sugars that provide energy for the growing embryo. Secretion of the soluble α-amylase occurs signal-independently by bulk flow (Denecke et al., 1990; Phillipson et al., 2001). However, signals are needed for the accumulation of proteins in the ER (Denecke et al., 1991; Contreras et al., 2004) or to target them to the vacuole (Bednarek et al., 1990; Holwerda et al., 1992; Koide et al., 1997; Frigerio et al., 1998). Therefore, sorting signals were fused to secretory proteins to generate reporter proteins to analyze protein sorting and transport in the endomembrane system.

The secretory α-amylase has frequently been used as reporter to study transport processes in the endomembrane system and it has an endogenous enzymatic activity whereby it can be detected. With the usage of different α-amylase-based reporter constructs, different transport routes in the endomembrane system were characterized (Leborgne-Castel et al., 1999; Pimpl et al., 2000; Phillipson et al., 2001; Pimpl et al., 2003; daSilva et al., 2004; daSilva et al., 2005; daSilva et al., 2006; Bottanelli et al., 2011; Gershlick et al., 2014).

To test if a nanobody-epitope interaction can occur in the endomembrane system we evolved a new approach. For this, we used α-amylase as quantifiable reporter for the readout and a vacuolar reporter as putative interactor. In case of an interaction, the vacuolar reporter is expected to reduce the secretion of α-amylase by redirecting it through the attachment of the vacuolar sorting signal. For this purpose, we fused the GFP epitope to the α-amylase, resulting in the secretory reporter α-amylase-GFP. The GFP-nanobody (Nb_G) was fused to the soluble vacuolar protein Aleu-RFP (Aleu-RFP-Nb_G) which carries the ssVSS NPIR.

After having verified that α-amylase-GFP is secreted efficiently into the culture medium of electrotransfected tobacco protoplasts, α-amylase-GFP was coexpressed with Aleu-RFP-Nb_G. Upon coexpression of the two different constructs, the secretion index (Denecke et al., 1990), a value that represents the secretion efficiency, is reduced to a value lower than one. This means that the transport of the secretory α-amylase-GFP is rerouted to vacuole after the nanobody-triggered attachment of the vacuolar sorting signal. In controls, the secretory α-amylase or the ER-retained α-amylase-HDEL (Phillipson et al., 2001) were coexpressed with Aleu-RFP-Nb_G. In both cases, the coexpressed Aleu-RFP-Nb_G did not influence the transport of the reporter protein due to the absence of a nanobody-epitope interaction.

Results show that the nanobody-epitope interaction is specific and occurs in the transit of the endomembrane system, since α-amylase-GFP was only rerouted to the vacuole after the nanobody-triggered attachment of the vacuolar sorting signal. Thus, this quantitative protein transport assay offers a good opportunity to study protein-protein interactions of soluble molecules.

7.3 Nanobody mediated lockdown of VSRs reveals ligand reloading in the Golgi (Früholz et al., in press)

Compartment specific VSR-ligand interaction analysis revealed that ligands are released in the TGN/EE from the receptors (Künzl et al., 2016). This, however, is also the location of the retromer complex, which is suggested to mediate the retrograde transport of VSR (Niemes et al., 2010b; Stierhof et al., 2012). Together with the demonstration that the post TGN/EE transport of soluble vacuolar proteins occurs independent of VSRs, it became clear that if VSRs do recycle back to a donor

compartment to reload ligands, then the TGN/EE would be the starting point for such a recycling (Künzl et al., 2016). However, the upstream target compartment of the VSR recycling route remains elusive.

In mammals, MPRs mediate the transport of lysosomal proteins towards the lysosome (Gonzalez-Noriega et al., 1980; Sahagian et al., 1981; Hoflack and Kornfeld, 1985). The CI-MPR binds ligands at the cell surface and transports them to the lysosome. There, ligands are released from the receptors due to the low compartmental pH (Gonzalez-Noriega et al., 1980). It was suggested the receptor-mediated transport can only be highly effective if receptors recycle continuously after ligand release and can thus go for hundreds of rounds for ligand transport (Rome et al., 1979; Gonzalez-Noriega et al., 1980; Sahagian and Neufeld, 1983). Recycling of MPRs was determined after their radioactive labeling (Braulke et al., 1987; Duncan and Kornfeld, 1988). This was only possible because a small amount (3-10%) of both MPRs are accessible at the PM (Braulke et al., 1987; Breuer et al., 1997). Oligosaccharides of PM-localizing MPRs were labeled with [^{3}H]galactose by exogenous galyctosyltransferases. Glycans of endocytosed MPRs were processed in the *trans*-Golgi cisternae, revealing that the CI-MPR and the CD-MPR recycle to the TGN (Duncan and Kornfeld, 1988). This strategy, however, was not applicable to study recycling of VSRs in plants. PM-localization of VSRs was only reported in growing lily and tobacco pollen tubes (Wang et al., 2011) and for overexpressed citrine-*At*VSR4 (Saint-Jean et al., 2010). Therefore, we have envisaged a novel strategy to verify VSR recycling.

To identify the target compartment of the VSR recycling route, a discrimination between VSRs on the anterograde and VSRs on the retrograde route is necessary. For this, we have developed a strategy for a post-translational GFP-labeling of VSRs that have reached the TGN/EE since VSRs are expected to conduct further ligand transport. With this method, we visualize only recycling receptors. Upon recycling of the GFP-labeled receptors to an upstream target compartment, we trigger their lockdown to block further anterograde transport via the specific interaction of a second nanobody-epitope pair.

Usually, translational fusions with fluorescent proteins are used to analyze the transport of VSRs. However, they become visible directly after synthesis and folding in the ER and the fluorescent signal persists throughout the lifespan of the protein. Hence, it is not possible to distinguish between VSRs on the anterograde and

VSRs on the retrograde route. A prerequisite to examine the VSR recycling route is that VSRs become visible in the TGN/EE earliest. Consequently, we have envisaged a system that allows a post-translational labeling of VSRs in the TGN/EE as it was also proposed by Robinson and Neuhaus (2016). Thereby, we have taken advantage of the TGN as being the EE in plants (Dettmer et al., 2006; Lam et al., 2007). For this purpose, the GFP-binding nanobody (Nb_G; (Kubala et al., 2010; Künzl et al., 2016)) was fused N-terminally to the full length VSR4 (Nb_G-VSR). Transiently expressed Nb_G-VSR in tobacco mesophyll protoplasts is then post-translationally labeled in the TGN/EE with exogenously supplied GFP upon endocytic uptake. The labeling GFP itself is a secretory protein, harvested from the culture medium of Sec-GFP expressing protoplasts. The harvested GFP is supplemented to a second population of protoplasts, expressing Nb_G-VSR for the endocytic uptake. Because of this post-translational GFP labeling strategy, it is now possible to distinguish between VSRs on the anterograde and VSRs on the retrograde route, since only new synthesized VSRs that have passed the TGN/EE at least once are GFP-labeled and can thus be detected by CLSM.

First, we tested for compartment specific post-translational labeling by expressing RFP-tagged membrane markers fused to the Nb_G for the ER (Nb_G-RFP-CNX), the *cis*-Golgi cisternae (Man1-RFP-Nb_G), the *trans*-Golgi cisternae (ST-RFP-Nb_G), the TGN/EE (SYP61-RFP-Nb_G) and for the MVB/LE (Nb_G-RFP-BP80). Protoplasts expressing these constructs were incubated with protoplast secreted GFP for the endocytic uptake. Endocytosed GFP was trapped in the TGN/EE and the MVB/LE due to the nanobody-epitope interaction between the Nb_G of the membrane marker and the endocytosed GFP. In contrast, no GFP labeling occurred in the *trans*- and *cis*-Golgi cisternae and in the ER. When these membrane markers were coexpressed with Sec-GFP, the specific GFP-nanobody-epitope interaction occurred and the GFP retained in the *cis*-/*trans*-Golgi cisternae or ER, respectively. The results show that a post-translational GFP-labeling is in principle possible for all Nb_G-tagged marker proteins.

Having identified that post-translational GFP-labeling is possible for proteins in the TGN/EE, we tested if it is possible to label a full length VSR with endocytosed GFP. It was shown recently that a full length VSR that is fluorescently tagged between the signal peptide and the coding sequence is functional (Saint-Jean et al., 2010). Accordingly, we tagged a VSR with the GFP-nanobody and a RFP (Nb_G-

RFP-VSR) and post-translationally labeled it with endocytosed GFP. Perfect colocalizing punctate signals were observed between the red-fluorescent VSR and the endocytosed GFP, demonstrating that the post-translational labeling is specific and efficient. Next, we wanted to identify the location of the colocalizing punctate signals. Therefore, an invisible Nb_G-tagged VSR (Nb_G-VSR) was coexpressed with RFP-tagged compartmental marker for the ER (RFP-CNX), the *cis*-Golgi cisternae (Man1-RFP), the *trans*-Golgi cisternae (ST-RFP), the TGN/EE (RFP-SYP61) and for the MVB/LE and vacuole (Aleu-RFP). The post-translational GFP-labeled VSR colocalized only with the TGN/EE marker leading to the conclusion that GFP-labeled VSRs localize under steady state conditions at the TGN/EE. Surprisingly, colocalization occurred neither with the MVB/LE and vacuolar marker Aleu-RFP, nor with markers for the *cis*-/*trans*-Golgi cisternae or the ER. Likewise endogenous VSRs were also localized by immunogold labeling in *Arabidopsis* root cells at the TGN/EE, however, labeling was also observed at the MVB/LE (Niemes et al., 2010b; Stierhof and El Kasmi, 2010; Viotti et al., 2010).

The steady-state localization at the TGN/EE can be explained by conceptual different scenario: either VSRs do not recycle at all as it is assumed for homology-transmembrane-RING-H2 (RMR) receptors, a receptor family that mediates the transport of soluble proteins to the protein storage vacuole (Shen et al., 2011; Occhialini et al., 2016), or the TGN/EE is the starting point of the retrograde recycling step of a bidirectional transport system, whereby the anterograde transport is faster than the retrograde. In order to test this hypothesis, we aimed a strategy to block further anterograde transport of VSRs from the target compartment after recycling. For this, we made use of a second nanobody epitope pair, to build a trap for the post-translational labeled and recycled VSR. The mammalian α-synuclein nanobody (Nb_S) recognizes a 23 amino acid linear epitope from α-synuclein (SYN) (Guilliams et al., 2013). This epitope (SYN) was fused to red-fluorescent membrane markers which serve as compartment specific membrane anchors (MA-RFP-Nb_S). To enable the trap, the SYN epitope was fused to GPF, resulting in the dual epitope linker protein GFP-SYN.

To identify the target compartment of the VSR recycling route, Nb_G-VSR and MA-RFP-Nb_S are coexpressed. Subsequently, the Nb_G-tagged VSR is post-translationally labeled with the dual epitope linker GFP-SYN in the TGN/EE after its endocytic uptake. Upon recycling of the GFP-SYN-labeled VSR to the upstream donor

compartment, the VSR is expected to be locked to the membrane anchor by the SYN-nanobody epitope interaction between the SNY epitope of the labeled VSR and the SYN-nanobody of the compartment specific membrane anchor.
To implement such a strategy, it is, however, mandatory to test if the SYN-nanobody epitope interaction also does occur in the lumen of secretory pathway compartments first. Therefore, a quantitative protein transport assay, as described in Früholz and Pimpl (2017) (see chapter **7.2**), was performed. This time however, the SYN epitope was fused to the secretory protein α-amylase (amy-SYN) and the Nb_S to the vacuolar-targeted protein Aleu-RFP, resulting in Aleu-RFP-Nb_S. After the verification that amy-SYN is secreted efficiently into the culture medium, amy-SYN was coexpressed with different amounts of Aleu-RFP-Nb_S. Upon coexpression of the two proteins, the transport of amy-SYN was deviated to the vacuole after the nanobody-epitope triggered attachment of the vacuolar sorting signal. Next, we tested if the SYN-nanobody epitope interaction can also occur *in vitro*. For this, membrane anchors for the ER (Nb_S-RFP-CNX), the *cis*-Golgi cisternae (Man1-RFP-Nb_S), the *trans*-Golgi cisternae (ST-RFP-Nb_S) and the TGN/EE (SYP61-RFP-Nb_S) as well as the corresponding RFP-tagged markers (RFP-CNX, Man1-RFP, ST-RFP and RFP-SYP61) were bound to RFP beads, magnetic agarose beads coupled with a RFP-binding protein that bind RFP-tagged proteins, in a bead binding assay and incubated under binding conditions (Kirsch et al., 1994; Watanabe et al., 2004; Künzl et al., 2016) with protoplast secreted GFP-SYN. Immunoblot analysis revealed that GFP-SYN bound to all compartment anchors, whereas no interaction occurred in controls were the membrane markers were bound to RFP beads. To make sure that the SYN-tagged GFP does not prevent the nanobody-triggered labeling of the Nb_G-VSR, *in vitro* immunoprecipitations were performed. HA-tagged Nb_G-VSRs were bound to HA beads and incubated either with GFP or GFP-SYN under binding conditions (Kirsch et al., 1994; Watanabe et al., 2004; Künzl et al., 2016). Results show that GFP and GFP-SYN were immunoprecipitated respectively. Additionally, the localization of GFP-SYN labeled Nb_G-VSR was analyzed by CLSM. The GFP-SYN labeled VSR colocalized only with the TGN/EE marker and not with markers for the ER, *cis*-/*trans*-Golgi or the MVB/LE. The results underline that the steady state localization of labeled VSRs is not shifted when labeling them with the dual epitope linker GFP-SYN.

After having shown that the dual epitope linker GFP-SYN is bound by the GFP- and the SYN-nanobody, we applied our experimental approach to identify the target compartment of the VSR recycling route by blocking the anterograde VSR transport after recycling. The localization of the GFP-SYN labeled Nb_G-VSR shifted from the TGN/EE to the *trans*- and *cis*-Golgi cisternae when coexpressed with the *trans*-Golgi anchor ST-RFP-Nb_S or the *cis*-Golgi anchor Man1-RFP-Nb_S, respectively. This colocalization was never observed when the Golgi markers ST-RFP or Man1-RFP without the Nb_S for the lockdown were coexpressed. This demonstrates that the labeled VSRs were successfully locked in the *trans*- and *cis*-Golgi cisternae after recycling from the TGN/EE due to the SYN nanobody-epitope interaction between the labeled VSR and the compartment specific membrane anchor. To confirm that the lockdown of the GFP-SYN labeled VSR did not alter the localization of the anchors in the Golgi, protoplasts were incubated with Brefeldin A (BFA), a fungal toxin that causes the fusion between the Golgi stack and the ER in tobacco (Ritzenthaler et al., 2002). After BFA treatment, the punctae from the locked GFP-SYN labeled VSRs and the RFP-tagged Golgi anchors disappeared and signals appeared in the nuclear envelope, demonstrating that the lockdown did not alter the localization of the *cis*-/*trans*-Golgi cisternae anchors. In comparison, a GFP-SYN labeled and recycled VSR was never locked in the ER by the ER anchor Nb_S-RFP-CNX. As control, we coexpressed Nb_G-VSR and SYP61-RFP-Nb_S and labeled subsequently the VSR with the endocytosed dual epitope GFP-SYN resulting in a colocalization of the labeled VSR and the TGN/EE anchor. The same result was observed when the TGN/EE marker RFP-SYP61 was coexpressed. Together, these results identify the *cis*-Golgi cisternae as the target compartment of the VSR recycling route and show that VSRs do not recycle to compartments upstream of the Golgi stack.

We have shown previously that a soluble Nb_G-tagged LBD of VSR that is anchored to the Golgi marker Man1-GFP or ST-GFP by the GFP nanobody-epitope interaction can bind the ligand Aleu-RFP (Künzl et al., 2016). Based on this concept, we analyzed if also recycled full length VSRs can reload ligands in the Golgi stack, as is assumed for the concept of receptor-mediated transport that includes multiple rounds of ligand binding and release. Therefore, we locked a post-translational GFP-SYN labeled Nb_G-VSR in the *cis*-Golgi by the invisible anchor Man1-Nb_S after recycling. Additionally, we coexpressed the model ligand Aleu-RFP and

a blue fluorescent protein 2 (BFP2)-tagged Golgi marker (Man1-BFP2), to verify the Golgi localization of the VSR-ligand interaction. CLSM analysis showed that GFP-SYN labeled and recycled VSRs, locked by the *cis*-Golgi anchor Man1-Nb$_S$ colocalize with the ligand Aleu-RFP and the *cis*-Golgi marker Man1-BFP2, demonstrating that recycled VSR bind ligands in the *cis*-Golgi cisternae. The same result was observed when the *trans*-Golgi anchor ST-Nb$_S$ was used for the lockdown and ST-BFP2 as *trans*-Golgi marker. However, no colocalization between the labeled and locked VSR, the ligand and the Golgi marker occurred in the absence of the lockdown when either the Nb$_S$-tagged anchor was not coexpressed or when the Nb$_G$-VSR was labeled with GFP instead of GFP-SYN. In these cases, the VSRs localizes to the TGN/EE, a compartments whose environment does not promote VSR-ligand interaction (Künzl et al., 2016).
The use of our devised concept for a nanobody-epitope based labeling and tracking by the simultaneous use of two different nanobodies allowed us to identify the *cis*-Golgi cisternae as the target compartment of the VSR recycling route and to show that VSRs reload ligands after recycling for subsequent rounds of ligand transport. Together with our previous work (Künzl et al., 2016), we now postulate a new model for the VSR-mediated sorting of soluble vacuolar proteins in the plant endomembrane system, which is described in chapter **7.4**/**Figure 3**.

7.4 Closing remarks

Here, it was possible to decipher the core mechanisms of the VSR-mediated transport of soluble vacuolar proteins and to elucidate the implementation of a bidirectional operating receptor transport system in the plant endomembrane system. We have proven that the bidirectional VSR-mediated transport does indeed exist in plant cells and that it operates between the *cis*-Golgi cisternae and the TGN/EE. Concluding we came up with a revised model for the VSR-mediated transport in the plant endomembrane system (**Figure 3**).

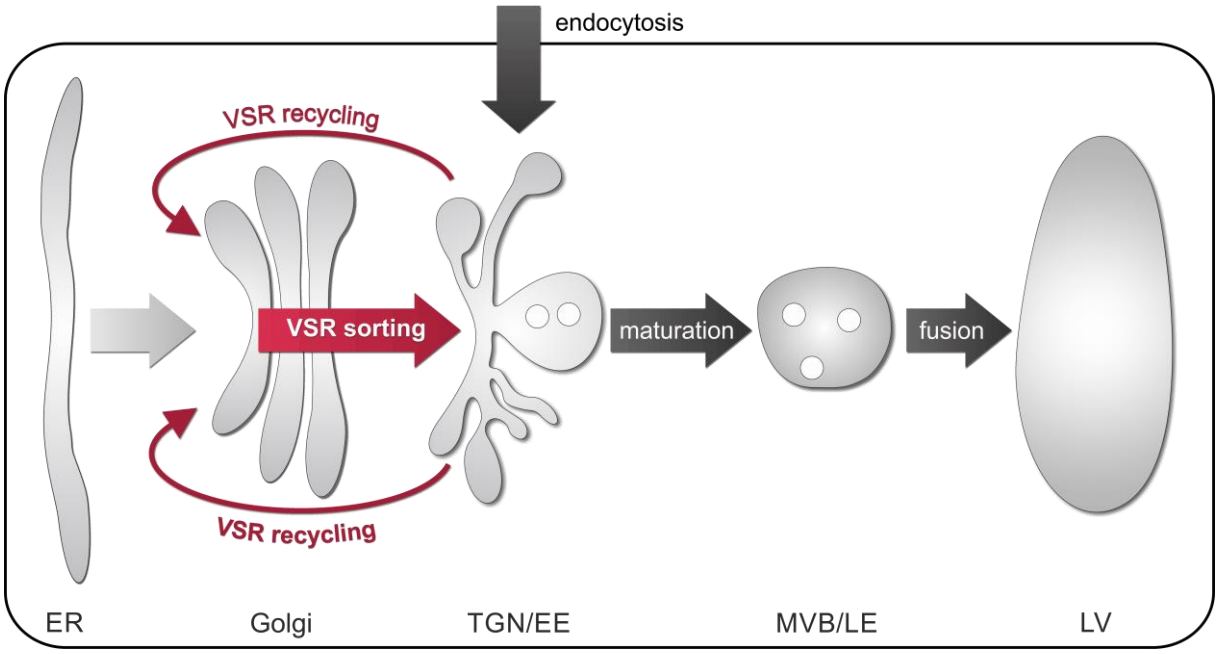

Figure 3: Revised model for receptor mediated sorting of soluble vacuolar proteins in the plant endomembrane system. Newly synthesized VSRs bind ligands in the early secretory pathway and transport them to the TGN/EE. There, ligands are released from the VSRs. Next, VSRs are recycled back to the *cis*-Golgi cisternae for further rounds of ligand transport. Post TGN/EE transport of soluble proteins like released ligands but also endocytosed proteins occurs independent of VSRs and leads per default to the lytic vacuole. Transport in this route is mediated by multivesicular bodies, the late endosomes (MVBs/LEs). They bud off the TGN/EE in a maturation-based step and confer cargo delivery by the ultimate fusion with the lytic vacuole (LV). (Früholz et al., in press)

Newly synthesized VSRs bind soluble vacuolar proteins after their synthesis and folding in the early secretory pathway (Watanabe et al., 2004; daSilva et al., 2005; Niemes et al., 2010b; Gershlick et al., 2014; Künzl et al., 2016) at neutral pH (Martiniere et al., 2013; Shen et al., 2013) and form a receptor-ligand complex. This complex is then transported to the TGN/EE were ligands are released (Künzl et al., 2016) due to the low pH of this compartment (Martiniere et al., 2013; Shen et al., 2013; Luo et al., 2015). The TGN/EE however is the most acidic compartment, with the MVB/LE being more alkaline than the TGN/EE, en route to the vacuole because the characteristic V-ATPases which are mainly responsible for the acidification localize there (Dettmer et al., 2006) and are absent in the MVBs/LEs (Viotti et al., 2013). Therefore, if pH is the driving force that defines binding and release, it cannot be assumed that an acidity driven release can indeed occur in any post-Golgi compartment than the TGN/EE. The identified compartments for ligand binding and release are in agreement with the postulated pH dependency for VSR ligand interaction *in vitro* (Kirsch et al., 1994; Cao et al., 2000). Post TGN/EE transport of released ligands and endocytosed soluble proteins to the lytic vacuole

occurs independently of VSRs and consequently by default. (Künzl et al., 2016). This transport occurs via maturation of the MVBs/LEs that bud off the TGN/EE (Scheuring et al., 2011; Singh et al., 2014) and finally deliver their cargo to the lytic vacuole by fusion (Scheuring et al., 2011). VSRs that have released their ligands in the TGN/EE recycle back to the *cis*-Golgi cisternae, the target compartment of the VSR recycling route (Früholz et al., in press) in a retromer-dependent manner (Oliviusson et al., 2006; Niemes et al., 2010b). There, VSRs reload ligands for further rounds of ligand transport to the TGN/EE (Früholz et al., in press). In this case, we assume that synthesized and folded ligands exit the ER passively in COPII-coated vesicles, which mediate the transport between the ER and the Golgi (Phillipson et al., 2001).

Assuming that the life span of VSRs exceeds by far the time it takes for a round of ligand transport, as reported for the mammalian MPRs (Rome et al., 1979) or the LDL receptor (Brown et al., 1983), it is plausible to assume that recycled VSRs mainly transport ligands from the *cis*-Golgi cisternae to the TGN/EE. At the same time only a few *de novo* synthesized VSRs might contribute to this transport during their first round of ligand transport.

Some recent publications from the mammalian field show that the WLM sorting motif of CI-MPRs, which is responsible for the recycling from the endosomes to the TGN (Seaman, 2007), interacts with the SNX dimers SNX1/2 with SNX5/6 rather than with the retromer subunit VPS35, as assumed previously (Kvainickas et al., 2017; Simonetti et al., 2017). Moreover they show that a VPS35 knock out had no effect on the CI-MPR distribution whereas it was shifted from the TGN to the endosomal membrane in SNX knockouts suggesting that the SNX dimers mediate the retrograde CI-MRP transport from the endosomes to the TGN rather than the retromer complex. With regard to these new results from the mammalian field is tempting to speculate that also in the plant endomembrane system VSRs might be recycled in an SNX-dependent manner rather than in a retromer-dependent manner. However, further experimental work is necessary to proof the speculated involvement of SNX in VSR recycling and it has to be clarified in which transport processes retromer is involved.

Our aforementioned model for the VSR-mediated transport of soluble vacuolar proteins proofs that ligands are released in the TGN/EE from the receptors and that their subsequent transport occurs by default. Further, VSRs are recycled from

this compartment. On the other hand, it was also reported that secretory cargo that is transported to the PM also passes the TGN/EE (Viotti et al., 2010). Based on these findings the question raises where and how the vacuolar, recycling and secretory route separate in the TGN/EE. It was suggested that two types of TGNs/EEs exist, a Golgi-associated TGN were mainly SV bud and a Golgi-independent or free TGN where mainly CCVs bud (Kang et al., 2011; Uemura et al., 2014). Thus, it is tempting to speculate that the SVs of the Golgi-associated TGN mediate the transport of secretory proteins to the PM and that the VSR-ligand complex persists until the Golgi-associated TGN matures into a Golgi-independent TGN. There, the VSR-ligand complex might dissociate, the VSR recycle back to the *cis*-Golgi and the ligands are delivered to the vacuole via maturation of the MVBs/LEs that bud off the Golgi-independent TGN (Kang et al., 2011; Robinson and Neuhaus, 2016). However, to proof this speculation a more detailed characterization of the TGN/EE is important to determine where the secretory and vacuolar pathway separate.

8. References

Ahmed, S.U., Bar-Peled, M., and Raikhel, N.V. (1997). Cloning and subcellular location of an Arabidopsis receptor-like protein that shares common features with protein-sorting receptors of eukaryotic cells. Plant physiology **114,** 325-336.

Ahmed, S.U., Rojo, E., Kovaleva, V., Venkataraman, S., Dombrowski, J.E., Matsuoka, K., and Raikhel, N.V. (2000). The plant vacuolar sorting receptor AtELP is involved in transport of NH2-terminal propeptide-containing vacuolar proteins in Arabidopsis thaliana. Journal of Cell Biology **149,** 1335-1344.

Anderson, R.G.W., Brown, M.S., Beisiegel, U., and Goldstein, J.L. (1982). Surface Distribution and Recycling of the Low-Density Lipoprotein Receptor as Visualized with Antireceptor Antibodies. Journal of Cell Biology **93,** 523-531.

Aniento, F., Gu, F., Parton, R.G., and Gruenberg, J. (1996). An endosomal beta COP is involved in the pH-dependent formation of transport vesicles destined for late endosomes. The Journal of cell biology **133,** 29-41.

Arighi, C.N., Hartnell, L.M., Aguilar, R.C., Haft, C.R., and Bonifacino, J.S. (2004). Role of the mammalian retromer in sorting of the cation-independent mannose 6-phosphate receptor. The Journal of cell biology **165,** 123-133.

Bandmann, V., and Homann, U. (2012). Clathrin-independent endocytosis contributes to uptake of glucose into BY-2 protoplasts. The Plant journal : for cell and molecular biology **70,** 578-584.

Bandmann, V., Muller, J.D., Kohler, T., and Homann, U. (2012). Uptake of fluorescent nano beads into BY2-cells involves clathrin-dependent and clathrin-independent endocytosis. FEBS letters **586,** 3626-3632.

Bar, M., and Avni, A. (2009). EHD2 inhibits ligand-induced endocytosis and signaling of the leucine-rich repeat receptor-like protein LeEix2. The Plant journal : for cell and molecular biology **59,** 600-611.

Bar, M., and Avni, A. (2012). Endocytosis of LeEix and EHD Proteins During Plant Defense Signalling. In Endocytosis in Plants (Springer), pp. 297-311.

Barberon, M., Zelazny, E., Robert, S., Conejero, G., Curie, C., Friml, J., and Vert, G. (2011). Monoubiquitin-dependent endocytosis of the IRON-REGULATED TRANSPORTER 1 (IRT1) transporter controls iron uptake in plants. P Natl Acad Sci USA **108,** E450-E458.

Barlowe, C. (1998). COPII and selective export from the endoplasmic reticulum. Biochimica et biophysica acta **1404,** 67-76.

Barlowe, C., Orci, L., Yeung, T., Hosobuchi, M., Hamamoto, S., Salama, N., Rexach, M.F., Ravazzola, M., Amherdt, M., and Schekman, R. (1994). Copii - a Membrane Coat Formed by Sec Proteins That Drive Vesicle Budding from the Endoplasmic-Reticulum. Cell **77,** 895-907.

Bednarek, S.Y., and Raikhel, N.V. (1991). The barley lectin carboxyl-terminal propeptide is a vacuolar protein sorting determinant in plants. The Plant cell **3,** 1195-1206.

Bednarek, S.Y., Wilkins, T.A., Dombrowski, J.E., and Raikhel, N.V. (1990). A carboxyl-terminal propeptide is necessary for proper sorting of barley lectin to vacuoles of tobacco. The Plant cell **2,** 1145-1155.

Boevink, P., Oparka, K., Santa Cruz, S., Martin, B., Betteridge, A., and Hawes, C. (1998). Stacks on tracks: the plant Golgi apparatus traffics on an

actin/ER network. The Plant journal : for cell and molecular biology **15,** 441-447.

Bonifacino, J.S., and Hurley, J.H. (2008). Retromer. Current opinion in cell biology **20,** 427-436.

Bottanelli, F., Foresti, O., Hanton, S., and Denecke, J. (2011). Vacuolar transport in tobacco leaf epidermis cells involves a single route for soluble cargo and multiple routes for membrane cargo. The Plant cell **23,** 3007-3025.

Brandizzi, F., and Barlowe, C. (2013). Organization of the ER-Golgi interface for membrane traffic control. Nat Rev Mol Cell Biol **14,** 382-392.

Braulke, T., and Bonifacino, J.S. (2009). Sorting of lysosomal proteins. Biochimica et biophysica acta **1793,** 605-614.

Braulke, T., Gartung, C., Hasilik, A., and Vonfigura, K. (1987). Is Movement of Mannose 6-Phosphate-Specific Receptor Triggered by Binding of Lysosomal-Enzymes. Journal of Cell Biology **104,** 1735-1742.

Breuer, P., Korner, C., Boker, C., Herzog, A., Pohlmann, R., and Braulke, T. (1997). Serine phosphorylation site of the 46-kDa mannose 6-phosphate receptor is required for transport to the plasma membrane in Madin-Darby canine kidney and mouse fibroblast cells. Molecular biology of the cell **8,** 567-576.

Brown, J.C., Jolliffe, N.A., Frigerio, L., and Roberts, L.M. (2003). Sequence-specific, Golgi-dependent vacuolar targeting of castor bean 2S albumin. The Plant journal : for cell and molecular biology **36,** 711-719.

Brown, M.S., Anderson, R.G., and Goldstein, J.L. (1983). Recycling receptors: the round-trip itinerary of migrant membrane proteins. Cell **32,** 663-667.

Cao, X., Rogers, S.W., Butler, J., Beevers, L., and Rogers, J.C. (2000). Structural requirements for ligand binding by a probable plant vacuolar sorting receptor. The Plant cell **12,** 493-506.

Casey, J.R., Grinstein, S., and Orlowski, J. (2010). Sensors and regulators of intracellular pH. Nat Rev Mol Cell Biol **11,** 50-61.

Chen, W.J., Goldstein, J.L., and Brown, M.S. (1990). NPXY, a sequence often found in cytoplasmic tails, is required for coated pit-mediated internalization of the low density lipoprotein receptor. The Journal of biological chemistry **265,** 3116-3123.

Chen, X., Irani, N.G., and Friml, J. (2011). Clathrin-mediated endocytosis: the gateway into plant cells. Current opinion in plant biology **14,** 674-682.

Collawn, J.F., Stangel, M., Kuhn, L.A., Esekogwu, V., Jing, S.Q., Trowbridge, I.S., and Tainer, J.A. (1990). Transferrin receptor internalization sequence YXRF implicates a tight turn as the structural recognition motif for endocytosis. Cell **63,** 1061-1072.

Contreras, I., Ortiz-Zapater, E., Castilho, L.M., and Aniento, F. (2000). Characterization of Cop I coat proteins in plant cells. Biochemical and biophysical research communications **273,** 176-182.

Contreras, I., Yang, Y., Robinson, D.G., and Aniento, F. (2004). Sorting signals in the cytosolic tail of plant p24 proteins involved in the interaction with the COPII coat. Plant & cell physiology **45,** 1779-1786.

daSilva, L.L., Foresti, O., and Denecke, J. (2006). Targeting of the plant vacuolar sorting receptor BP80 is dependent on multiple sorting signals in the cytosolic tail. The Plant cell **18,** 1477-1497.

daSilva, L.L., Snapp, E.L., Denecke, J., Lippincott-Schwartz, J., Hawes, C., and Brandizzi, F. (2004). Endoplasmic reticulum export sites and Golgi

bodies behave as single mobile secretory units in plant cells. The Plant cell **16,** 1753-1771.

daSilva, L.L., Taylor, J.P., Hadlington, J.L., Hanton, S.L., Snowden, C.J., Fox, S.J., Foresti, O., Brandizzi, F., and Denecke, J. (2005). Receptor salvage from the prevacuolar compartment is essential for efficient vacuolar protein targeting. The Plant cell **17,** 132-148.

De Marcos Lousa, C., Gershlick, D.C., and Denecke, J. (2012). Mechanisms and concepts paving the way towards a complete transport cycle of plant vacuolar sorting receptors. The Plant cell **24,** 1714-1732.

Denecke, J., Botterman, J., and Deblaere, R. (1990). Protein secretion in plant cells can occur via a default pathway. The Plant cell **2,** 51-59.

Denecke, J., De Rycke, R., and Botterman, J. (1992). Plant and mammalian sorting signals for protein retention in the endoplasmic reticulum contain a conserved epitope. EMBO J **11,** 2345-2355.

Denecke, J., Goldman, M.H., Demolder, J., Seurinck, J., and Botterman, J. (1991). The tobacco luminal binding protein is encoded by a multigene family. The Plant cell **3,** 1025-1035.

Dettmer, J., Hong-Hermesdorf, A., Stierhof, Y.D., and Schumacher, K. (2006). Vacuolar H+-ATPase activity is required for endocytic and secretory trafficking in Arabidopsis. The Plant cell **18,** 715-730.

Dhonukshe, P., Aniento, F., Hwang, I., Robinson, D.G., Mravec, J., Stierhof, Y.D., and Friml, J. (2007). Clathrin-mediated constitutive endocytosis of PIN auxin efflux carriers in Arabidopsis. Current biology : CB **17,** 520-527.

Duncan, J.R., and Kornfeld, S. (1988). Intracellular movement of two mannose 6-phosphate receptors: return to the Golgi apparatus. The Journal of cell biology **106,** 617-628.

Dupree, P., and Sherrier, D.J. (1998). The plant Golgi apparatus. Biochimica et biophysica acta **1404,** 259-270.

Etxeberria, E., Gonzalez, P., Baroja-Fernandez, E., and Romero, J.P. (2006). Fluid phase endocytic uptake of artificial nano-spheres and fluorescent quantum dots by sycamore cultured cells: evidence for the distribution of solutes to different intracellular compartments. Plant signaling & behavior **1,** 196-200.

Fan, L., Li, R., Pan, J., Ding, Z., and Lin, J. (2015). Endocytosis and its regulation in plants. Trends in plant science **20,** 388-397.

Ferguson, S.S., Downey, W.E., 3rd, Colapietro, A.M., Barak, L.S., Menard, L., and Caron, M.G. (1996). Role of beta-arrestin in mediating agonist-promoted G protein-coupled receptor internalization. Science **271,** 363-366.

Foresti, O., Gershlick, D.C., Bottanelli, F., Hummel, E., Hawes, C., and Denecke, J. (2010). A recycling-defective vacuolar sorting receptor reveals an intermediate compartment situated between prevacuoles and vacuoles in tobacco. The Plant cell **22,** 3992-4008.

Frigerio, L., de Virgilio, M., Prada, A., Faoro, F., and Vitale, A. (1998). Sorting of phaseolin to the vacuole is saturable and requires a short C-terminal peptide. The Plant cell **10,** 1031-1042.

Frigerio, L., Jolliffe, N.A., Di Cola, A., Felipe, D.H., Paris, N., Neuhaus, J.M., Lord, J.M., Ceriotti, A., and Roberts, L.M. (2001). The internal propeptide of the ricin precursor carries a sequence-specific determinant for vacuolar sorting. Plant physiology **126,** 167-175.

Früholz, S., and Pimpl, P. (2017). Analysis of Nanobody-Epitope Interactions in Living Cells via Quantitative Protein Transport Assays. Methods Mol Biol **1662,** 171-182.

Früholz, S., Fäßler, F., Kolukisaoglu, Ü., and Pimpl, P. (in press). Nanobody mediated lockdown of VSRs reveals ligand reloading in the Golgi. Nat Commun.

Fujimoto, M., Arimura, S., Ueda, T., Takanashi, H., Hayashi, Y., Nakano, A., and Tsutsumi, N. (2010). Arabidopsis dynamin-related proteins DRP2B and DRP1A participate together in clathrin-coated vesicle formation during endocytosis. Proc Natl Acad Sci U S A **107,** 6094-6099.

Gao, C., Cai, Y., Wang, Y., Kang, B.H., Aniento, F., Robinson, D.G., and Jiang, L. (2014). Retention mechanisms for ER and Golgi membrane proteins. Trends in plant science **19,** 508-515.

Geldner, N., Anders, N., Wolters, H., Keicher, J., Kornberger, W., Muller, P., Delbarre, A., Ueda, T., Nakano, A., and Jurgens, G. (2003). The Arabidopsis GNOM ARF-GEF mediates endosomal recycling, auxin transport, and auxin-dependent plant growth. Cell **112,** 219-230.

Gershlick, D.C., Lousa, C.D., Foresti, O., Lee, A.J., Pereira, E.A., Dasilva, L.L., Bottanelli, F., and Denecke, J. (2014). Golgi-Dependent Transport of Vacuolar Sorting Receptors Is Regulated by COPII, AP1, and AP4 Protein Complexes in Tobacco. The Plant cell.

Goldstein, J.L., and Brown, M.S. (1974). Binding and degradation of low density lipoproteins by cultured human fibroblasts. Comparison of cells from a normal subject and from a patient with homozygous familial hypercholesterolemia. The Journal of biological chemistry **249,** 5153-5162.

Gonzalez-Noriega, A., Grubb, J.H., Talkad, V., and Sly, W.S. (1980). Chloroquine inhibits lysosomal enzyme pinocytosis and enhances lysosomal enzyme secretion by impairing receptor recycling. The Journal of cell biology **85,** 839-852.

Guilliams, T., El-Turk, F., Buell, A.K., O'Day, E.M., Aprile, F.A., Esbjorner, E.K., Vendruscolo, M., Cremades, N., Pardon, E., Wyns, L., Welland, M.E., Steyaert, J., Christodoulou, J., Dobson, C.M., and De Genst, E. (2013). Nanobodies raised against monomeric alpha-synuclein distinguish between fibrils at different maturation stages. Journal of molecular biology **425,** 2397-2411.

Hadlington, J.L., and Denecke, J. (2000). Sorting of soluble proteins in the secretory pathway of plants. Current opinion in plant biology **3,** 461-468.

Hamers-Casterman, C., Atarhouch, T., Muyldermans, S., Robinson, G., Hamers, C., Songa, E.B., Bendahman, N., and Hamers, R. (1993). Naturally occurring antibodies devoid of light chains. Nature **363,** 446-448.

Hanton, S.L., Renna, L., Bortolotti, L.E., Chatre, L., Stefano, G., and Brandizzi, F. (2005). Diacidic motifs influence the export of transmembrane proteins from the endoplasmic reticulum in plant cells. The Plant cell **17,** 3081-3093.

Happel, N., Honing, S., Neuhaus, J.M., Paris, N., Robinson, D.G., and Holstein, S.E. (2004). Arabidopsis mu A-adaptin interacts with the tyrosine motif of the vacuolar sorting receptor VSR-PS1. The Plant journal : for cell and molecular biology **37,** 678-693.

Hara-Kuge, S., Kuge, O., Orci, L., Amherdt, M., Ravazzola, M., Wieland, F.T., and Rothman, J.E. (1994). En bloc incorporation of coatomer subunits

during the assembly of COP-coated vesicles. The Journal of cell biology **124,** 883-892.

Hicke, L., and Riezman, H. (1996). Ubiquitination of a yeast plasma membrane receptor signals its ligand-stimulated endocytosis. Cell **84,** 277-287.

Hillmer, S., Movafeghi, A., Robinson, D.G., and Hinz, G. (2001). Vacuolar storage proteins are sorted in the cis-cisternae of the pea cotyledon Golgi apparatus. The Journal of cell biology **152,** 41-50.

Hinz, G., Colanesi, S., Hillmer, S., Rogers, J.C., and Robinson, D.G. (2007). Localization of vacuolar transport receptors and cargo proteins in the Golgi apparatus of developing Arabidopsis embryos. Traffic **8,** 1452-1464.

Hoflack, B., and Kornfeld, S. (1985). Purification and characterization of a cation-dependent mannose 6-phosphate receptor from murine P388D1 macrophages and bovine liver. The Journal of biological chemistry **260,** 12008-12014.

Holwerda, B.C., Padgett, H.S., and Rogers, J.C. (1992). Proaleurain Vacuolar Targeting Is Mediated by Short Contiguous Peptide Interactions. The Plant cell **4,** 307-318.

Huotari, J., and Helenius, A. (2011). Endosome maturation. EMBO J **30,** 3481-3500.

Inada, N., and Ueda, T. (2014). Membrane trafficking pathways and their roles in plant-microbe interactions. Plant & cell physiology **55,** 672-686.

Jaillais, Y., Fobis-Loisy, I., Miege, C., Rollin, C., and Gaude, T. (2006). AtSNX1 defines an endosome for auxin-carrier trafficking in Arabidopsis. Nature **443,** 106-109.

Jaillais, Y., Santambrogio, M., Rozier, F., Fobis-Loisy, I., Miege, C., and Gaude, T. (2007). The retromer protein VPS29 links cell polarity and organ initiation in plants. Cell **130,** 1057-1070.

Jensen, D., and Schekman, R. (2011). COPII-mediated vesicle formation at a glance. Journal of cell science **124,** 1-4.

Jolliffe, N.A., Brown, J.C., Neumann, U., Vicre, M., Bachi, A., Hawes, C., Ceriotti, A., Roberts, L.M., and Frigerio, L. (2004). Transport of ricin and 2S albumin precursors to the storage vacuoles of Ricinus communis endosperm involves the Golgi and VSR-like receptors. The Plant journal : for cell and molecular biology **39,** 821-833.

Kang, B.H., Nielsen, E., Preuss, M.L., Mastronarde, D., and Staehelin, L.A. (2011). Electron tomography of RabA4b- and PI-4Kbeta1-labeled trans Golgi network compartments in Arabidopsis. Traffic **12,** 313-329.

Kasai, K., Takano, J., Miwa, K., Toyoda, A., and Fujiwara, T. (2011). High boron-induced ubiquitination regulates vacuolar sorting of the BOR1 borate transporter in Arabidopsis thaliana. The Journal of biological chemistry **286,** 6175-6183.

Kim, H., Kang, H., Jang, M., Chang, J.H., Miao, Y., Jiang, L., and Hwang, I. (2010). Homomeric interaction of AtVSR1 is essential for its function as a vacuolar sorting receptor. Plant physiology **154,** 134-148.

Kirsch, T., Saalbach, G., Raikhel, N.V., and Beevers, L. (1996). Interaction of a potential vacuolar targeting receptor with amino- and carboxyl-terminal targeting determinants. Plant physiology **111,** 469-474.

Kirsch, T., Paris, N., Butler, J.M., Beevers, L., and Rogers, J.C. (1994). Purification and initial characterization of a potential plant vacuolar targeting receptor. Proc Natl Acad Sci U S A **91,** 3403-3407.

Koide, Y., Hirano, H., Matsuoka, K., and Nakamura, K. (1997). The N-terminal propeptide of the precursor to sporamin acts as a vacuole-targeting signal even at the C terminus of the mature part in tobacco cells. Plant physiology **114,** 863-870.

Kornfeld, S., and Mellman, I. (1989). The biogenesis of lysosomes. Annu Rev Cell Biol **5,** 483-525.

Kubala, M.H., Kovtun, O., Alexandrov, K., and Collins, B.M. (2010). Structural and thermodynamic analysis of the GFP:GFP-nanobody complex. Protein science : a publication of the Protein Society **19,** 2389-2401.

Künzl, F., Früholz, S., Fäßler, F., Li, B., and Pimpl, P. (2016). Receptor-mediated sorting of soluble vacuolar proteins ends at the trans-Golgi network/early endosome. Nat Plants**,** 16017.

Kvainickas, A., Jimenez-Orgaz, A., Nagele, H., Hu, Z., Dengjel, J., and Steinberg, F. (2017). Cargo-selective SNX-BAR proteins mediate retromer trimer independent retrograde transport. The Journal of cell biology.

Lam, S.K., Siu, C.L., Hillmer, S., Jang, S., An, G., Robinson, D.G., and Jiang, L. (2007). Rice SCAMP1 defines clathrin-coated, trans-golgi-located tubular-vesicular structures as an early endosome in tobacco BY-2 cells. The Plant cell **19,** 296-319.

Leborgne-Castel, N., Jelitto-Van Dooren, E.P., Crofts, A.J., and Denecke, J. (1999). Overexpression of BiP in tobacco alleviates endoplasmic reticulum stress. The Plant cell **11,** 459-470.

Letourneur, F., and Klausner, R.D. (1992). A novel di-leucine motif and a tyrosine-based motif independently mediate lysosomal targeting and endocytosis of CD3 chains. Cell **69,** 1143-1157.

Letourneur, F., Gaynor, E.C., Hennecke, S., Demolliere, C., Duden, R., Emr, S.D., Riezman, H., and Cosson, P. (1994). Coatomer Is Essential for Retrieval of Dilysine-Tagged Proteins to the Endoplasmic-Reticulum. Cell **79,** 1199-1207.

Li, R., Liu, P., Wan, Y., Chen, T., Wang, Q., Mettbach, U., Baluska, F., Samaj, J., Fang, X., Lucas, W.J., and Lin, J. (2012). A membrane microdomain-associated protein, Arabidopsis Flot1, is involved in a clathrin-independent endocytic pathway and is required for seedling development. The Plant cell **24,** 2105-2122.

Li, Y.B., Rogers, S.W., Tse, Y.C., Lo, S.W., Sun, S.S.M., Jauh, G.Y., and Jiang, L.W. (2002). BP-80 and homologs are concentrated on post-Golgi, probable lytic prevacuolar compartments. Plant and Cell Physiology **43,** 726-742.

Lu, D.P., Lin, W.W., Gao, X.Q., Wu, S.J., Cheng, C., Avila, J., Heese, A., Devarenne, T.P., He, P., and Shan, L.B. (2011). Direct Ubiquitination of Pattern Recognition Receptor FLS2 Attenuates Plant Innate Immunity. Science **332,** 1439-1442.

Luo, F., Fong, Y.H., Zeng, Y., Shen, J., Jiang, L., and Wong, K.B. (2014). How vacuolar sorting receptor proteins interact with their cargo proteins: crystal structures of apo and cargo-bound forms of the protease-associated domain from an Arabidopsis vacuolar sorting receptor. The Plant cell **26,** 3693-3708.

Luo, Y., Scholl, S., Doering, A., Zhang, Y., Irani, N.G., Di Rubbo, S., Neumetzler, L., Krishnamoorthy, P., Van Houtte, I., Mylle, E., Bischoff, V., Vernhettes, S., Winne, J., Friml, J., Stierhof, Y.D., Schumacher, K.,

Persson, S., and Russinova, E. (2015). V-ATPase activity in the TGN/EE is required for exocytosis and recycling in Arabidopsis. Nat Plants **1**.

Marcusson, E.G., Horazdovsky, B.F., Cereghino, J.L., Gharakhanian, E., and Emr, S.D. (1994). The Sorting Receptor for Yeast Vacuolar Carboxypeptidase-Y Is Encoded by the Vps10 Gene. Cell **77,** 579-586.

Martiniere, A., Bassil, E., Jublanc, E., Alcon, C., Reguera, M., Sentenac, H., Blumwald, E., and Paris, N. (2013). In vivo intracellular pH measurements in tobacco and Arabidopsis reveal an unexpected pH gradient in the endomembrane system. The Plant cell **25,** 4028-4043.

Martins, S., Dohmann, E.M.N., Cayrel, A., Johnson, A., Fischer, W., Pojer, F., Satiat-Jeunemaitre, B., Jaillais, Y., Chory, J., Geldner, N., and Vert, G. (2015). Internalization and vacuolar targeting of the brassinosteroid hormone receptor BRI1 are regulated by ubiquitination. Nat Commun **6**.

Miller, E.A., and Barlowe, C. (2010). Regulation of coat assembly-sorting things out at the ER. Current opinion in cell biology **22,** 447-453.

Miller, S.E., Sahlender, D.A., Graham, S.C., Honing, S., Robinson, M.S., Peden, A.A., and Owen, D.J. (2011). The molecular basis for the endocytosis of small R-SNAREs by the clathrin adaptor CALM. Cell **147,** 1118-1131.

Montesinos, J.C., Pastor-Cantizano, N., Robinson, D.G., Marcote, M.J., and Aniento, F. (2014). Arabidopsis p24delta5 and p24delta9 facilitate Coat Protein I-dependent transport of the K/HDEL receptor ERD2 from the Golgi to the endoplasmic reticulum. The Plant journal : for cell and molecular biology **80,** 1014-1030.

Muyldermans, S. (2001). Single domain camel antibodies: current status. J Biotechnol **74,** 277-302.

Muyldermans, S. (2013). Nanobodies: natural single-domain antibodies. Annu Rev Biochem **82,** 775-797.

Nakamura, K., and Matsuoka, K. (1993). Protein targeting to the vacuole in plant cells. Plant physiology **101,** 1-5.

Neuhaus, J.M., Sticher, L., Meins, F., Jr., and Boller, T. (1991). A short C-terminal sequence is necessary and sufficient for the targeting of chitinases to the plant vacuole. Proc Natl Acad Sci U S A **88,** 10362-10366.

Niemes, S., Labs, M., Scheuring, D., Krueger, F., Langhans, M., Jesenofsky, B., Robinson, D.G., and Pimpl, P. (2010a). Sorting of plant vacuolar proteins is initiated in the ER. The Plant journal : for cell and molecular biology **62,** 601-614.

Niemes, S., Langhans, M., Viotti, C., Scheuring, D., San Wan Yan, M., Jiang, L., Hillmer, S., Robinson, D.G., and Pimpl, P. (2010b). Retromer recycles vacuolar sorting receptors from the trans-Golgi network. The Plant journal : for cell and molecular biology **61,** 107-121.

Occhialini, A., Gouzerh, G., Di Sansebastiano, G.P., and Neuhaus, J.M. (2016). Dimerization of the Vacuolar Receptors AtRMR1 and -2 from Arabidopsis thaliana Contributes to Their Localization in the trans-Golgi Network. Int J Mol Sci **17**.

Oliviusson, P., Heinzerling, O., Hillmer, S., Hinz, G., Tse, Y.C., Jiang, L., and Robinson, D.G. (2006). Plant retromer, localized to the prevacuolar compartment and microvesicles in Arabidopsis, may interact with vacuolar sorting receptors. The Plant cell **18,** 1239-1252.

Olson, L.J., Hindsgaul, O., Dahms, N.M., and Kim, J.J.P. (2008). Structural insights into the mechanism of pH-dependent ligand binding and release by

the cation-dependent mannose 6-phosphate receptor. Journal of Biological Chemistry **283,** 10124-10134.

Orci, L., Stamnes, M., Ravazzola, M., Amherdt, M., Perrelet, A., Sollner, T.H., and Rothman, J.E. (1997). Bidirectional transport by distinct populations of COPI-coated vesicles. Cell **90,** 335-349.

Ordenes, V.R., Moreno, I., Maturana, D., Norambuena, L., Trewavas, A.J., and Orellana, A. (2012). In vivo analysis of the calcium signature in the plant Golgi apparatus reveals unique dynamics. Cell Calcium **52,** 397-404.

Paez Valencia, J., Goodman, K., and Otegui, M.S. (2016). Endocytosis and Endosomal Trafficking in Plants. Annu Rev Plant Biol **67,** 309-335.

Paris, N., Rogers, S.W., Jiang, L., Kirsch, T., Beevers, L., Phillips, T.E., and Rogers, J.C. (1997). Molecular cloning and further characterization of a probable plant vacuolar sorting receptor. Plant physiology **115,** 29-39.

Pastor-Cantizano, N., Montesinos, J.C., Bernat-Silvestre, C., Marcote, M.J., and Aniento, F. (2016). p24 family proteins: key players in the regulation of trafficking along the secretory pathway. Protoplasma **253,** 967-985.

Pelham, H.R.B., and Rothman, J.E. (2000). The debate about transport in the Golgi - Two sides of the same coin? Cell **102,** 713-719.

Phillipson, B.A., Pimpl, P., daSilva, L.L., Crofts, A.J., Taylor, J.P., Movafeghi, A., Robinson, D.G., and Denecke, J. (2001). Secretory bulk flow of soluble proteins is efficient and COPII dependent. The Plant cell **13,** 2005-2020.

Pimpl, P., Hanton, S.L., Taylor, J.P., Pinto-daSilva, L.L., and Denecke, J. (2003). The GTPase ARF1p controls the sequence-specific vacuolar sorting route to the lytic vacuole. The Plant cell **15,** 1242-1256.

Pimpl, P., Movafeghi, A., Coughlan, S., Denecke, J., Hillmer, S., and Robinson, D.G. (2000). In situ localization and in vitro induction of plant COPI-coated vesicles. The Plant cell **12,** 2219-2236.

Pimpl, P., Taylor, J.P., Snowden, C., Hillmer, S., Robinson, D.G., and Denecke, J. (2006). Golgi-mediated vacuolar sorting of the endoplasmic reticulum chaperone BiP may play an active role in quality control within the secretory pathway. The Plant cell **18,** 198-211.

Pryor, P.R., Jackson, L., Gray, S.R., Edeling, M.A., Thompson, A., Sanderson, C.M., Evans, P.R., Owen, D.J., and Luzio, J.P. (2008). Molecular basis for the sorting of the SNARE VAMP7 into endocytic clathrin-coated vesicles by the ArfGAP Hrb. Cell **134,** 817-827.

Ritzenthaler, C., Nebenfuhr, A., Movafeghi, A., Stussi-Garaud, C., Behnia, L., Pimpl, P., Staehelin, L.A., and Robinson, D.G. (2002). Reevaluation of the effects of brefeldin A on plant cells using tobacco bright yellow 2 cells expressing Golgi-targeted green fluorescent protein and COPI antisera. The Plant cell **14,** 237-261.

Robatzek, S., Chinchilla, D., and Boller, T. (2006). Ligand-induced endocytosis of the pattern recognition receptor FLS2 in Arabidopsis. Genes Dev **20,** 537-542.

Robinson, D.G., and Pimpl, P. (2014). Receptor-mediated transport of vacuolar proteins: a critical analysis and a new model. Protoplasma **251,** 247-264.

Robinson, D.G., and Neuhaus, J.M. (2016). Receptor-mediated sorting of soluble vacuolar proteins: myths, facts, and a new model. Journal of experimental botany **67,** 4435-4449.

Rogers, J.C. (1985). Two barley alpha-amylase gene families are regulated differently in aleurone cells. The Journal of biological chemistry **260,** 3731-3738.

Rohrer, J., and Kornfeld, R. (2001). Lysosomal hydrolase mannose 6-phosphate uncovering enzyme resides in the trans-Golgi network. Molecular biology of the cell **12,** 1623-1631.

Rome, L.H., Weissmann, B., and Neufeld, E.F. (1979). Direct demonstration of binding of a lysosomal enzyme, alpha-L-iduronidase, to receptors on cultured fibroblasts. Proc Natl Acad Sci U S A **76,** 2331-2334.

Ron, M., and Avni, A. (2004). The receptor for the fungal elicitor ethylene-inducing xylanase is a member of a resistance-like gene family in tomato. The Plant cell **16,** 1604-1615.

Rothbauer, U., Zolghadr, K., Muyldermans, S., Schepers, A., Cardoso, M.C., and Leonhardt, H. (2008). A versatile nanotrap for biochemical and functional studies with fluorescent fusion proteins. Mol Cell Proteomics **7,** 282-289.

Rothbauer, U., Zolghadr, K., Tillib, S., Nowak, D., Schermelleh, L., Gahl, A., Backmann, N., Conrath, K., Muyldermans, S., Cardoso, M.C., and Leonhardt, H. (2006). Targeting and tracing antigens in live cells with fluorescent nanobodies. Nat Methods **3,** 887-889.

Russinova, E., Borst, J.W., Kwaaitaal, M., Cano-Delgado, A., Yin, Y., Chory, J., and de Vries, S.C. (2004). Heterodimerization and endocytosis of Arabidopsis brassinosteroid receptors BRI1 and AtSERK3 (BAK1). The Plant cell **16,** 3216-3229.

Sahagian, G.G., and Neufeld, E.F. (1983). Biosynthesis and turnover of the mannose 6-phosphate receptor in cultured Chinese hamster ovary cells. The Journal of biological chemistry **258,** 7121-7128.

Sahagian, G.G., Distler, J., and Jourdian, G.W. (1981). Characterization of a membrane-associated receptor from bovine liver that binds phosphomannosyl residues of bovine testicular beta-galactosidase. Proc Natl Acad Sci U S A **78,** 4289-4293.

Saint-Jean, B., Seveno-Carpentier, E., Alcon, C., Neuhaus, J.M., and Paris, N. (2010). The cytosolic tail dipeptide Ile-Met of the pea receptor BP80 is required for recycling from the prevacuole and for endocytosis. The Plant cell **22,** 2825-2837.

Sanderfoot, A.A., Ahmed, S.U., Marty-Mazars, D., Rapoport, I., Kirchhausen, T., Marty, F., and Raikhel, N.V. (1998). A putative vacuolar cargo receptor partially colocalizes with AtPEP12p on a prevacuolar compartment in Arabidopsis roots. Proc Natl Acad Sci U S A **95,** 9920-9925.

Scheuring, D., Kunzl, F., Viotti, C., Yan, M.S., Jiang, L., Schellmann, S., Robinson, D.G., and Pimpl, P. (2012). Ubiquitin initiates sorting of Golgi and plasma membrane proteins into the vacuolar degradation pathway. BMC plant biology **12,** 164.

Scheuring, D., Viotti, C., Kruger, F., Kunzl, F., Sturm, S., Bubeck, J., Hillmer, S., Frigerio, L., Robinson, D.G., Pimpl, P., and Schumacher, K. (2011). Multivesicular bodies mature from the trans-Golgi network/early endosome in Arabidopsis. The Plant cell **23,** 3463-3481.

Schoberer, J., and Strasser, R. (2011). Sub-compartmental organization of Golgi-resident N-glycan processing enzymes in plants. Molecular plant **4,** 220-228.

Schornack, S., Fuchs, R., Huitema, E., Rothbauer, U., Lipka, V., and Kamoun, S. (2009). Protein mislocalization in plant cells using a GFP-binding chromobody. The Plant journal : for cell and molecular biology **60,** 744-754.

Seaman, M.N. (2004). Cargo-selective endosomal sorting for retrieval to the Golgi requires retromer. The Journal of cell biology **165,** 111-122.

Seaman, M.N. (2007). Identification of a novel conserved sorting motif required for retromer-mediated endosome-to-TGN retrieval. Journal of cell science **120,** 2378-2389.

Shen, J., Ding, Y., Gao, C., Rojo, E., and Jiang, L. (2014). N-linked glycosylation of AtVSR1 is important for vacuolar protein sorting in Arabidopsis. The Plant journal : for cell and molecular biology.

Shen, J., Zeng, Y., Zhuang, X., Sun, L., Yao, X., Pimpl, P., and Jiang, L. (2013). Organelle pH in the Arabidopsis endomembrane system. Molecular plant **6,** 1419-1437.

Shen, Y., Wang, J., Ding, Y., Lo, S.W., Gouzerh, G., Neuhaus, J.M., and Jiang, L. (2011). The rice RMR1 associates with a distinct prevacuolar compartment for the protein storage vacuole pathway. Molecular plant **4,** 854-868.

Shimada, T., Kuroyanagi, M., Nishimura, M., and Hara-Nishimura, I. (1997). A pumpkin 72-kDa membrane protein of precursor-accumulating vesicles has characteristics of a vacuolar sorting receptor. Plant & cell physiology **38,** 1414-1420.

Shimada, T., Fuji, K., Tamura, K., Kondo, M., Nishimura, M., and Hara-Nishimura, I. (2003). Vacuolar sorting receptor for seed storage proteins in Arabidopsis thaliana. P Natl Acad Sci USA **100,** 16095-16100.

Shimada, T., Koumoto, Y., Li, L., Yamazaki, M., Kondo, M., Nishimura, M., and Hara-Nishimura, I. (2006). AtVPS29, a putative component of a retromer complex, is required for the efficient sorting of seed storage proteins. Plant & cell physiology **47,** 1187-1194.

Simonetti, B., Danson, C.M., Heesom, K.J., and Cullen, P.J. (2017). Sequence-dependent cargo recognition by SNX-BARs mediates retromer-independent transport of CI-MPR. The Journal of cell biology.

Singh, M.K., Kruger, F., Beckmann, H., Brumm, S., Vermeer, J.E., Munnik, T., Mayer, U., Stierhof, Y.D., Grefen, C., Schumacher, K., and Jurgens, G. (2014). Protein delivery to vacuole requires SAND protein-dependent Rab GTPase conversion for MVB-vacuole fusion. Current biology : CB **24,** 1383-1389.

Staehelin, L.A., and Moore, I. (1995). The Plant Golgi-Apparatus - Structure, Functional-Organization and Trafficking Mechanisms. Annu Rev Plant Phys **46,** 261-288.

Stael, S., Wurzinger, B., Mair, A., Mehlmer, N., Vothknecht, U.C., and Teige, M. (2012). Plant organellar calcium signalling: an emerging field. Journal of experimental botany **63,** 1525-1542.

Stierhof, Y.D., and El Kasmi, F. (2010). Strategies to improve the antigenicity, ultrastructure preservation and visibility of trafficking compartments in Arabidopsis tissue. Eur J Cell Biol **89,** 285-297.

Stierhof, Y.D., Viotti, C., Scheuring, D., Sturm, S., and Robinson, D.G. (2012). Sorting nexins 1 and 2a locate mainly to the TGN. Protoplasma.

Strasser, R. (2014). Biological significance of complex N-glycans in plants and their impact on plant physiology. Frontiers in plant science **5,** 363.

Takano, J., Miwa, K., Yuan, L., von Wiren, N., and Fujiwara, T. (2005). Endocytosis and degradation of BOR1, a boron transporter of Arabidopsis thaliana, regulated by boron availability. Proc Natl Acad Sci U S A **102,** 12276-12281.

Takano, J., Tanaka, M., Toyoda, A., Miwa, K., Kasai, K., Fuji, K., Onouchi, H., Naito, S., and Fujiwara, T. (2010). Polar localization and degradation of Arabidopsis boron transporters through distinct trafficking pathways. Proc Natl Acad Sci U S A **107,** 5220-5225.

Takeuchi, M., Ueda, T., Sato, K., Abe, H., Nagata, T., and Nakano, A. (2000). A dominant negative mutant of sar1 GTPase inhibits protein transport from the endoplasmic reticulum to the Golgi apparatus in tobacco and Arabidopsis cultured cells. The Plant journal : for cell and molecular biology **23,** 517-525.

Traub, L.M. (2009). Tickets to ride: selecting cargo for clathrin-regulated internalization. Nat Rev Mol Cell Biol **10,** 583-596.

Tse, Y.C., Mo, B., Hillmer, S., Zhao, M., Lo, S.W., Robinson, D.G., and Jiang, L. (2004). Identification of multivesicular bodies as prevacuolar compartments in Nicotiana tabacum BY-2 cells. The Plant cell **16,** 672-693.

Uemura, T., Suda, Y., Ueda, T., and Nakano, A. (2014). Dynamic behavior of the trans-golgi network in root tissues of Arabidopsis revealed by super-resolution live imaging. Plant & cell physiology **55,** 694-703.

Viotti, C., Bubeck, J., Stierhof, Y.D., Krebs, M., Langhans, M., van den Berg, W., van Dongen, W., Richter, S., Geldner, N., Takano, J., Jurgens, G., de Vries, S.C., Robinson, D.G., and Schumacher, K. (2010). Endocytic and secretory traffic in Arabidopsis merge in the trans-Golgi network/early endosome, an independent and highly dynamic organelle. The Plant cell **22,** 1344-1357.

Viotti, C., Kruger, F., Krebs, M., Neubert, C., Fink, F., Lupanga, U., Scheuring, D., Boutte, Y., Frescatada-Rosa, M., Wolfenstetter, S., Sauer, N., Hillmer, S., Grebe, M., and Schumacher, K. (2013). The endoplasmic reticulum is the main membrane source for biogenesis of the lytic vacuole in Arabidopsis. The Plant cell **25,** 3434-3449.

Wang, H., Zhuang, X.H., Hillmer, S., Robinson, D.G., and Jiang, L.W. (2011). Vacuolar sorting receptor (VSR) proteins reach the plasma membrane in germinating pollen tubes. Molecular plant **4,** 845-853.

Watanabe, E., Shimada, T., Kuroyanagi, M., Nishimura, M., and Hara-Nishimura, I. (2002). Calcium-mediated association of a putative vacuolar sorting receptor PV72 with a propeptide of 2S albumin. The Journal of biological chemistry **277,** 8708-8715.

Watanabe, E., Shimada, T., Tamura, K., Matsushima, R., Koumoto, Y., Nishimura, M., and Hara-Nishimura, I. (2004). An ER-localized form of PV72, a seed-specific vacuolar sorting receptor, interferes the transport of an NPIR-containing proteinase in Arabidopsis leaves. Plant & cell physiology **45,** 9-17.

Xiang, L., Etxeberria, E., and Van den Ende, W. (2013). Vacuolar protein sorting mechanisms in plants. FEBS J **280,** 979-993.

Yang, Y.D., Elamawi, R., Bubeck, J., Pepperkok, R., Ritzenthaler, C., and Robinson, D.G. (2005). Dynamics of COPII vesicles and the Golgi apparatus in cultured Nicotiana tabacum BY-2 cells provides evidence for transient association of Golgi stacks with endoplasmic reticulum exit sites. The Plant cell **17,** 1513-1531.

Yu, A., Xing, Y., Harrison, S.C., and Kirchhausen, T. (2010). Structural analysis of the interaction between Dishevelled2 and clathrin AP-2 adaptor, a critical step in noncanonical Wnt signaling. Structure **18,** 1311-1320.

9. Appendix

9.1 Receptor-mediated sorting of soluble vacuolar proteins ends at the *trans*-Golgi network/early endosome

Fabian Künzl, **Simone Früholz**, Florian Fäßler, Beibei Li and Peter Pimpl

Nature Plants 2, Article number: 16017 (2016), doi:10.1038/nplants.2016.17
(https://www.nature.com/articles/nplants201617)

Vacuolar sorting receptors transport ligands from the ER and the Golgi to the TGN/EE

Fabian Künzl, Simone Früholz, Florian Fäßler, Beibei Li and Peter Pimpl*

Center for Plant Molecular Biology (ZMBP), University of Tübingen, Germany

* **Corresponding author:**
Peter Pimpl, ZMBP, University of Tübingen, Auf der Morgenstelle 32, D-72076 Tübingen
Tel: +49-7071-2978889
Fax: +49-7071-295797
e-mail: peter.pimpl@zmbp.uni-tuebingen.de

Running title: Compartment-specific analysis of VSR-ligand interaction

Abstract

Sorting of soluble vacuolar proteins is of vital importance for plant cells and requires that vacuolar sorting receptors (VSRs) bind and release their cargo ligands. However, it is controversial, where in the endomembrane system these interactions occur. Here, we present an *in vivo* analysis of VSR-ligand interactions for all compartments of the vacuolar transport route. For this, we have developed compartment-specific VSR sensors and performed FRET-FLIM analysis to monitor for ligand binding. We show that VSRs bind ligands in the ER and in the Golgi, but not in the *trans*-Golgi network/early endosome (TGN/EE) nor in multivesicular late endosomes (MVBs/LEs). This implies that *post*-TGN/EE trafficking of ligands towards the vacuole is VSR-independent. We verify this by demonstrating that also non-VSR-ligands are delivered to the vacuole from the TGN/EE after endocytic uptake. Thus, we postulate that vacuolar sorting receptors transport ligands from the ER and the Golgi to the TGN/EE, followed by a VSR-independent default flow onwards to the vacuole.

Introduction

Soluble vacuolar proteins and their corresponding vacuolar sorting receptors (VSRs) were identified in plants more than twenty years ago[1,2]. However, the mechanism of VSR-mediated sorting as implemented in the plant endomembrane system[3] is still not yet understood. Vacuolar sorting signals of soluble plant proteins are encoded by short peptide motifs within the amino acid sequence[1]. The first VSR was isolated from detergent-solubilised Golgi and clathrin-coated vesicle (CCV) fractions at neutral pH using synthetic peptides containing sorting signals[5]. VSRs are type I transmembrane proteins encoded by a gene family unique to plants[4-6]. They bind ligands via a structured N-terminal luminal binding domain (LBD) consisting of a protease associated domain, a central domain and three epidermal growth factor repeats[7,8]. VSRs also carry sorting signals for their own transport in the cytosolic C-terminus[9-11]. Based on assumed similarities to the lysosomal sorting machinery in mammals concerning receptor localisation and pH dependency of ligand binding, it was proposed almost twenty years ago that VSR-mediated sorting in plants occurs via CCV-facilitated transport from the *trans*-Golgi to a prevacuolar compartment, where ligands dissociate due to the lower pH.
In the intervening years, major discoveries have challenged this model: the *trans*-Golgi network (TGN) in plants was identified as the early endosome (EE)[12,13] that is distinct from the Golgi stack[14]. This hybrid structure (TGN/EE) has now been shown to be the most acidic compartment *en route* to the vacuole[15-17]. The TGN/EE harbours the retromer complex necessary for recycling of the VSRs[18,19]. Most important, however, was the demonstration that the TGN/EE is the source for the biogenesis of the prevacuolar compartment, the multivesicular late endosome (MVB/LE), which confers transport by fusion with the vacuole[20]. These recent findings still await integration into the proposed concept of VSR-mediated sorting. In order to determine the compartments that constitute the framework for the bi-directional receptor transport, it is of paramount importance to firstly identify the locations at which VSRs bind or release their ligands.
To this end, we have developed genetically encoded VSR sensors that allow for non-invasive compartment-specific detection of VSR-ligand interactions *in vivo*. We assembled VSR sensors from a soluble LBD of a VSR and a compartment-specific green fluorescent protein (GFP)-containing membrane markers via antibody-epitope interaction.

For this, we utilised the antigen-binding capability of the V_HH domain of a heavy-chain antibody[21], termed nanobody (Nb), that was recently raised against GFP in alpacas (*Lama paco*)[22,23]. Based on the amino acid sequence of this anti-GFP Nb, we have generated a coding sequence for the expression of a soluble GFP-binding LBD fusion protein (LBD-Nb). VSR sensor assembly occurs upon coexpression of this LBD-Nb with a compartment-specific membrane marker protein that exposes GFP in the compartmental lumen, thereby reconstituting a GFP-tagged membrane protein.

We monitored for VSR-ligand interaction by coexpression of the self-assembling sensors with red fluorescent protein (RFP) ligands in a comprehensive approach, combining localisation analysis with Förster-resonance energy transfer-fluorescence lifetime imaging microscopy (FRET-FLIM). We firstly analysed the localisation of assembled sensors and the soluble ligands to test whether the presence of the sensor results in coaccumulation of ligands, as a preliminary indication for VSR-ligand interaction. In the second step, we applied FRET-FLIM to either verify or negate VSR-ligand interactions[24,25]. This is possible since FRET occurs only across short distances between 1 and 10 nm, thus allowing to differentiate between interaction-dependent and -independent colocalisation of proteins[24].

With this novel strategy, we were able to show that VSRs bind ligands only in the ER and in the Golgi stack, but not in *post*-Golgi compartments such as the TGN/EE or the MVB/LE. This suggests that *post*-TGN/EE trafficking of soluble proteins towards the vacuole is independent of VSR-ligand interactions. Confirmation of this conclusion was provided by identifying the vacuole as being the default location for soluble proteins of the endocytic route that merges with the biosynthetic vacuolar route at the TGN/EE. Consequently, we postulate a two-stage process for vacuolar transport of soluble proteins. Firstly, VSRs confer the transport of ligands to the TGN/EE, followed by a VSR-independent default flow onwards to the vacuole via budding of MVBs/LEs and their fusion with the vacuole.

RESULTS

Compartment-specific targeting via nanobody-mediated protein assembly

The challenge in using genetically encoded reporters for non-invasive compartment-specific analysis *in vivo* is to achieve their precise targeting[26]. This is particularly true for the analysis of the Golgi stack, the TGN/EE and the MVB/LE, since sorting signals specific for these compartments are largely unknown. A common targeting strategy is the use of translational fusions between reporter domains and membrane marker proteins. This is however subject to topology restrictions of the fusion partners and it has to be mentioned that the N-terminal LBD of the type I VSRs can only be fused to type I membrane marker proteins[27]. Type I membrane markers, however, are only known for the ER and the MVB/LE but neither for the Golgi stack nor the TGN/EE. To overcome these constraints, we developed a targeting strategy based on nanobody-mediated protein assembly. To demonstrate successful targeting, we have generated a construct consisting of a fluorescent LBD fused to an anti-GFP nanobody [23] as a soluble VSR (LBD-RFP-Nb) that can be used in combination with epitope (GFP)-tagged membrane marker proteins to assemble compartment-specific VSR sensors *in vivo* (Fig. 1a). To rule out that the soluble VSR bears intrinsic sorting signals that compromise targeting, we first analysed its transport properties (Fig. 1b-d). Fluorescence signals of LBD-RFP-Nb are largely absent in cells but appear when ER export is prevented by Sec12 overproduction[28]. To test for nanobody-mediated protein assembly in all compartments *en route* to the vacuole, we have expressed the soluble VSR with membrane anchors for ER (GFP-CNX), Golgi (Man1-GFP), TGN/EE (SYP61-GFP) and MVBs/LEs (GFP-BP80; Fig. 1e-i, Supplementary Table 1). In all cases, strong red-fluorescence signals from LBD-RFP-Nb become detectable and colocalise precisely with the respective anchor due to nanobody-epitope interaction at the inner leaflet of the compartmental membrane. This is most evident for the colocalising signals at the ring-shaped periphery of the Golgi (Fig. 1f) and at ring-like MVB/LE structures after treatment with wortmannin (WM)[29] (Fig. 1i). Together, these data show that nanobody-epitope interactions persist in the lumen of all compartments along the vacuolar route, irrespective of their individual biochemical properties.

Assembled VSR sensors possess ligand-binding competence

We have generated a soluble LBD-Nb fusion protein for coexpression with the GFP-based membrane anchors. Due to the nanobody-epitope interaction, both molecules constitute a green-fluorescent membrane protein, employed as compartment-specific VSR sensors. Usage of these sensors together with a red-fluorescent ligand allows testing for receptor-ligand interactions via sensor-ligand colocalisation analysis and via FRET-FLIM as an intensity-independent approach to detect FRET[24]. For this, we used the established model ligand Aleu-RFP. This soluble vacuolar reporter carries 24 amino acids from the *Petunia* thiol protease aleurain that contains the sequence-specific vacuolar sorting motif NPIR[30].

Upon coexpression, binding of Aleu-RFP to the anchored LBD of the sensor triggers close proximity of the RFP from the ligand and the GFP upstream of the LBD within the sensor and thus allows for FRET to occur. In this situation, excited-stage energy from the donor GFP is transferred to the acceptor RFP of the ligand, thereby reducing the fluorescence lifetime of GFP[24]. Consequently, lack of ligand binding does not alter the fluorescence lifetime, even if both fluorophores colocalise interaction-independently in the same compartment (Fig. 2a).

During the course of VSR-mediated sorting, ligand binding is reversible. Therefore, we expected to identify compartments *en route* to the vacuole that either support or restrict ligand binding. To rule out that the experiments were compromised by differences in the ligand-binding competence of the LBD-Nb in the context of different membrane anchors, we first confirmed the ligand-binding capability of all VSR sensors *in vitro* (Fig 2b, Supplementary Fig. 1). For this, we assembled sensors in the ER, Golgi, TGN/EE and MVB/LE (Supplementary Fig. 2) and immunoprecipitated them by using GFP antibodies in bead-binding assays. For direct comparison of their ligand-binding capabilities, we incubated the bead-bound VSR sensors with the ligand Aleu-RFP[30] at binding conditions[2]. In all cases, Aleu-RFP was coprecipitated while secretory Sec-RFP in control experiments was not. This demonstrates that all assembled VSR sensors possess ligand-binding competence.

VSR-ligand interaction occurs in the ER but not in the MVB/LE

We have recently shown that placement of LBDs in the lumen of the ER triggers accumulation of ligands, suggesting VSR-ligand binding[27]. Consistently, assembly

of VSR sensors in the ER also retains the ligand Aleu-RFP, preventing vacuolar delivery (Fig. 3a,b). To test whether this accumulation is indeed due to VSR-ligand interaction, we performed FRET-FLIM. We took advantage of the fact that the ER marker GFP-Calnexin (CNX) induces sheet-like ER cisternae without affecting ER function[31], resulting in an enlarged signal surface facilitating FLIM recording. The analysis revealed a highly significant reduction of the GFP lifetime in the presence of the ligand, with values well within the range of recently reported protein-protein interactions using this pair of fluorophores for FRET-FLIM in plants[25].

In sharp contrast, fluorescence lifetime was not influenced by the ER-localising non-ligand RFP-HDEL and the secretory marker Sec-RFP, even if present in the ER at high levels upon inhibition of ER export by brefeldin A (BFA), or in the absence of the LBD-Nb as binding partner (Fig. 3c, Supplementary Fig. 3a). This direct comparison between the model ligand Aleu-RFP with the non-ligands RFP-HDEL and Sec-RFP (±BFA) reveals that the recorded reduction of fluorescence lifetime is specific for VSR-ligand interaction, thus identifying the ER as a compartment that promotes VSR-ligand binding.

Receptor-mediated transport of ligands is completed by their release. With the MVB/LE being the last morphologically characterised compartment *en route* to the vacuole, ligands should be released from receptors here at the latest. At steady-state conditions, Aleu-RFP localises to the MVB/LE in addition to the vacuole, which is not altered by the LBD-Nb after sensor assembly (Fig. 3d,e). Therefore, it is difficult to judge VSR-ligand interactions in this compartment solely by the assessment of localisation. FRET-FLIM analysis however revealed that these colocalising ligands do not influence the fluorescence lifetime of the VSR sensor (Fig. 3f, Supplementary Fig. 3b). Reduction of fluorescence lifetime of the GFP in the sensor can only be triggered in controls by direct attachment of RFP to the sensor via nanobody-epitope interaction (LBD-RFP-Nb, compare to Fig. 1h). This demonstrates that the VSR sensors do not bind ligands in this compartment. To extend the analysis, we applied the drug WM which induces enlargement of MVBs/LEs by homotypic fusion[29]. The resulting ring-like structures now reveal a differential distribution, with signals from the VSR sensor being present at the limiting membrane while signals from Aleu-RFP locate to the compartmental lumen (Fig 3g). This also suggests that ligands do not bind to VSRs in this transit compartment towards the vacuole, since this would indeed result in close proximity

of the fluorophores (compare to Fig. 1i). Together, these data demonstrate that ligands do interact with the VSR sensors in the ER and that they do not interact in the MVB/LE. These findings furthermore reveal that only a combination of localisation analysis and FRET-FLIM allows for a reliable assessment of whether a given compartment supports or restricts VSR-ligand binding.

VSR-ligand interaction occurs in the Golgi stack but not in the TGN/EE

Having identified the ER as compartment that supports ligand binding and MVBs/LEs as compartments that do not, we next tested Golgi and TGN/EE for possible VSR-ligand interactions. The *cis*-Golgi marker α-mannosidase 1 (Man1)-GFP does not colocalise with Aleu-RFP, whose punctate signals represent MVBs/LEs (Fig. 4a, compare to Fig. 3d,g). Assembly of VSR sensors in the Golgi however causes colocalisation of Aleu-RFP with all GFP-labelled VSR sensors (Fig. 4b). These colocalising signals appear in addition to the RFP signals from punctate MVBs/LEs and the vacuole. The redistribution of Aleu-RFP to the Golgi can be emphasised by the employment of transport competitors for the endogenous VSRs[32], which reduce vacuolar delivery. The competitor HA-BP80, a HA-epitope-tagged LBD-deletion mutant of BP80, reduces RFP signals in MVBs/LEs and in the vacuole, but does not alter Golgi-colocalisation of the VSR sensors with Aleu-RFP (Fig. 4c). The colocalising signals at the inner leaflet of the Golgi membrane are similar to the signals previously seen for the LBD-RFP-Nb targeted to this compartment (compare to Fig. 1f). This suggests an interaction between the sensors and ligands.

FRET-FLIM analysis revealed a highly significant reduction of the fluorescence lifetime of the donor GFP in the VSR sensor (Fig. 4d, Supplementary Fig. 4a). This reduction depends on the presence of the LBD, demonstrating that the Golgi-localisation of Aleu-RFP is caused by interaction with the VSR sensor. We have also assessed VSR-ligand interaction in the *trans*-face of the stack by using the *trans*-Golgi marker sialyltransferase (ST)-GFP for VSR sensor assembly (Fig. 4e). Aleu-RFP does also not colocalise with the membrane marker ST-GFP (Fig. 4f). In the presence of the LBD-Nb, the distribution pattern of Aleu-RFP shifts, resulting in colocalisation of the ligand and sensor (Fig.4g, Supplementary Fig. 4b), suggesting an interaction to occur. This was verified by FRET-FLIM analysis (Fig.

4h), revealing that Aleu-RFP causes a highly significant decrease of the fluorescence lifetime, which does not occur in the absence of the LBD-Nb.
The situation in the TGN/EE yields another picture. Here, assembly of VSR sensors does not cause colocalisation of the ligand Aleu-RFP (Fig. 5a-c), questioning the occurrence of VSR-ligand interactions. FRET-FLIM analysis of the TGN/EE-localising VSR sensor revealed that Aleu-RFP does not influence the fluorescence lifetime of the sensor, a situation identical to control experiments where the non-ligand Sec-RFP was used instead (Fig. 5d, Supplementary Fig. 5). To demonstrate that protein-protein interactions can shorten the lifetime in the TGN, we attached the red-fluorescent LBD (LBD-RFP-Nb) via nanobody-epitope interaction to the membrane anchor SYP61-GFP. This control confirmed the assembly of VSR sensors in the TGN/EE as illustrated in Fig. 1g and proves that the principle of FRET-FLIM interaction analysis is also applicable to this compartment (Fig. 5d).
Together, these data favour the idea that VSRs and ligands do not interact in the TGN/EE. Consequently, it is tempting to speculate that the VSRs in this compartment have already released their ligands. This however would imply that these VSRs bind ligands upstream of the TGN/EE. To verify this hypothesis, we blocked the arrival of the TGN/EE-targeted VSR sensor with the drug BFA, causing retention of sensors and ligands in the ER (Fig. 5e). BFA-induced ER localisation causes a drastic increase of the fluorescence lifetime of SYP61-GFP-based sensors, with values being identical to those of ER-targeted GFP-CNX-based sensors (compare to Fig. 3c). Under these conditions, coexpressed Aleu-RFP strongly reduces fluorescence lifetime of the SYP61-GFP-based sensor, demonstrating ligand binding. This does not occur in the presence of Sec-RFP (Fig. 5f, Supplementary Fig. 5). The capability of the TGN/EE-targeted VSR sensor to bind ligands in the ER was furthermore confirmed by coimmunoprecipitation (Fig. 5g). Here, only BFA-triggered ER-localisation of the VSR sensor resulted in coimmunoprecipitation of the ligand Aleu-RFP, which does not occur if the sensor localises to the TGN/EE. (Fig. 5g, compare to Fig.3a-c). Altogether, our data demonstrate that VSRs bind their ligands very early in the secretory pathway and release ligands upon arrival in the TGN/EE.

VSRs do not mediate *post*-TGN/EE transport of soluble proteins to the vacuole

The compartment-specific analysis identified the ER and the Golgi as compartments that promote VSR-ligand binding while the TGN/EE and the MVB/LE restrict this interaction. This suggests that VSRs do not contribute to the *post*-TGN/EE transport of soluble vacuolar proteins towards the vacuole. Receptor-independent transport from the TGN/EE to the vacuole furthermore implies that this route does not require sorting signals and is thus the default route for soluble proteins.

To test for this hypothesis, we have developed a strategy to analyse *post*-TGN/EE transport of soluble proteins lacking vacuolar sorting signals. Since these signals are required for the VSR-mediated sorting to the TGN/EE via the biosynthetic pathway, we took advantage of the early endosomal properties of the TGN/EE and targeted soluble proteins to the TGN/EE via the endocytic route. For these experiments, we used triple (3x) RFP from the culture medium of 3xRFP-secreting protoplasts as a fluorescent reporter protein for endocytic uptake. The use of a reporter that was secreted by protoplasts ensures that this reporter does neither carry cryptic intrinsic vacuolar sorting signals nor signs of damage that could possibly trigger vacuolar degradation via mechanisms of quality control later on [33,34].

Incubation of cells expressing cytosolic GFP (Cyt-GFP) with 3xRFP results in vacuolar delivery of this reporter (Fig. 6a). Consequently, the endocytosed reporter is recovered as soluble protein from cellular extracts and does not cofractionate with membranes (Fig 6b). To prove that the reporter reaches the vacuole via the TGN/EE and the MVB/LE, we used the protoplast-secreted anti-GFP nanobody fusion 3xRFP-Nb, which is also delivered to the vacuole in endocytic uptake assays (Fig. 6c). This time however, we used cells expressing GFP-membrane anchors either at the cell surface (SYP132-GFP), the TGN/EE (SYP61-GFP) or the MVB/LE (GFP-BP80). In all cases, the reporter 3xRFP-Nb colocalised with the respective membrane anchor due to nanobody-mediated assembly (Fig. 6d-f), demonstrating its transport via the endocytic route. Together, this shows that soluble proteins reach the vacuole from the TGN/EE independent of sorting receptors, defining the vacuole as being the default location of *post*-TGN/EE transport of soluble proteins.

Discussion

V_HH domains of heavy-chain antibodies from camelids, termed nanobodies, are the smallest polypeptides capable of epitope-binding[35]. The specificity of this interaction together with their size of only 13 kDa turns an ever increasing number of engineered nanobodies into powerful tools for research, diagnostics and therapeutics[35]. Amongst first applications for nanobodies was their use as chromobodies[22]. These fusion proteins between a nanobody and a fluorescent protein have been expressed in the cytosol of plant cells, allowing for specific detection of proteins by the nanobody-mediated attachment of a fluorescent reporter[36,37] but also for manipulation of protein function, possibly by masking of functional domains of the target protein by reporter-attachment[37].

Here, we have employed an anti-GFP nanobody to develop novel VSR sensors for the analysis of VSR-ligand interactions in the lumen of the compartments of the endomembrane system. These sensors assemble via nanobody-triggered interaction from a soluble LBD-nanobody fusion protein with an epitope-tagged compartment-specific membrane anchor. We see this strategy as an approach to overcome current limitations with respect to compartment-specific targeting of functional protein domains, allowing for the analysis of protein-protein interactions *in vivo* that does not redundantise the analysis of the intricate interaction between unmodified full-length VSR and endogenous ligands in the future.

The use of this system allows now for the first time the direct linkage of the type I LBD with type II membrane anchors for the Golgi and the TGN/EE, thus enabling the use of the very same sensing protein at different locations, rather than employing VSR trafficking mutants that exhibit altered distributions[11,16].

We demonstrate that VSR-ligand interactions occur in the ER and Golgi, but don't occur in the TGN/EE or MVBs/LEs (Fig. 6g). These data are in agreement with previous observations, showing that LBDs, when fused to the ER retrieval signal HDEL[32,38] or to the transmembrane domain of an ER-marker[27], cause accumulation of soluble vacuolar proteins. Moreover, VSRs have been initially isolated from solubilised Golgi fractions with immobilised sorting signals at neutral pH[2], which is also found in these compartments[15,16]. Release of ligands was suggested to occur at low pH[2] and in combination with the initial localisation of VSRs at the Golgi and at prevacuoles, it was suggested that VSRs transport their

ligands between these compartments[5]. Since then, localisation analysis was refined and VSRs were also found in *trans*-Golgi cisternae[39], TGN/EE[18,40], MVBs/LEs[18,29,41] and even at the PM[11,42], implying that the sole use of localisation data of receptors is insufficient to judge the ligand-binding status of VSRs[3]. Our data show ligand binding of the SYP61-GFP-based sensor *in vitro* and *in vivo*. However, this depends strictly on its intracellular localisation, with demonstrated binding in the ER but the complete lack thereof in the TGN/EE, suggesting that ligands have been released in the TGN/EE.

We employed FRET-FLIM analysis to monitor for VSR-ligand interactions. The fluorescence lifetime is an intrinsic property of a fluorophore and depends on the environmental pH[43], with decreasing pH lowering lifetime. The FLIM data obtained for the VSR sensor reveals compartment-specific fluorescence lifetimes, thus reflecting on relative compartmental pH. Recorded fluorescence lifetimes were longest in the ER, falling off in *cis*- to *trans*-Golgi and were shortest in the TGN/EE, suggesting that the TGN/EE exhibits a low pH that could have triggered the release of the ligand. This is also supported by recently reported pH values for intracellular compartments[15-17], identifying the TGN/EE with pH values ranging from 6.3-5.5 as being the most acidic compartment of the vacuolar route and MVBs/LEs possessing either similar[15] or an even slightly more alkaline pH[16], whilst the pH was highest in the ER (pH 7.1-7.5)[15-17]. Together, our data are in full agreement with the originally proposed concept of pH-dependent binding and release of ligands[2].

Another key factor modulating VSR-ligand interaction is calcium[44], possibly due to conformational changes induced by Ca^{2+}-binding to an EGF repeat within the LBD[7,44]. Ca^{2+} facilitates ligand binding and prevents release, even at a pH of 4[44], showing that Ca^{2+} supports ligand binding at unfavourable pH[3]. Experimental data on compartmental Ca^{2+} concentrations are scarce. The presence of Ca^{2+} pumps in the ER and the tonoplast suggests that concentrations are the highest there, with an estimate from 50 µM to 5 mM[45], falling off to the nanomolar range in compartments *en route* to the vacuole like the Golgi [46]. Together, this suggests that VSR-mediated sorting depends on an intricate interplay between pH, Ca^{2+} and possibly other factors that differ between the compartments in order to trigger ligand binding and release.

Release of ligands in the TGN implies that further anterograde transport of soluble proteins to the vacuole is independent of VSRs. This is in full agreement with the TGN-localisation of the VSR-recycling retromer complex[18,19] and the observation that MVBs/LEs originate at the TGN/EE[20] and fuse with the vacuole. This scenario does not necessitate VSRs for the ligands to be exported from the TGN/EE. Consequently, all soluble proteins would share the fate of the very same passive vacuolar delivery via the MVB/LE. Indeed, our endocytic uptake assays with secreted non-ligand proteins revealed vacuolar delivery after fluid phase endocytosis. We have traced the endocytosed reporter in the TGN/EE and the MVB/LE, thus confirming the operation of such a passive vacuolar delivery via the endocytic pathway. Alternatively, it could be speculated that secreted soluble proteins might possess positive sorting information for yet unidentified receptors that mediate endocytosis and TGN/EE export. A prerequisite for such a scenario however would be that these receptors do not bind the secretory proteins already in the TGN/EE to prevent vacuolar delivery prior to reaching the PM. However, together with previously reported findings that even endocytosed polystyrene beads reach the vacuole via the endocytic route[47], it seems justified to postulate that the vacuole is the default location for soluble proteins of the endocytic route, which consequently does not require a receptor-mediated transport step between the TGN/EE and the MVB/LE for vacuolar delivery.

METHODS

Plant materials. *Nicotiana tabacum* L. SR1 was grown on Murashige and Skoog medium supplemented with 2% sucrose, 0.5 g/L MES and 0.8 % Agar at pH 5.7 in 16/8 h light–dark cycles at 22 °C.

Plasmid constructs. All constructs are given in Supplemental Table 1. DNA manipulations were performed according to established procedures, using pUC[48]-/pGreenII[34]-based vectors and *Escherichia coli* MC1061. A anti-GFP nanobody (Nb) sequence was generated by reverse-translation of the aa sequence[23], optimised for *Arabidopsis*-specific codon-usage (EMBOSS Backtranseq), modified with N-/C-terminal HA-/6x-His-tags and chemically-synthesised (GeneArt Gene

Synthesis). LBD-RFP-Nb was assembled from AtVSR4 (GenBank accession NM_127036)-LBD, RFP[34] and Nb. Compartment-specific anchors uniformly carried EGFP (GenBank accession BAQ19368), warranting comparable spectroscopical properties. All red-fluorescent reporters are based on monomeric-RFP[34]. 3xRFP/3xRFP-Nb carry the N-terminal signal peptide of Sec-RFP. Correct localisation of all generated marker/reporter-fluorophore fusions was verified.

Protoplast isolation and gene expression. Protoplasts were isolated and electro-transfected as described[49], using the square-wave pulse generator EPI-2500 (Fischer, Heidelberg). 10-50 ng/µL$_{transformation}$ plasmid DNA were transfected; expression occurred for 18-24 h at 25 °C in the dark.

Biosynthesis of fluorescent reporters. Protoplast-secreted reporters (3xRFP/ 3xRFP-Nb) for endocytic uptake experiments were obtained from cell-free culture medium after expression, harvesting, sonication and clearance, ruling out contaminations with reporter-synthesising cells during uptake-experiments. For endocytic uptake, populations of protoplasts expressing GFP markers were supplemented with cleared reporter-containing medium for 24 h.

Confocal microscopy and statistical analysis. Imaging was performed using a Leica TCS-SP8 CLSM, with a x63 (1.2 NA) water immersion objective. Fluorophores were excited (ex) and emission (em) was detected by line switching in sequential mode using HyD detectors: CFP (ex/em: 458 nm/464-525 nm), GFP (ex/em: 488 nm/496-525 nm), and RFP (ex/em: 561 nm/569-636 nm). Pinholes were adjusted to 1 Airy unit for each wavelength. *Post*-acquisition image-processing was performed using Adobe Photoshop CS3 (v10.0.1) and CorelDraw X6 (v16.0.0.707). Calculation of the linear Pearson's correlation coefficient (r_p) and nonlinear Spearman's rank correlation coefficient (r_s) of red and green fluorescent signals and ROI selection was performed as previously described, with threshold levels set to 10. For statistics, correlation coefficients of 10 individually analysed cells per experiment were considered and are given as mean values with standard errors of the mean. Statistical significance was calculated using ANOVA, followed by Tukey's HSD test.

Fluorescence lifetime imaging microscopy. Data acquisition was performed with a Leica TCS-SP8 equipped with a PicoHarp-300-TCSPC-module, a PDL-808

Sepia multichannel-picosecond pulsed-diode-laser-driver and was analysed using SymPhoTime v5.3.2.2 (PicoQuant). GFP was excited with a 470 nm laser (LDH-P-C-470B) at 40 MHz pulse-frequency. Emission was recorded at 496-525 nm by time-correlated single-photon- counting (TCSPC) until reaching a count of 500 photons per pixel. To calculate fluorescence lifetimes, TCSPC histograms were reconvoluted with an instrumental-response-function (IRF) and fitted against a bi-exponential decay function. Only fittings giving χ^2 values between 0.9 and 1.4 were considered. All fluorescence signals of organellar markers were specifically selected with the software's 'region of interest' selection tools to avoid potential miscalculations caused by background noise. In case of GFP-BP80, vacuolar background fluorescence, as seen in addition to punctate endosomal signals, was excluded from lifetime calculations. All selected signals of a cell were recorded and calculated as mean lifetime. Per experimental condition, 12-20 cells were independently analysed, thus representing a total of more than 200 individual Golgi stacks, TGNs/EEs or MVBs/LEs. For statistics, calculated lifetimes of all cells were averaged. Error bars indicate standard errors of the mean. Statistical significance was calculated as above.

Harvesting, protein extraction and immunoblotting. Cell-free medium was harvested after flotation of cells for 5 min at 80 g, using syringes and sealed pre-punctured tubes. Proteins from medium-samples were precipitated as described[50]. After resealing, cells were diluted 5-fold with 250 mM NaCl and sedimented by centrifugation as above. Cells were extracted by sonication in extraction buffer (100 mM Tris, pH 7.8, 200 mM NaCl, 1 mM EDTA, 2 % β-mercaptoethanol and 0.2 % Triton X-100) for PAGE/WB analysis or in 2x binding buffer (40 mM HEPES, 300 mM NaCl, 2 mM $CaCl_2$, 2 mM $MgCl_2$, pH 7.1) for (Co-)IP/ligand binding analysis. Extracts were cleared by centrifugation at 20,000 g for 15 min at 4 °C. For SDS-PAGE/WB, all processed samples/beads were finally mixed 1:1 with 2x Xtreme loading dye[33] and denatured for 5 min at 95 °C. SDS-PAGE/WB was performed as described[33]. Antibodies used: mouse monoclonal anti-GFP (Roche 11814460001, 1:1,000), rat monoclonal anti-RFP (ChromoTek, 1:1,000) and rat monoclonal anti-HA-Peroxidase (Roche 12013819001, 1:2,500).

Immunoprecipitation and ligand binding. For IP/Co-IP and binding assays, sensors were assembled *in vivo* (+/- ligands/BFA) and extracted 1:1 in 2x binding buffer. Immunoprecipitation was performed overnight with rabbit polyclonal GFP antibodies (Life Technologies A6455)-coupled Protein A beads (10001D, Life Technologies) at 4 °C. Beads were 3x washed with binding buffer and either immediately processed for SDS-PAGE/WB or incubated with Aleu-RFP/Sec-RFP (controls), which were in parallel samples transiently expressed and recovered from cell extracts/medium as described above, prior to processing for SDS-PAGE/WB. For cellular fractionation by osmotic shock, cells were resuspended in a 4-fold volume of Tris buffer (50 mM Tris, pH 8.0, 1 mM EDTA) and cleared. Supernatant (S) was recovered, the membrane pellet (P) was resuspended in the initial volume of extraction buffer, and S-/P-samples were processed for SDS-PAGE/WB.

References

1 Holwerda, B. C., Padgett, H. S. & Rogers, J. C. Proaleurain vacuolar targeting is mediated by short contiguous peptide interactions. *Plant Cell* **4,** 307-318 (1992).

2 Kirsch, T., Paris, N., Butler, J. M., Beevers, L. & Rogers, J. C. Purification and initial characterization of a potential plant vacuolar targeting receptor. *Proc. Natl. Acad. Sci. USA* **91,** 3403-3407 (1994).

3 Robinson, D. G. & Pimpl, P. Receptor-mediated transport of vacuolar proteins: a critical analysis and a new model. *Protoplasma* **251,** 247-264, doi:10.1007/s00709-013-0542-7 (2014).

4 Ahmed, S. U., Bar-Peled, M. & Raikhel, N. V. Cloning and subcellular location of an Arabidopsis receptor-like protein that shares common features with protein-sorting receptors of eukaryotic cells. *Plant Physiol.* **114,** 325-336 (1997).

5 Paris, N. *et al.* Molecular cloning and further characterization of a probable plant vacuolar sorting receptor. *Plant Physiol.* **115,** 29-39 (1997).

6 De Marcos Lousa, C., Gershlick, D. C. & Denecke, J. Mechanisms and concepts paving the way towards a complete transport cycle of plant vacuolar sorting receptors. *Plant Cell* **24,** 1714-1732, doi:10.1105/tpc.112.095679 (2012).

7 Cao, X., Rogers, S. W., Butler, J., Beevers, L. & Rogers, J. C. Structural requirements for ligand binding by a probable plant vacuolar sorting receptor. *Plant Cell* **12,** 493-506 (2000).

8 Luo, F. *et al.* How vacuolar sorting receptor proteins interact with their cargo proteins: crystal structures of apo and cargo-bound forms of the protease-associated domain from an Arabidopsis vacuolar sorting receptor. *Plant Cell* **26,** 3693-3708, doi:10.1105/tpc.114.129940 (2014).

9 daSilva, L. L., Foresti, O. & Denecke, J. Targeting of the plant vacuolar sorting receptor BP80 is dependent on multiple sorting signals in the cytosolic tail. *Plant Cell* **18,** 1477-1497 (2006).
10 Kim, H. *et al.* Homomeric interaction of AtVSR1 is essential for its function as a vacuolar sorting receptor. *Plant Physiol.* **154,** 134-148 (2010).
11 Saint-Jean, B., Seveno-Carpentier, E., Alcon, C., Neuhaus, J. M. & Paris, N. The cytosolic tail dipeptide Ile-Met of the pea receptor BP80 is required for recycling from the prevacuole and for endocytosis. *Plant Cell* **22,** 2825-2837 (2010).
12 Dettmer, J., Hong-Hermesdorf, A., Stierhof, Y. D. & Schumacher, K. Vacuolar H+-ATPase activity is required for endocytic and secretory trafficking in Arabidopsis. *Plant Cell* **18,** 715-730 (2006).
13 Lam, S. K. *et al.* BFA-induced compartments from the Golgi apparatus and trans-Golgi network/early endosome are distinct in plant cells. *Plant J.* **60,** 865-881 (2009).
14 Foresti, O. & Denecke, J. Intermediate organelles of the plant secretory pathway: identity and function. *Traffic* **9,** 1599-1612 (2008).
15 Shen, J. *et al.* Organelle pH in the *Arabidopsis* Endomembrane System. *Mol Plant* **6,** 1419-1437, doi:10.1093/mp/sst079 (2013).
16 Martiniere, A. *et al.* In Vivo Intracellular pH Measurements in Tobacco and Arabidopsis Reveal an Unexpected pH Gradient in the Endomembrane System. *Plant Cell* **25,** 4028-4043, doi:10.1105/tpc.113.116897 (2013).
17 Luo, Y. *et al.* V-ATPase activity in the TGN/EE is required for exocytosis and recycling in Arabidopsis. *Nature Plants* **1,** 15094, doi:10.1038/nplants.2015.94 (2015).
18 Niemes, S. *et al.* Retromer recycles vacuolar sorting receptors from the trans-Golgi network. *Plant J.* **61,** 107-121 (2010).
19 Stierhof, Y. D., Viotti, C., Scheuring, D., Sturm, S. & Robinson, D. G. Sorting nexins 1 and 2a locate mainly to the TGN. *Protoplasma* **250,** 235-240, doi:10.1007/s00709-012-0399-1 (2013).
20 Scheuring, D. *et al.* Multivesicular bodies mature from the trans-Golgi network/early endosome in Arabidopsis. *Plant Cell* **23,** 3463-3481, doi:10.1105/tpc.111.086918 (2011).
21 Hamers-Casterman, C. *et al.* Naturally occurring antibodies devoid of light chains. *Nature* **363,** 446-448, doi:10.1038/363446a0 (1993).
22 Rothbauer, U. *et al.* Targeting and tracing antigens in live cells with fluorescent nanobodies. *Nature methods* **3,** 887-889, doi:10.1038/nmeth953 (2006).
23 Kubala, M. H., Kovtun, O., Alexandrov, K. & Collins, B. M. Structural and thermodynamic analysis of the GFP:GFP-nanobody complex. *Protein Sci.* **19,** 2389-2401, doi:10.1002/pro.519 (2010).
24 Bucherl, C. A., Bader, A., Westphal, A. H., Laptenok, S. P. & Borst, J. W. FRET-FLIM applications in plant systems. *Protoplasma* **251,** 383-394, doi:10.1007/s00709-013-0595-7 (2014).
25 Kriechbaumer, V. *et al.* Reticulomics: Protein-protein interaction studies with two plasmodesmata-localised reticulon family proteins identify binding partners enriched at plasmodesmata, ER and the plasma membrane. *Plant Physiol.*, doi:10.1104/pp.15.01153 (2015).
26 Martiniere, A., Desbrosses, G., Sentenac, H. & Paris, N. Development and properties of genetically encoded pH sensors in plants. *Frontiers in plant science* **4,** 523, doi:10.3389/fpls.2013.00523 (2013).

27 Niemes, S. *et al.* Sorting of plant vacuolar proteins is initiated in the ER. *Plant J.* **62,** 601-614 (2010).
28 Nishikawa, S., Hirata, A. & Nakano, A. Inhibition of endoplasmic reticulum (ER)-to-Golgi transport induces relocalization of binding protein (BiP) within the ER to form the BiP bodies. *Mol. Biol. Cell* **5,** 1129-1143 (1994).
29 Tse, Y. C. *et al.* Identification of multivesicular bodies as prevacuolar compartments in Nicotiana tabacum BY-2 cells. *Plant Cell* **16,** 672-693 (2004).
30 Humair, D., Hernandez Felipe, D., Neuhaus, J. M. & Paris, N. Demonstration in yeast of the function of BP-80, a putative plant vacuolar sorting receptor. *Plant Cell* **13,** 781-792 (2001).
31 Runions, J., Brach, T., Kuhner, S. & Hawes, C. Photoactivation of GFP reveals protein dynamics within the endoplasmic reticulum membrane. *J Exp Bot* **57,** 43-50 (2006).
32 daSilva, L. L. *et al.* Receptor salvage from the prevacuolar compartment is essential for efficient vacuolar protein targeting. *Plant Cell* **17,** 132-148 (2005).
33 Pimpl, P. *et al.* Golgi-mediated vacuolar sorting of the endoplasmic reticulum chaperone BiP may play an active role in quality control within the secretory pathway. *Plant Cell* **18,** 198-211 (2006).
34 Scheuring, D. *et al.* Ubiquitin initiates sorting of Golgi and plasma membrane proteins into the vacuolar degradation pathway. *BMC plant biology* **12,** 164-180, doi:10.1186/1471-2229-12-164 (2012).
35 Muyldermans, S. Nanobodies: natural single-domain antibodies. *Annu. Rev. Biochem.* **82,** 775-797, doi:10.1146/annurev-biochem-063011-092449 (2013).
36 Rocchetti, A., Hawes, C. & Kriechbaumer, V. Fluorescent labelling of the actin cytoskeleton in plants using a cameloid antibody. *Plant methods* **10,** 12, doi:10.1186/1746-4811-10-12 (2014).
37 Schornack, S. *et al.* Protein mislocalization in plant cells using a GFP-binding chromobody. *Plant J.* **60,** 744-754, doi:10.1111/j.1365-313X.2009.03982.x (2009).
38 Watanabe, E. *et al.* An ER-Localized Form of PV72, a Seed-Specific Vacuolar Sorting Receptor, Interferes the Transport of an NPIR-Containing Proteinase in Arabidopsis Leaves. *Plant Cell Physiol.* **45,** 9-17 (2004).
39 Hillmer, S., Movafeghi, A., Robinson, D. G. & Hinz, G. Vacuolar storage proteins are sorted in the cis-cisternae of the pea cotyledon Golgi apparatus. *J. Cell Biol.* **152,** 41-50 (2001).
40 Hinz, G., Colanesi, S., Hillmer, S., Rogers, J. C. & Robinson, D. G. Localization of vacuolar transport receptors and cargo proteins in the Golgi apparatus of developing Arabidopsis embryos. *Traffic* **8,** 1452-1464 (2007).
41 Viotti, C. *et al.* Endocytic and Secretory Traffic in Arabidopsis Merge in the Trans-Golgi Network/Early Endosome, an Independent and Highly Dynamic Organelle. *Plant Cell* **22,** 1344-1357 (2010).
42 Wang, H., Zhuang, X., Hillmer, S., Robinson, D. G. & Jiang, L. Vacuolar Sorting Receptor (VSR) Proteins Reach the Plasma Membrane in Germinating Pollen Tubes. *Mol Plant* **4,** 845-853 (2011).
43 Schmitt, F. J. *et al.* eGFP-pHsens as a highly sensitive fluorophore for cellular pH determination by fluorescence lifetime imaging microscopy (FLIM). *Biochim. Biophys. Acta* **1837,** 1581-1593, doi:10.1016/j.bbabio.2014.04.003 (2014).

44 Watanabe, E., Shimada, T., Kuroyanagi, M., Nishimura, M. & Hara-Nishimura, I. Calcium-mediated association of a putative vacuolar sorting receptor PV72 with a propeptide of 2S albumin. *J. Biol. Chem.* **277,** 8708-8715 (2002).
45 Stael, S. *et al.* Plant organellar calcium signalling: an emerging field. *J Exp Bot* **63,** 1525-1542, doi:10.1093/jxb/err394 (2012).
46 Ordenes, V. R. *et al.* In vivo analysis of the calcium signature in the plant Golgi apparatus reveals unique dynamics. *Cell Calcium* **52,** 397-404, doi:10.1016/j.ceca.2012.06.008 (2012).
47 Etxeberria, E., Gonzalez, P., Baroja-Fernandez, E. & Romero, J. P. Fluid phase endocytic uptake of artificial nano-spheres and fluorescent quantum dots by sycamore cultured cells: evidence for the distribution of solutes to different intracellular compartments. *Plant Signal Behav* **1,** 196-200 (2006).
48 Phillipson, B. A. *et al.* Secretory bulk flow of soluble proteins is efficient and COPII dependent. *Plant Cell* **13,** 2005-2020 (2001).
49 Bubeck, J. *et al.* The syntaxins SYP31 and SYP81 control ER-Golgi trafficking in the plant secretory pathway. *Traffic* **9,** 1629-1652 (2008).
50 Pimpl, P., Hanton, S. L., Taylor, J. P., Pinto-DaSilva, L. L. & Denecke, J. The GTPase ARF1p Controls the Sequence-Specific Vacuolar Sorting Route to the Lytic Vacuole. *Plant Cell* **15,** 1242-1256 (2003).

Acknowledgments

We thank Sébastien Peter (Institute of Physical and Theoretical Chemistry, University of Tübingen) for technical support and helpful discussions on FRET-FLIM. We would like to thank Diana Vranjkovic and Natalie Gerling for technical help. The financial support of the Deutsche Forschungsgemeinschaft (PI 769/1-2 and the Collaborative Research Centre SFB 1101 “Molecular Encoding of Specificity in Plant Processes” and TPA03) and the Deutscher Akademischer Austauschdienst (Project 57057314) is gratefully acknowledged.

Author contributions

F.K., F.F., S.F and P.P. designed and analysed the experiments. F.K., S.F., F.F. and B.L. performed experiments. F.K. and P.P. wrote the manuscript.

Additional information

Correspondence and requests for materials should be addressed to P.P.

Competing interests

The authors declare no competing financial interests.

Figure Legends and Tables

Figure 1. Compartment-specific targeting of luminal ligand-binding domains (LBDs) in the plant endomembrane system via nanobody-epitope interactions. (**a**) Nanobody (Nb)-mediated sensor assembly by coexpression of soluble LBD-RFP-Nb with luminal GFP-epitope-exposing type I/II membrane proteins. (**b**) Immunodetection of LBD-RFP-NB ± Sec12 overproduction in cells/medium (C)/(M) using α-HA. Loading control: coexpressed Golgi marker ERD2-CFP (α-GFP), mock-transfection (co). (**c**,**d**) CLSM analysis of cells from (**b**). Soluble/secreted LBD-RFP-Nb accumulates with ERD2-CFP in the ER upon Sec12 overproduction (+Sec12). (**e**-**i**) Sensor assembly by coexpression of LBD-RFP-Nb with the epitope-tagged anchors (**e**) GFP-CNX (type I) in the ER, (**f**) Man1-GFP (type II) in the Golgi, (**g**) SYP61-GFP (type II) in the TGN/EE, (**h**,**i)** GFP-BP80 (type I) in the MVB/LE, and (**i**) in wortmannin-induced (+WM, 30 µM, 1 h) ring-like MVB/LE structures (arrowheads). Inlays: **c**,**f**-**i** magnifications; **d**,**e** cortical sections. Scale bars (µm): 5/2.5 (inlays).

Figure 2. All assembled VSR sensors are ligand-binding competent. (**a**) Principle of compartment-specific VSR-ligand interaction-analysis via FRET-FLIM. Expression of GFP-tagged membrane anchors with soluble LBD-Nbs reconstitutes fluorescent VSR sensors. Binding of red-fluorescent ligands (Aleu-RFP) leads to close proximity and thus FRET, thereby shortening the fluorescence lifetime of GFP. (**b**) Immunoblot revealing ligand-binding capability of all VSR sensors *in vitro*. Sensors were assembled by coexpression of LBD-Nb with either GFP-CNX, Man1-GFP, SYP61-GFP, or GFP-BP80 in tobacco protoplasts, immunoprecipitated (anti-GFP antibody-coated beads, IP: α-GFP), and incubated with Aleu-RFP. Immunoblots (IB) were probed with antibodies to detect anchors (α-GFP), LBD-Nb (α-HA) and Aleu-RFP/Sec-RFP (α-RFP).

Figure 3. Analysis of VSR-ligand interaction identifies the ER as compartment that favours ligand binding whilst the MVB/LE restricts ligand binding.

(**a,b**) Assembly of ER-localising VSR sensors from GFP-CNX+LBD-Nb retains coexpressed vacuolar Aleu-RFP in the ER. (**c**) FRET-FLIM reveals Aleu-RFP-

triggered FRET/reduced fluorescence lifetime compared to controls expressing RFP-HDEL, Sec-RFP, or ΔLBD-Nb. (**d,e**) Coexpressed Aleu-RFP and GFP-BP80 colocalise in MVBs/LEs also upon sensor assembly (GFP-BP80+LBD-Nb). (**f**) FRET-FLIM revealing that Aleu-RFP doesn't trigger FRET/reduce fluorescence lifetime of MVB/LE-localising sensors compared to controls with Nb-mediated attachment of RFP (LBD-RFP-Nb, see Fig. 1). (**g**) Differential distribution of GFP-BP80 and Aleu-RFP in wortmannin-induced ring-like MVB/LE-structures (30 µM, 1 h) is not altered by sensor assembly (+LBD-Nb). FLIM data are presented as mean ± s.e.m. fluorescence lifetime of *n*=12/17 (**c**/**f**) measurements. Significance was calculated using ANOVA, followed by Tukey's HSD test (*** $P<0.001$ compared to every other group; NS, not significant). Images (right) showing fluorescence intensity/lifetime of sensors. Scale bars (µm): 5/2.5 (inlays). Inlays: **a**,**b**, cortical section; **d**,**e**: magnifications.

Figure 4. The Golgi provides ligand-binding conditions for VSRs. (**a**) Coexpressed *cis*-Golgi marker Man1-GFP and the soluble vacuolar reporter Aleu-RFP don't colocalise. (**b**) Assembly of Golgi-localised VSR sensors from Man1-GFP+LBD-Nb retains Aleu-RFP in the Golgi (arrowheads). (**c**) Golgi retention is highlighted by reduction of Aleu-RFP signals in MVBs/LEs and vacuoles by coexpression of the VSR-transport competitor HA-BP80. (**d**) FRET-FLIM analysis identifies the Golgi as compartment favouring ligand binding. Coexpression of Aleu-RFP causes FRET-triggered decrease of fluorescence lifetime of the sensor, which doesn't occur in the absence of the LBD (ΔLBD-Nb). (**e**) VSR sensor assembly in the *trans*-Golgi by coexpression of LBD-RFP-Nb with the marker ST-GFP. (**f**,**g**) Golgi retention of Aleu-RFP caused by assembly of VSR sensors from ST-GFP+LBD-Nb. (**h**) FRET-FLIM analysis demonstrates ligand binding in the *trans*-Golgi. Golgi movement was reduced by application of 4 µm LatB 1 h prior to FLIM. Data are presented/calculated as in Fig. 3, *n*=12 measurements. Scale bars (µm): 5/2.5 (inlays). Inlays: magnifications.

Figure 5. The TGN/EE does not provide ligand-binding conditions for VSRs. (**a**,**b**) Aleu-RFP doesn't colocalise with the TGN/EE marker SYP61-GFPand is not retained upon sensor assembly (SYP61-GFP+LBD-Nb). Inlays: magnification. (**c**) Pearson's (r_P) and Spearman's (r_S) correlation (PSC) coefficients of SYP61-

GFP/Aleu-RFP signals from **a**,**b**, with colocalising SYP61-GFP/LBD-RFP-Nb (see Fig. 1g) for comparison. Statistical analysis/annotations as in Fig. 3, *n*=10 cells, *** *P*<0.001. (**d**) Aleu-RFP doesn't trigger FRET/reduce fluorescence lifetime of TGN/EE-localising sensors (identical to Sec-RFP in negative controls). FRET is triggered in positive controls by attachment of RFP (LBD-RFP-Nb, see Fig. 1). (**e**) BFA-induced ER coaccumulation of sensors (SYP61-GFP+LBD-Nb) and Aleu-RFP (+BFA). Inlay: cortical section. (**f**) Coexpression of SYP61-GFP-based sensors with Aleu-RFP or Sec-RFP ±BFA. Aleu-RFP triggers FRET/reduces fluorescence lifetime only in the presence of BFA due to redistribution of sensors/ligands to the binding-favouring ER. Data in **d**,**f** are presented/calculated as in Fig. 3, *n*=17/20 (**d**/**f**) measurements. TGN/EE movement was reduced by application of 4 µm LatB 1 h prior to FLIM. (**g**) Proteins were expressed as indicated (± BFA), sensors were immunoprecipitated (anti-GFP antibody-coated beads, IP: α-GFP), and immunoblotted (IB). Total extracts (T) and immunoprecipitates (IP) were probed with α-GFP (Anchor), α-HA (LBD-Nb), and α-RFP (Aleu-RFP/Sec-RFP), revealing ligand binding of SYP61-GFP-based sensors in the ER (+BFA, black arrowhead) but not in the TGN/EE (-BFA, white arrowhead). For **e**-**g**, BFA (36 µM) was applied after transfection. Scale bars (µm): 5/2.5 (inlays).

Figure 6. Vacuolar delivery of endocytosed soluble proteins does not depend on sorting signals. (**a**) Endocytic uptake and vacuolar delivery of 3xRFP by Cyt-GFP-expressing protoplasts. (**b**) Immunoblot of cellular extracts after uptake of 3xRFP, osmotic shock (total proteins, T), and fractionation into membrane (M) and soluble (S) fractions identify endocytosed 3xRFP as soluble protein (left). Cells expressing the plasma membrane marker RFP-TMD23 served as fractionation control (right). (**c**) Endocytic uptake and vacuolar delivery of nanobody-tagged reporter 3xRFP-Nb (compare to **a**). (**d**-**f**) Mapping of the transport route to the vacuole by nanobody-mediated anchoring of endocytosed 3xRFP-Nb in the TGN/EE and MVB/LE. Incubation of cells exposing GFP at (**d**) the surface (SYP132-GFP), (**e**) the TGN/EE (SYP61-GFP) or (**f**) the MVB/LE (GFP-BP80) with 3xRFP-Nb leads to accumulation of the reporter at the corresponding locations, demonstrating that endocytosed non-VSR-ligand 3xRFP-Nb transits the TGN/EE and MVB/LE *en route* to the vacuole. Inlays:

magnifications. Scale bars (µm): 5/2.5 (inlays). (**g**) Concept of sorting and transport of soluble vacuolar proteins. The ER and the Golgi provide binding conditions (green) for VSR-ligand interaction, while the *post*-Golgi compartments TGN/EE and MVB/LE do not (red).

Supplementary Figure 1. Uncropped immunoblot. Detection of the immunoprecipitated compartmental markers GFP-CNX, Man1-GFP, SYP61-GFP, and GFP-BP80 as illustrated in Figure 2b. Concentration series (c1-c3) were loaded in SDS-PAGE to equalise the amounts of markers for the detection of the coexpressed/coimmunoprecipitated LBD-Nb. Sections cut for Figure 2b are highlighted by black rectangles. The Immunoblot (IB) was probed with α-GFP.

Supplementary Figure 2. The assembly of VSR sensors does not influence the localisation of the membrane anchors. Protoplasts were transfected with plasmids encoding for the indicated proteins and incubated 24 h before CLSM analysis. (**a**-**d**) Sensors were assembled from LBD-Nb and the GFP-tagged membrane anchors and localisation was compared to RFP-tagged derivatives of the respective compartmental marker. (**a**) Colocalisation with RFP-CNX in the ER, (**b**) colocalisation with Man1-RFP in the Golgi, (**c**) colocalisation with RFP-SYP61 in the TGN/EE, and (**d**) colocalisation with RFP-BP80 in the MVB/LE. Inlays in **a**-**d**: magnifications. Scale bars (µm): 5/2.5 µm (inlays). (**e**) Pearson's (r_P) and Spearman's (r_S) correlation (PSC) coefficients calculated for green and red signals as shown in **a**-**d** demonstrating colocalisation. PSC coefficients are presented as mean ± s.e.m (n = 10 individual cells). Statistical significance was calculated using ANOVA, followed by Tukey's HSD test (*** $P < 0.001$).

Supplementary Figure 3. Representative CLSM images of cells analysed by FRET-FLIM to asses VSR-ligand binding in the ER and the MVB/LE. (**a**) FLIM data for the ER. The diagram shows the fluorescence lifetimes from Figure 3c plus additional controls analysed 6 h after application of 36 µM BFA. The different experimental groups are represented by Latin numbers (I-VI). A representative image is given for each group ensuring expression of tested fluorescent pairs. (**b**) FLIM data for the MVB/LE. The diagram shows the fluorescence lifetimes from Figure 3f. The different experimental groups are represented by Latin numbers (I-

IV). A representative image is given for each group ensuring expression of tested fluorescent pairs. Scale bars: 5 µm. Statistics: *** *P*<0.001; NS, not significant.

Supplementary Figure 4. Representative CLSM images of cells analysed by FRET-FLIM to asses VSR-ligand binding in the Golgi. (**a**) FLIM data for the *cis*-Golgi. The diagram shows the fluorescence lifetimes from Figure 4d. The different experimental groups are represented by Latin numbers (I-IV). A representative image is given for each group ensuring expression of tested fluorescent pairs. (**b**) FLIM data for the *trans*-Golgi. The diagram shows the fluorescence lifetimes from Figure 4h. The different experimental groups are represented by Latin numbers (I-IV). A representative image is given for each group ensuring expression of tested fluorescent pairs. Scale bars: 5 µm. Statistics: *** *P*<0.001; NS, not significant.

Supplementary Figure 5. Representative CLSM images of cells analysed by FRET-FLIM to asses VSR-ligand binding in the TGN/EE. (**a**) The diagram shows the fluorescence lifetimes from Figure 5d,f (± BFA) in direct comparison. The different experimental groups are represented by Latin numbers (I-IV). A representative image is given for each group ensuring expression of tested fluorescent pairs. Scale bars: 5 µm. Statistics: *** *P*<0.001; NS, not significant.

Figure 1

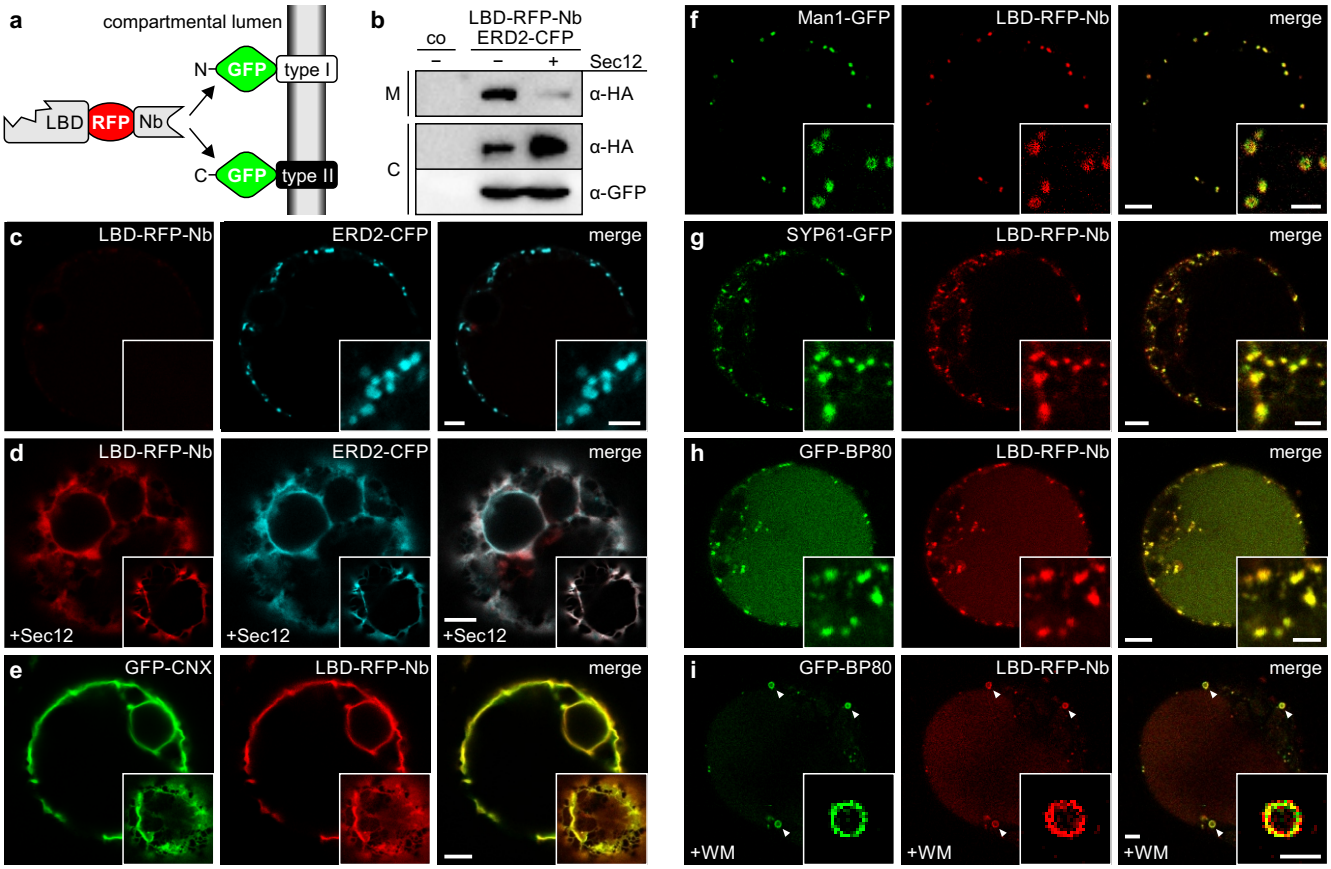

Figure 1. Compartment-specific targeting of luminal ligand-binding domains (LBDs) in the plant endomembrane system via nanobody-epitope interactions. (**a**) Nanobody (Nb)-mediated sensor assembly by coexpression of soluble LBD-RFP-Nb with luminal GFP-epitope-exposing type I/II membrane proteins. (**b**) Immunodetection of LBD-RFP-NB ± Sec12 overproduction in cells/medium (C)/(M) using α-HA. Loading control: coexpressed Golgi marker ERD2-CFP (α-GFP), mock-transfection (co). (**c**,**d**) CLSM analysis of cells from (**b**). Soluble/secreted LBD-RFP-Nb accumulates with ERD2-CFP in the ER upon Sec12 overproduction (+Sec12). (**e-i**) Sensor assembly by coexpression of LBD-RFP-Nb with the epitope-tagged anchors (**e**) GFP-CNX (type I) in the ER, (**f**) Man1-GFP (type II) in the Golgi, (**g**) SYP61-GFP (type II) in the TGN/EE, (**h**,**i**) GFP-BP80 (type I) in the MVB/LE, and (**i**) in wortmannin-induced (+WM, 30 µM, 1 h) ring-like MVB/LE structures (arrowheads). Inlays: **c**,**f-i** magnifications; **d**,**e** cortical sections. Scale bars (µm): 5/2.5 (inlays).

Figure 2

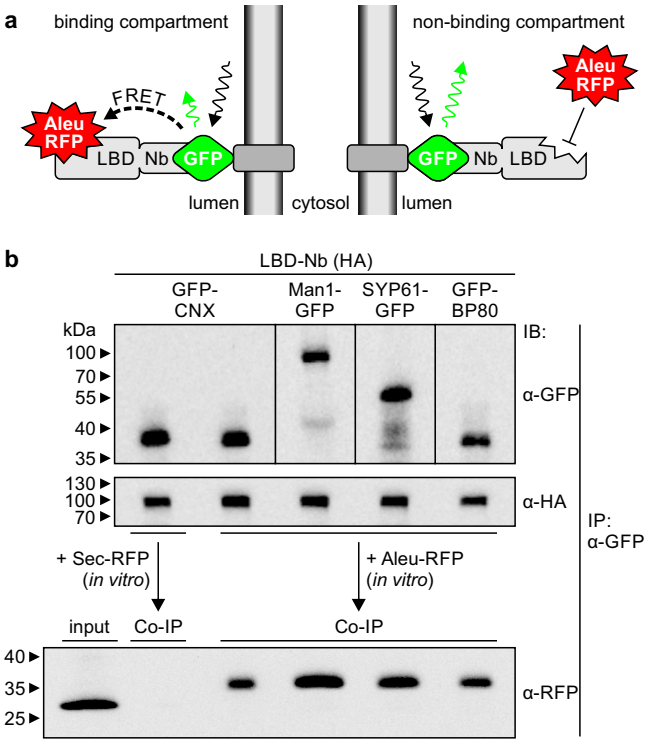

Figure 2. All assembled VSR sensors are ligand-binding competent. (**a**) Principle of compartment-specific VSR-ligand interaction-analysis via FRET-FLIM. Expression of GFP-tagged membrane anchors with soluble LBD-Nbs reconstitutes fluorescent VSR sensors. Binding of red-fluorescent ligands (Aleu-RFP) leads to close proximity and thus FRET, thereby shortening the fluorescence lifetime of GFP. (**b**) Immunoblot revealing ligand-binding capability of all VSR sensors *in vitro*. Sensors were assembled by coexpression of LBD-Nb with either GFP-CNX, Man1-GFP, SYP61-GFP, or GFP-BP80 in tobacco protoplasts, immunoprecipitated (anti-GFP antibody-coated beads, IP: α-GFP), and incubated with Aleu-RFP. Immunoblots (IB) were probed with antibodies to detect anchors (α-GFP), LBD-Nb (α-HA) and Aleu-RFP/Sec-RFP (α-RFP).

Figure 3

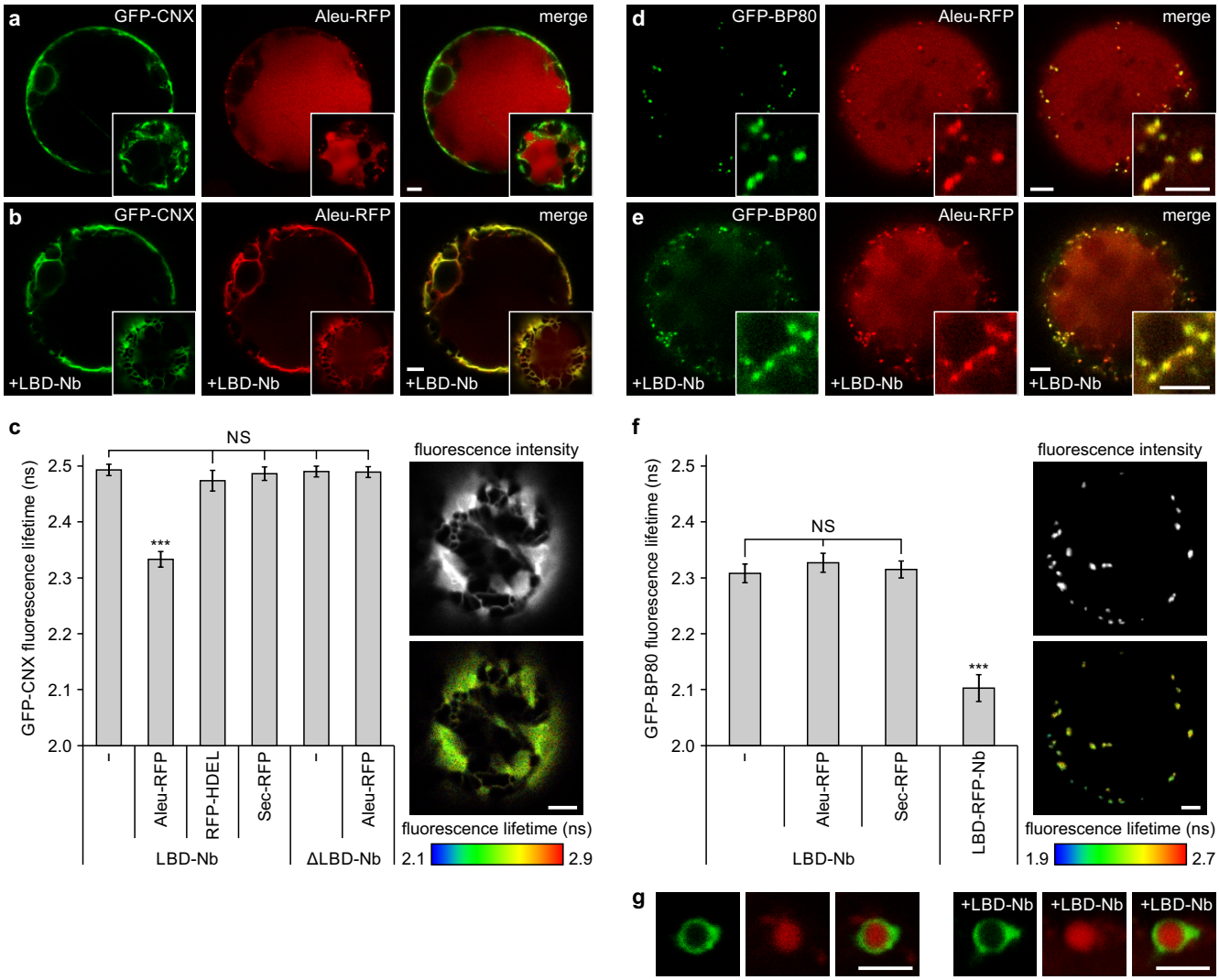

Figure 3. Analysis of VSR-ligand interaction identifies the ER as compartment that favours ligand binding whilst the MVB/LE restricts ligand binding. (**a**,**b**) Assembly of ER-localising VSR sensors from GFP-CNX+LBD-Nb retains coexpressed vacuolar Aleu-RFP in the ER. (**c**) FRET-FLIM reveals Aleu-RFP-triggered FRET/reduced fluorescence lifetime compared to controls expressing RFP-HDEL, Sec-RFP, or ΔLBD-Nb. (**d**,**e**) Coexpressed Aleu-RFP and GFP-BP80 colocalise in MVBs/LEs also upon sensor assembly (GFP-BP80+LBD-Nb). (**f**) FRET-FLIM revealing that Aleu-RFP doesn't trigger FRET/reduce fluorescence lifetime of MVB/LE-localising sensors compared to controls with Nb-mediated attachment of RFP (LBD-RFP-Nb, see Fig. 1). (**g**) Differential distribution of GFP-BP80 and Aleu-RFP in wortmannin-induced ring-like MVB/LE-structures (30 µM, 1 h) is not altered by sensor assembly (+LBD-Nb). FLIM data are presented as mean ± s.e.m. fluorescence lifetime of *n*=12/17 (**c**/**f**) measurements. Significance was calculated using ANOVA, followed by Tukey's HSD test (*** *P*<0.001 compared to every other group; NS, not significant). Images (right) showing fluorescence intensity/lifetime of sensors. Scale bars (µm): 5/2.5 (inlays). Inlays: **a**,**b**, cortical section; **d**,**e**: magnifications.

Figure 4

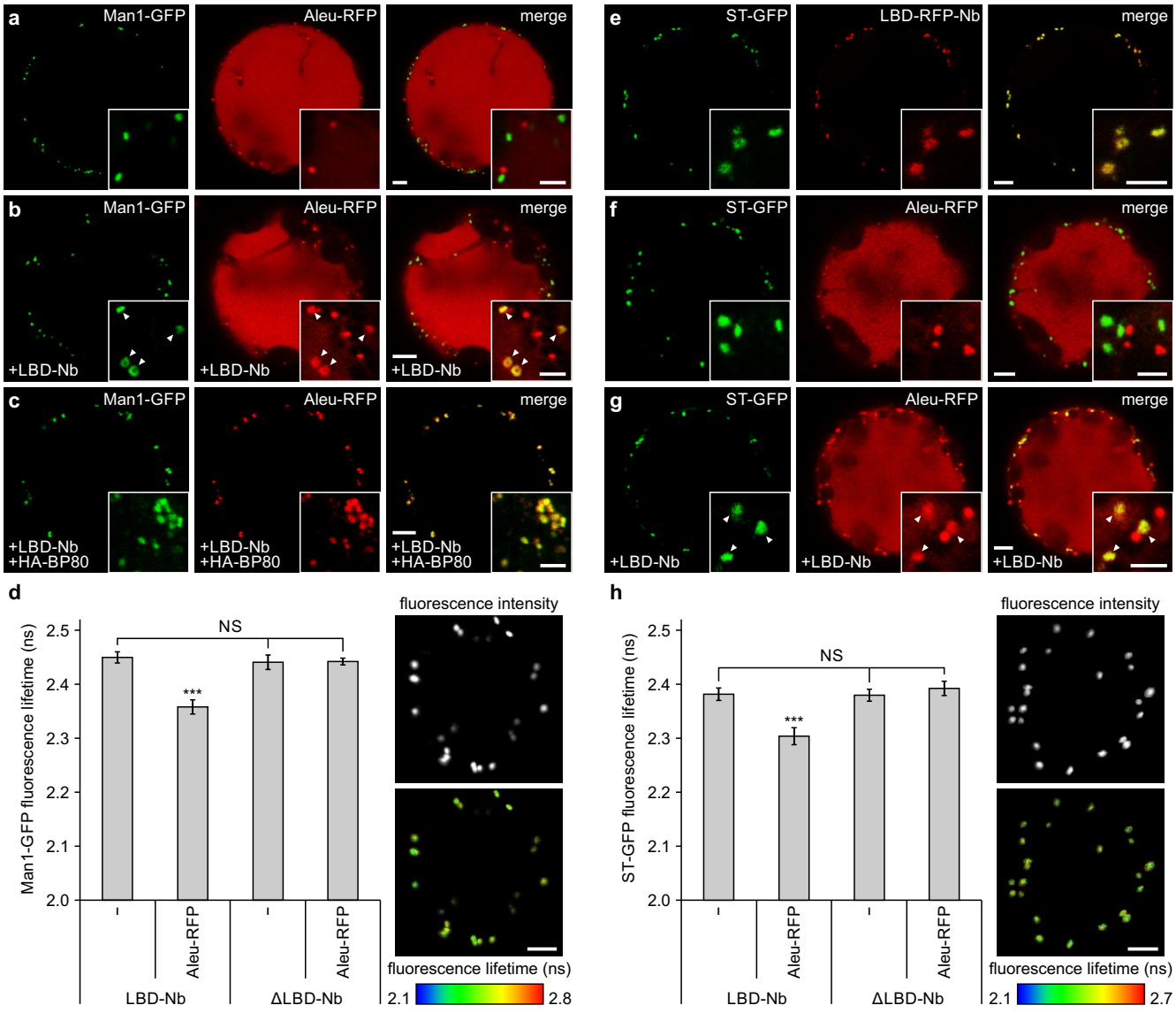

Figure 4. The Golgi provides ligand-binding conditions for VSRs. (**a**) Coexpressed *cis*-Golgi marker Man1-GFP and the soluble vacuolar reporter Aleu-RFP don't colocalise. (**b**) Assembly of Golgi-localised VSR sensors from Man1-GFP+LBD-Nb retains Aleu-RFP in the Golgi (arrowheads). (**c**) Golgi retention is highlighted by reduction of Aleu-RFP signals in MVBs/LEs and vacuoles by coexpression of the VSR-transport competitor HA-BP80. (**d**) FRET-FLIM analysis identifies the Golgi as compartment favouring ligand binding. Coexpression of Aleu-RFP causes FRET-triggered decrease of fluorescence lifetime of the sensor, which doesn't occur in the absence of the LBD (ΔLBD-Nb). (**e**) VSR sensor assembly in the *trans*-Golgi by coexpression of LBD-RFP-Nb with the marker ST-GFP. (**f**,**g**) Golgi retention of Aleu-RFP caused by assembly of VSR sensors from ST-GFP+LBD-Nb. (**h**) FRET-FLIM analysis demonstrates ligand binding in the *trans*-Golgi. Golgi movement was reduced by application of 4 µm latrunculin B 1 h prior to FLIM. Data are presented/calculated as in Fig. 3, *n*=12 measurements. Scale bars (µm): 5/2.5 (inlays). Inlays: magnifications.

Figure 5

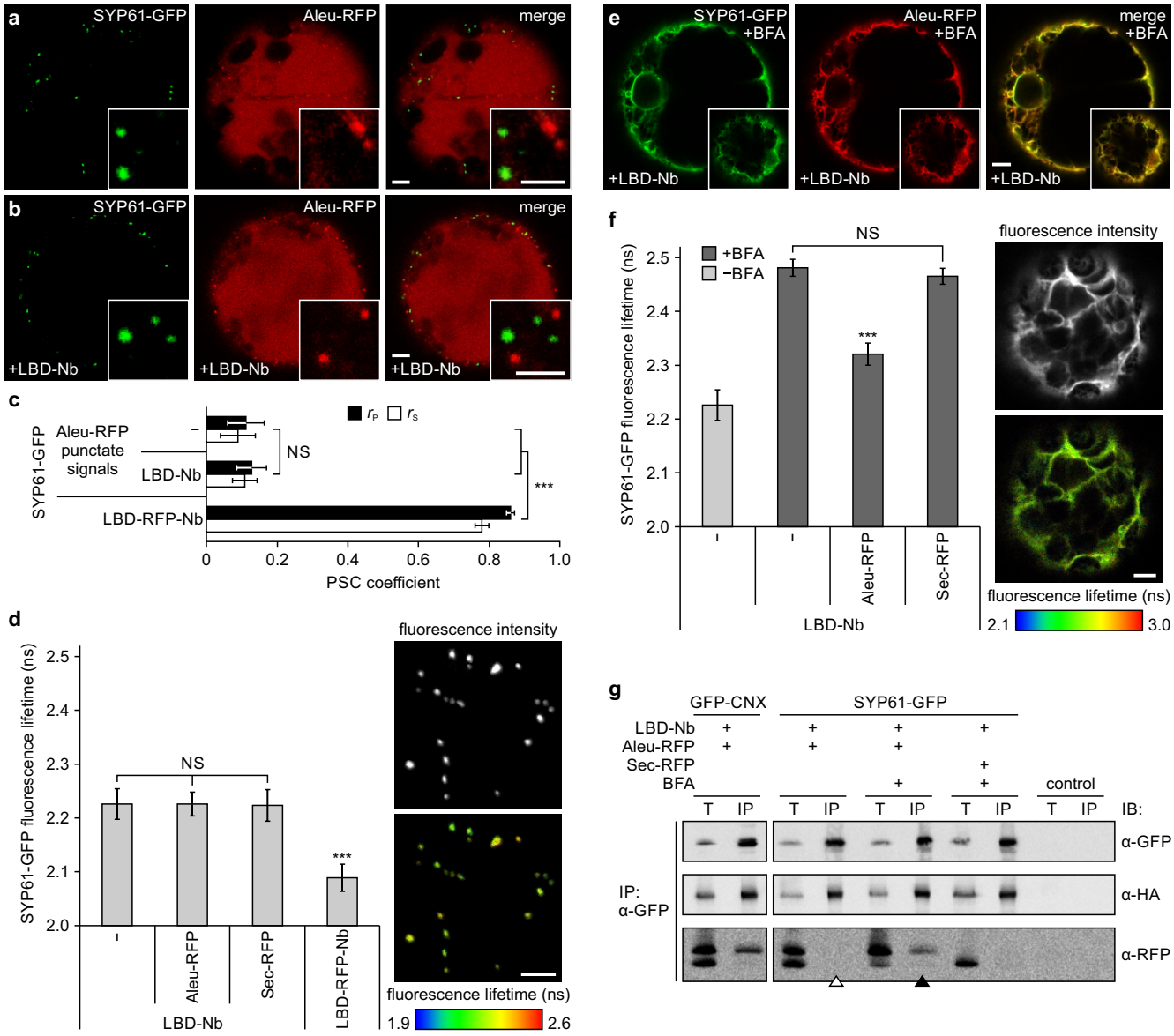

Figure 5. The TGN/EE does not provide ligand-binding conditions for VSRs. (**a**,**b**) Aleu-RFP doesn't colocalise with the TGN/EE marker SYP61-GFPand is not retained upon sensor assembly (SYP61-GFP+LBD-Nb). Inlays: magnification. (**c**) Pearson's (r_P) and Spearman's (r_S) correlation (PSC) coefficients of SYP61-GFP/Aleu-RFP signals from **a**,**b**, with colocalising SYP61-GFP/LBD-RFP-Nb (see Fig. 1g) for comparison. Statistical analysis/annotations as in Fig. 3, n=10 cells, *** P<0.001. (**d**) Aleu-RFP doesn't trigger FRET/reduce fluorescence lifetime of TGN/EE-localising sensors (identical to Sec-RFP in negative controls). FRET is triggered in positive controls by attachment of RFP (LBD-RFP-Nb, see Fig. 1). (**e**) BFA-induced ER coaccumulation of sensors (SYP61-GFP+LBD-Nb) and Aleu-RFP (+BFA). Inlay: cortical section. (**f**) Coexpression of SYP61-GFP-based sensors with Aleu-RFP or Sec-RFP ±BFA. Aleu-RFP triggers FRET/reduces fluorescence lifetime only in the presence of BFA due to redistribution of sensors/ligands to the binding-favouring ER. Data in **d**,**f** are presented/calculated as in Fig. 3, n=17/20 (**d**/**f**) measurements. TGN/EE movement was reduced by application of 4 µm latrunculin B 1 h prior to FLIM. (**g**) Proteins were expressed as indicated (± BFA), sensors were immunoprecipitated (anti-GFP antibody-coated beads, IP: α-GFP), and immunoblotted (IB). Total extracts (T) and immunoprecipitates (IP) were probed with α-GFP (Anchor), α-HA (LBD-Nb), and α-RFP (Aleu-RFP/Sec-RFP), revealing ligand binding of SYP61-GFP-based sensors in the ER (+BFA, black arrowhead) but not in the TGN/EE (-BFA, white arrowhead). For **e**-**g**, BFA (36 µM) was applied after transfection. Scale bars

Figure 6

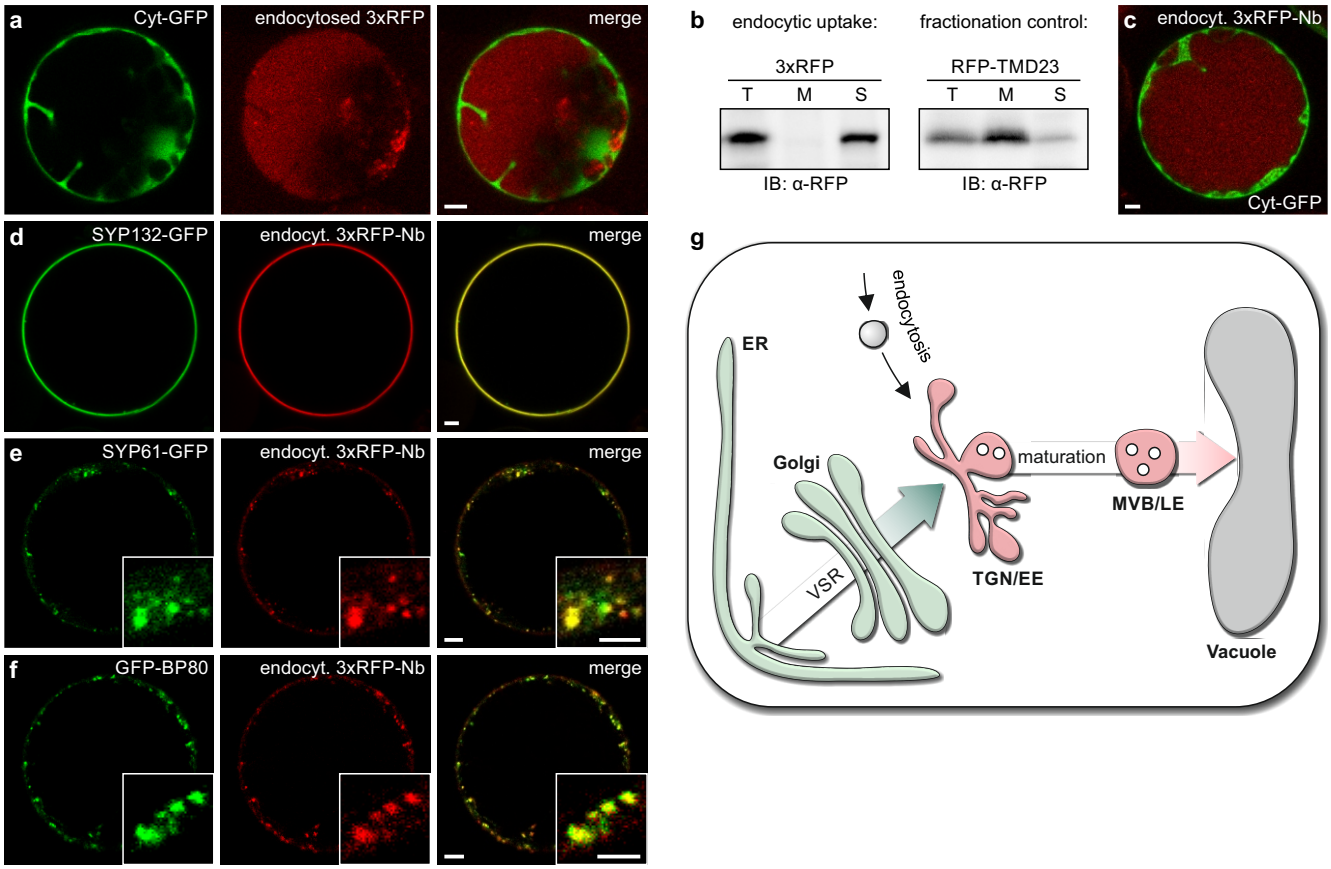

Figure 6. Vacuolar delivery of endocytosed soluble proteins does not depend on sorting signals. (**a**) Endocytic uptake and vacuolar delivery of 3xRFP by Cyt-GFP-expressing protoplasts. (**b**) Immunoblot of cellular extracts after uptake of 3xRFP, osmotic shock (total proteins, T), and fractionation into membrane (M) and soluble (S) fractions identify endocytosed 3xRFP as soluble protein (left). Cells expressing the plasma membrane marker RFP-TMD23 served as fractionation control (right). (**c**) Endocytic uptake and vacuolar delivery of nanobody-tagged reporter 3xRFP-Nb (compare to **a**). (**d**-**f**) Mapping of the transport route to the vacuole by nanobody-mediated anchoring of endocytosed 3xRFP-Nb in the TGN/EE and MVB/LE. Incubation of cells exposing GFP at (**d**) the surface (SYP132-GFP), (**e**) the TGN/EE (SYP61-GFP) or (**f**) the MVB/LE (GFP-BP80) with 3xRFP-Nb leads to accumulation of the reporter at the corresponding locations, demonstrating that endocytosed non-VSR-ligand 3xRFP-Nb transits the TGN/EE and MVB/LE *en route* to the vacuole. Inlays: magnifications. Scale bars (µm): 5/2.5 (inlays). (**g**) Concept of sorting and transport of soluble vacuolar proteins. The ER and the Golgi provide binding conditions (green) for VSR-ligand interaction, while the *post*-Golgi compartments TGN/EE and MVB/LE do not (red).

Supplementary Figure 1

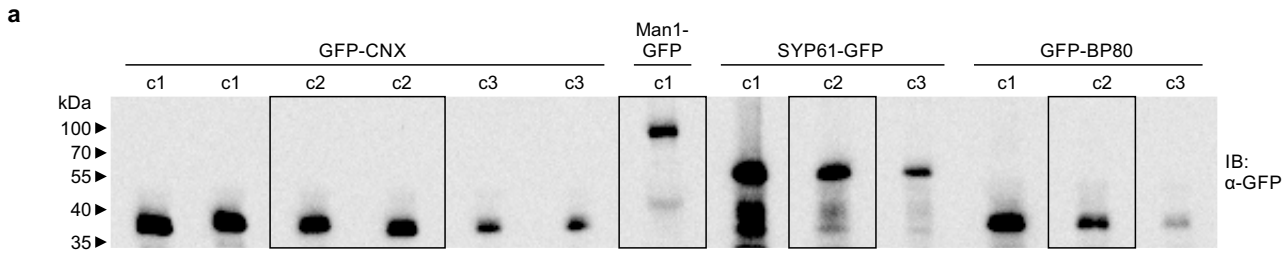

Supplementary Figure 1. Uncropped immunoblot. Detection of the immunoprecipitated compartmental markers GFP-CNX, Man1-GFP, SYP61-GFP, and GFP-BP80 as illustrated in Figure 2b. Concentration series (c1-c3) were loaded in SDS-PAGE to equalise the amounts of markers for the detection of the coexpressed/coimmunoprecipitated LBD-Nb. Sections cut for Figure 2b are highlighted by black rectangles. The Immunoblot (IB) was probed with α-GFP.

Supplementary Figure 2

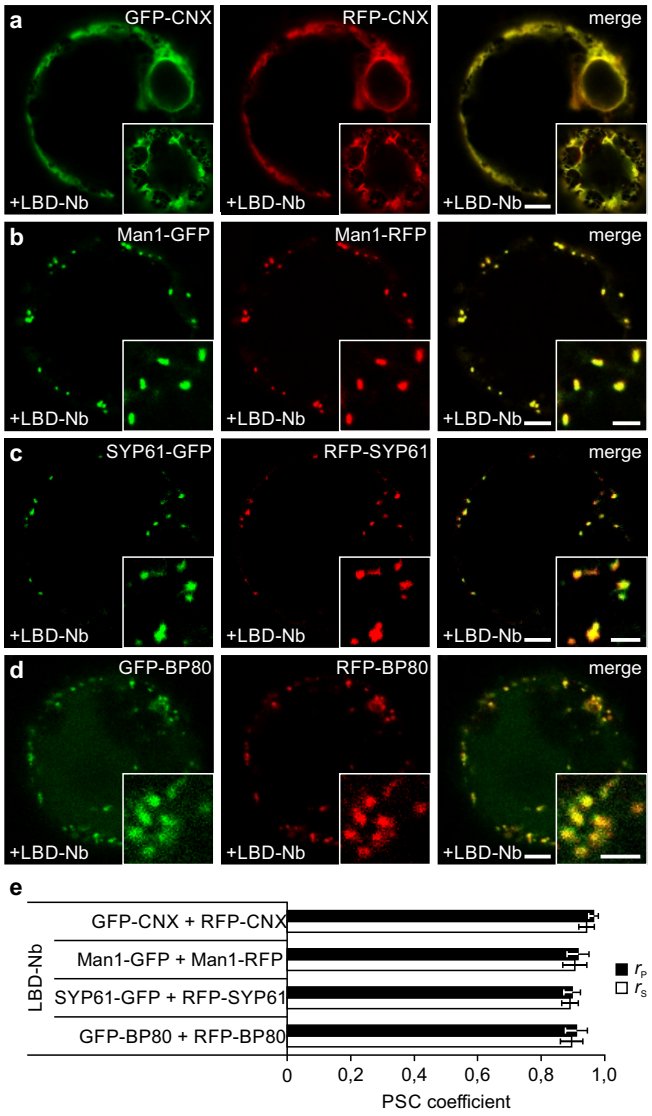

Supplementary Figure 2. The assembly of VSR sensors does not influence the localisation of the membrane anchors. Protoplasts were transfected with plasmids encoding for the indicated proteins and incubated 24 h before CLSM analysis. (**a**-**d**) Sensors were assembled from LBD-Nb and the GFP-tagged membrane anchors and localisation was compared to RFP-tagged derivatives of the respective compartmental marker. (**a**) Colocalisation with RFP-CNX in the ER, (**b**) colocalisation with Man1-RFP in the Golgi, (**c**) colocalisation with RFP-SYP61 in the TGN/EE, and (**d**) colocalisation with RFP-BP80 in the MVB/LE. Inlays in **a**-**d**: magnifications. Scale bars (µm): 5/2.5 µm (inlays). (**e**) Pearson's (r_P) and Spearman's (r_S) correlation (PSC) coefficients calculated for green and red signals as shown in **a**-**d** demonstrating colocalisation. PSC coefficients are presented as mean ± s.e.m (n = 10 individual cells). Statistical significance was calculated using ANOVA, followed by Tukey's HSD test (***

Supplementary Figure 3

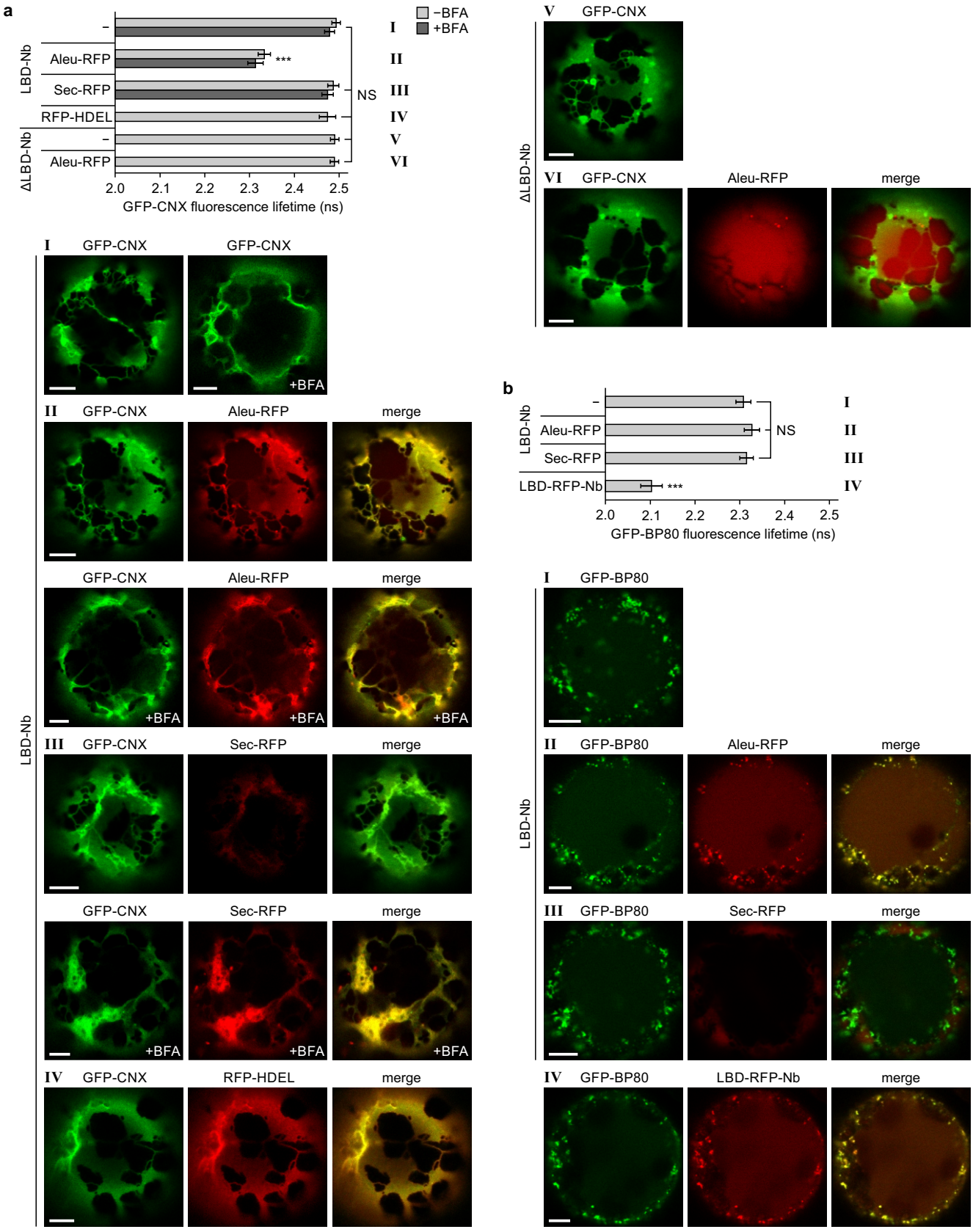

Supplementary Figure 3. Representative CLSM images of cells analysed by FRET-FLIM to assess VSR-ligand binding in the ER and the MVB/LE. (**a**) FLIM data for the ER. The diagram shows the fluorescence lifetimes from Figure 3c plus additional controls analysed 6 h after application of 36 µM BFA. The different experimental groups are represented by Latin numbers (I-VI). A representative image is given for each group ensuring expression of tested fluorescent pairs. (**b**) FLIM data for the MVB/LE. The diagram shows the fluorescence lifetimes from Figure 3f. The different experimental groups are represented by Latin numbers (I-IV). A representative image is given for each group ensuring expression of tested fluorescent pairs. Scale bars: 5 µm. Statistics: *** P<0.001; NS, not significant.

Supplementary Figure 4

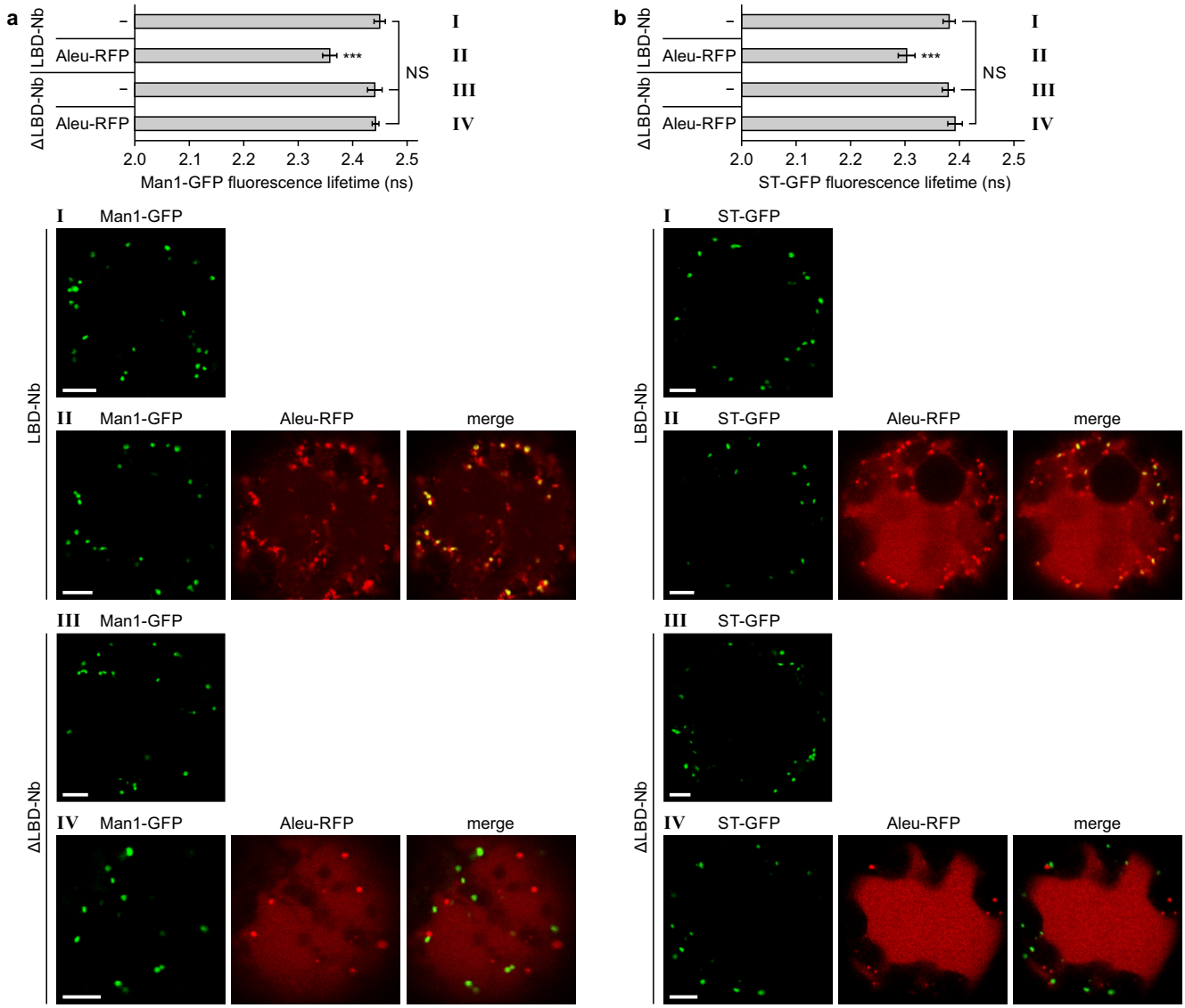

Supplementary Figure 4. Representative CLSM images of cells analysed by FRET-FLIM to assess VSR-ligand binding in the Golgi. (**a**) FLIM data for the *cis*-Golgi. The diagram shows the fluorescence lifetimes from Figure 4d. The different experimental groups are represented by Latin numbers (I-IV). A representative image is given for each group ensuring expression of tested fluorescent pairs. (**b**) FLIM data for the *trans*-Golgi. The diagram shows the fluorescence lifetimes from Figure 4h. The different experimental groups are represented by Latin numbers (I-IV). A representative image is given for each group ensuring expression of tested fluorescent pairs. Scale bars: 5 µm. Statistics: *** $P<0.001$; NS, not significant.

Supplementary Figure 5

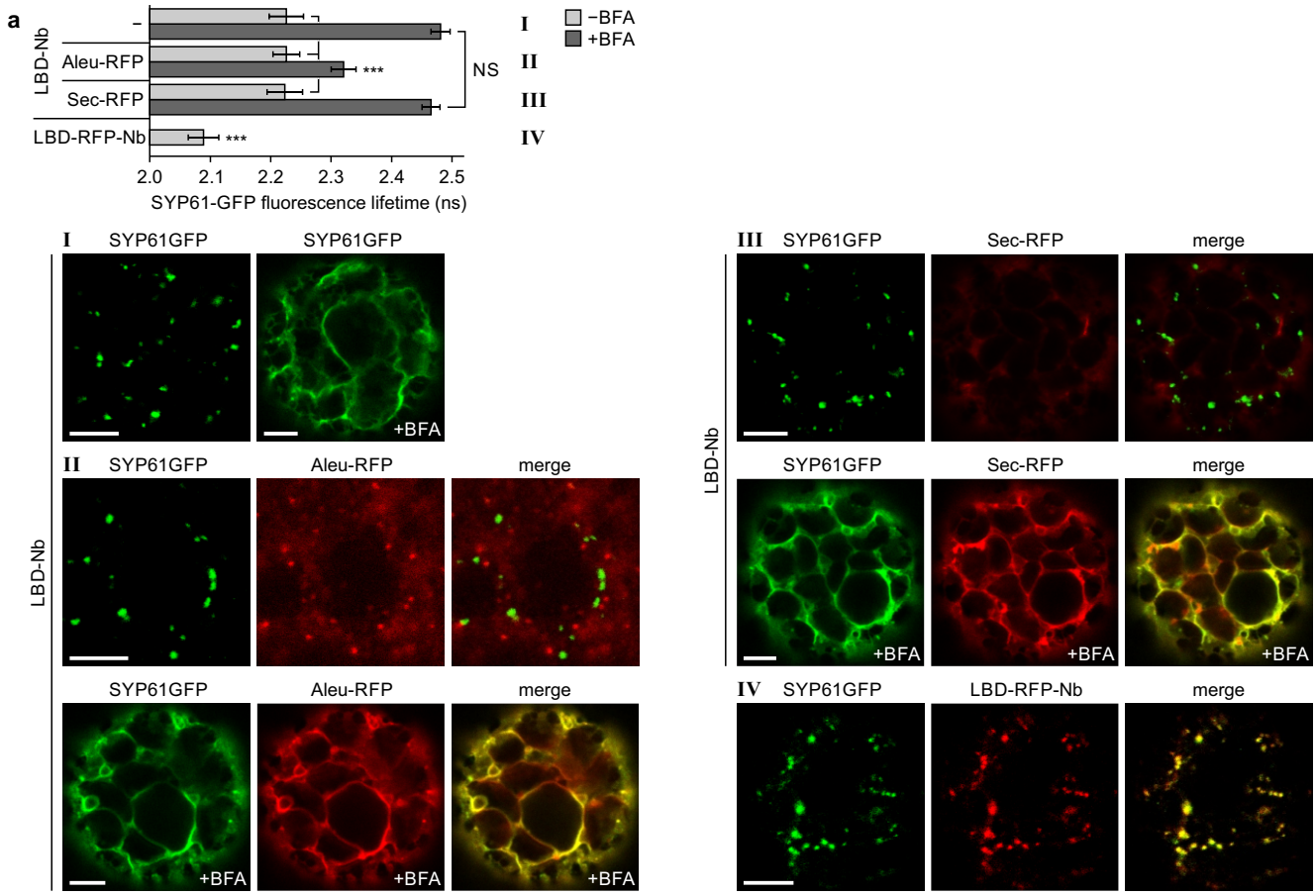

Supplementary Figure 5. Representative CLSM images of cells analysed by FRET-FLIM to assess VSR-ligand binding in the TGN/EE. (**a**) The diagram shows the fluorescence lifetimes from Figure 5d,f (± BFA) in direct comparison. The different experimental groups are represented by Latin numbers (I-IV). A representative image is given for each group ensuring expression of tested fluorescent pairs. Scale bars: 5 µm. Statistics: *** $P<0.001$; NS, not significant.

Supplementary Table 1

	Primers	Sequence (5'-3' direction)	Template	Recipient Vector
LBD-RFP-Nb (pBL14)	LBD_*Nhe*I_S	AGCTGAGCTAGCATGAA GCAGCTTCTATGTTA	first strand cDNA from 3-day-old *A. thaliana* seedlings	pCN1[1]; modified to contain following strategic restriction sites: P35S-*Nhe*I-CDS-*Bam*HI-T3nos
	LBD_*Sal*I_AS	GCTGATGTCGACGCAAG TGTCATGGTCTCTCA		
	mRFP_*Sal*I_S	TGCCGGGTCGACATGGC CTCCTCCGAGGACGT	pFK12[1]	
	mRFP_*Kpn*I_AS	TCCTTAGGTACCTGCTCC AGTGCTGTGGCGGC		
	PLUS: anti-GFP nanobody (*Kpn*I/*Bam*HI); chemically synthesised			
LBD-Nb (pFF29)	LBD_*Nhe*I_S	AGCTGAGCTAGCATGAA GCAGCTTCTATGTTA	first strand cDNA from 3-day-old *A. thaliana* seedlings	pBL14 (see above); cut *Kpn*I/*Nhe*I
	LBD_*Kpn*I_AS	CGTATTGGTACCGCAAGT GTCATGGTCTCTCA		
ΔLBD-Nb (pFK120)	Nb_*Nhe*I_S	AGTCTAGCTAGCGCCATG TATCCTTATGATGTTCC	pBL14 (see above)	RFP-TMD23 in pCN1[1]; cut *Bam*HI/*Nhe*I to keep the N-terminal signal peptide of RFP-TMD23
	Nb_*Bam*HI_AS	TGCTTCGGATCCCTAATG AT		
Cyt-RFP-Nb (pFF31)	mRFP_*Cla*I_S	AGTCTAATCGATGGCCTC CTCCGAGGACGT	pBL14 (see above)	RFP-TMD23 in pCN1[1]; cut *Bam*HI/*Cla*I
	Nb_*Bam*HI_AS	TGCTTCGGATCCCTAATG AT		
GFP-CNX (pFF4)	EGFP_*Nhe*I_S	GCATGAGCTAGCGCCAT GGTGAGCAAGGGCGAGG	pJB13[2]	pFK120 (see above); cut *Bam*HI/*Nhe*I
	EGFP_*Not*I_AS	AGTCTAGCGGCCGCCCT TGTACAGCTCGTCCATGC		
	CNX-TMD_*Not*I_S	GATCCGGCGGCCGCGAA CTGATTGAGAAAGCCGA	pSLH6[3]	
	CNX-CT_*Bam*HI_AS	TGCTTCGGATCCTCTAGA GC		
GFP-BP80 (pFF3)	BP80a-TMD_*Not*I_S	AGTCTAGCGGCCGCATC AGTAAGACGGGTTCACA	pLL38[3]	pFF4 (see above); cut *Bam*HI/*Not*I
	BP80a-CT_*Bam*HI_AS	TGCTTCGGATCCCTTAGG CA		
Man1-GFP (pFF6)	Man1_*Nhe*I_S	GCATGAGCTAGCATGGC GAGAGGGAGCAGATC	pBP30[4]	pBL14 (see above); cut *Bam*HI/*Nhe*I
	Man1_*Not*I_AS	AGTCTAGCGGCCGCCAC TAGTTCTAGAAAAAGGT		
	EGFP_*Not*I_S	AGTCTAGCGGCCGCATG GTGAGCAAGGGCGAGGA	pJB13[2]	
	EGFP_*Bam*HI_AS	AGCTGAGGATCCTTACTT GTACAGCTCGTCCA		
SYP61-GFP (pFF25)	SYP61_*Nhe*I_S	AGTCTAGCTAGCATGTCT TCAGCTCAAGATCC	pDS13[5]	pFF6 (see above); cut *Not*I/*Nhe*I
	SYP61_*Not*I_AS	GCTGTAGCGGCCGCCGG TCAAGAAGACAAGAACGA		
SYP132-GFP (FF13)	SYP132_*Nhe*I_S	AGTCTAGCTAGCATGAAC GATCTTCTGAAGGG	RFP-SYP132[6]	pFF6 (see above); cut *Not*I/*Nhe*I
	SYP132_*Not*I_AS	GATCCGGCGGCCGCCAG CACTCTTGTTTTTCCAAG		
Cyt-RFP (pFK98)	mRFP_*Nhe*I_S	AGTCTAGCTAGCATGGCC TCCTCCGAGGACG	pFK12[1]	pGD5[5]; cut *Bam*HI/*Nhe*I
	mRFP_*Bam*HI_AS	AGTCTAGGATCCTTATGC TCCAGTACTGTGGCGGC		

Sec-RFP (pFF14)	SP_*Xho*I_*Sal*I_S	TCGAGATGAAAGCCTTCA CACTCGCTCTCTTCTTAG CTCTTTCCCTCTATCTCC TGCCCAATCCAGCCATGA CG	Complementary oligonucleotides to assemble the coding sequence of the GFP-spo N-terminal signal peptide[3]	pCN1[1]; modified to contain following strategic restriction sites: P35S-*Xho*I-CDS-*Spe*I-T3nos
	SP_*Sal*I_*Xho*I_AS	TCGACGTCATGGCTGGAT TGGGCAGGAGATAGAGG GAAAGAGCTAAGAAGAG AGCGAGTGTGAAGGCTTT CATC		
	mRFP_*Sal*I_S	CTCTATGTCGACTATGGC CTCCTCCGAGGACGT	pFK12[1]	
	mRFP_*Spe*I_AS	AGTCTAACTAGTTTATGC TCCAGTACTGTGGCGGC		
Aleu-RFP (pFF15)	Aleu_*Xho*I_S	AGTCTACTCGAGATGTCT CGTCTGTCACTCCT	aleu-GFP[7]	pFF14 (see above); cut *Spe*I/*Xho*I
	Aleu_*Nhe*I_AS	CATTGCGCTAGCGCTTTC CA		
	mRFP_*Nhe*I_S	CTTTCTGCTAGCGCCATG GC	pFK12[1]	
	mRFP_*Spe*I_AS	AGTCTAACTAGTTTATGC TCCAGTACTGTGGCGGC		
3xRFP (pSF70)	mRFP_*Sal*I_S	TGCCGGGTCGACGATGG CCTCCTCCGAGGACGT	pFK12[1]	pFF14 (see above); cut *Spe*I/*Sal*I to keep the N-terminal signal peptide of pFF14
	mRFP_*Nde*I_AS	TTCGGACATATGTGCTCC AGTACTGTGGCGGC		
	mRFP_*Nde*I_S	AGTCTACATATGGCCTCC TCCGAGGACG	pFK12[8]	
	mRFP_*Nhe*I_AS	AGTCTAGCTAGCTGCTCC AGTACTGTGGC		
	mRFP_*Nhe*I_S	GTTGACTGCTAGCGCCAT GGCCTCCTC	pFK12[1]	
	mRFP_*Spe*I_AS	CTGCAACTAGTTTATGCT CCAGTACTGTGGCGGC		
3xRFP-Nb (pSF71)	mRFP_*Nhe*I_S	AGTCTAGCTAGCATGGCC TCCTCCGAGGACG	pFK12[1]	pSF70 (see above); cut *Hind*III/*Nhe*I
	mRFP_*Kpn*I_AS	TCCTTAGGTACCTGCTCC AGTGCTGTGGCGGC		
	PLUS: anti-GFP nanobody-T3nos (*Kpn*I/*Hind*III), subcloned from pBL14 (see above)			
RFP-CNX (pLBY13)	CNX-TMD_*Sal*I_S	AGTCTAGTCGACGGAACT GATTGAGAAAGCCGAG	pSLH6[3]	RFP-TMD23 in pCN1[1]; cut *Bam*HI/*Sal*I
	CNX-CT_*Bam*HI_AS	AGTCTAGGATCCCTAATT ATCACGTCTCGGTT		
GFP-SYP61 (pFK94)	EGFP_*Nco*I_S	AGTCTACCATGGTGAGCA AGGGCGAGG	pJB13[2]	pDS13[5]; cut *Cla*I/*Nco*I
	EGFP_*Cla*I_AS	AGTCTAATCGATGCTCCA CCCTTGTACAGCTCGTCC ATGC		
RFP-SYP61 (pML4)	mRFP_*Nhe*I_S	AGTCTAGCTAGCATGGCC TCCTCCGAGGACG	pBP30[4]	pGD5[5]; cut *Bam*HI/*Nhe*I
	mRFP_*Cla*I_AS	GCTGTAATCGATGCGGC GCCGGTGGAGTGGCGGC		
	PLUS: SYP61 (*Cla*I/*Bam*HI), subcloned from pDS13 [5]			

RFP-BP80 (pFK121)	BP80a-SP_*Nhe*I_S	TCCTTAGCTAGCATGAAG CAGCTTCTGTGTTA	pJLH21[3]	pGD5[5]; cut *Bam*HI/*Nhe*I
	BP80a-SP_*Not*I_AS	AGTCTAGCGGCCGCGAG CCTCGCTAAAAGGGGAA		
	mRFP_*Not*I_S	AGTCTAGCGGCCGCATG GCCTCCTCCGAGGACGT	pBP30[4]	
	mRFP_*Sal*I_AS	AGTCTAGTCGACCGGCG CCGGTGGAGTGGCGGC		
	BP80a-TMD_*Sal*I_S	GCTGATGTCGACTTTCAC AAGTGAAATCAGCG	pLL38[3]	
	BP80a-CT_*Bam*HI_AS	TGCTTCGGATCCCTTAGG CA		
HA-BP80 (pFK119)	SP_*Cla*I_S	CTCTATATCGATGAGGCT TT	pFK120 (see above)	pFF3 (see above); cut *Not*I/*Cla*I
	HA_*Not*I_AS	AGTCTAGCGGCCGCCAG CATAATCAGGAACATCA		
ST-GFP (pSF83)	ST_*Nhe*I_S	ACTGCAGCTAGCATGATT CATACCAACTTGAA	ST-YFP[9]	pFF03 (see above); cut *Not*I/*Nhe*I
	ST_*Not*I_AS	CTAGCAGCGGCCGCGGG CCACTTTCTCCTGGCTCT		
RFP-HDEL (pFK 123)	sp_*Cla*I_S	CTCTATATCGATGAGGCT TTGTAAATTCACAG	pFK12[1]	RFP-TMD23 in pCN1[1]; cut *Bam*HI/*Cla*I
	RFP-HDEL_*Bam*HI_AS	AGTCTAGGATCCCTAAAG CTCATCATGTGCTCCAGT ACTGTGGCG		

Established plasmids used in this study

Cyt-GFP[10]	Cytosolic GFP
ERD2-CFP[9]	*cis*-Golgi marker
Man1-RFP[4]	*cis*-Golgi marker
Sec12[11]	Guanine nucleotide exchange factor (GEF) for the GTPase Sar1p

References

1 Scheuring, D. *et al.* Ubiquitin initiates sorting of Golgi and plasma membrane proteins into the vacuolar degradation pathway. *BMC plant biology* **12,** 164-180, (2012).

2 Bubeck, J. *et al.* The syntaxins SYP31 and SYP81 control ER-Golgi trafficking in the plant secretory pathway. *Traffic* **9,** 1629-1652, (2008).

3 daSilva, L. L. *et al.* Receptor salvage from the prevacuolar compartment is essential for efficient vacuolar protein targeting. *Plant Cell* **17,** 132-148, (2005).

4 Nebenfuhr, A. *et al.* Stop-and-go movements of plant Golgi stacks are mediated by the acto-myosin system. *Plant Physiol.* **121,** 1127-1142, (1999).

5 Niemes, S. *et al.* Retromer recycles vacuolar sorting receptors from the trans-Golgi network. *Plant J.* **61,** 107-121, (2010).

6 Reichardt, I. *et al.* Mechanisms of functional specificity among plasma-membrane syntaxins in Arabidopsis. *Traffic* **12,** 1269-1280, (2011).

7 Humair, D., Hernandez Felipe, D., Neuhaus, J. M. & Paris, N. Demonstration in yeast of the function of BP-80, a putative plant vacuolar sorting receptor. *Plant Cell* **13,** 781-792, (2001).

8 Robinson, D. G. *et al.* Trying to make sense of retromer. *Trends Plant Sci.* **17,** 431-439, (2012).

9 Brandizzi, F. *et al.* The destination for single-pass membrane proteins is influenced markedly by the length of the hydrophobic domain. *Plant Cell* **14,** 1077-1092, (2002).

10 Scheuring, D. *et al.* Multivesicular bodies mature from the trans-Golgi network/early endosome in Arabidopsis. *Plant Cell* **23,** 3463-3481, (2011).

11 Phillipson, B. A. *et al.* Secretory bulk flow of soluble proteins is COPII dependent. *Plant Cell* **13,** 2005-2020, (2001).

9.2 Analysis of nanobody-epitope interactions in living cells via quantitative protein transport assays

Simone Früholz and Peter Pimpl

Methods in Molecular Biology, 1662, 171-182
https://link.springer.com/protocol/10.1007%2F978-1-4939-7262-3_15

Analysis of nanobody-epitope interactions in living cells via quantitative protein transport assays

Simone Früholz and Peter Pimpl*

Center for Plant Molecular Biology, University of Tübingen, Auf der Morgenstelle 32, 72076 Tübingen, Germany

*e-mail: peter.pimpl@zmbp.uni-tuebingen.de

Running head: Nanobody-epitope interaction analysis

Abstract

Over the past decades, quantitative protein transport analyses have been used to elucidate the sorting and transport of proteins in the endomembrane system of plants. Here, we have applied our knowledge about transport routes and the corresponding sorting signals to establish an *in vivo* system for testing specific interactions between soluble proteins.

Here, we describe the use of quantitative protein transport assays in tobacco mesophyll protoplasts to test for interactions occurring between a GFP-binding nanobody and its GFP epitope. For this we use a secreted GFP-tagged α-amylase as a reporter together with a vacuolar-targeted RFP-tagged nanobody. The interaction between these proteins is then revealed by a transport alteration of the secretory reporter due to the interaction-triggered attachment of the vacuolar sorting signal.

Key words nanobody-epitope interaction, GFP nanobody, epitope-tagging, electrotransfection, α-amylase, enzymatic assay, endomembrane system, secretory pathway, secretion index, protoplasts

1. Introduction

The secretory pathway is of vital importance for all eukaryotic cells, since it manufactures, stores and distributes macromolecules, lipids and proteins as cargo to intra- and extracellular locations. Probably the best characterized secretory protein in plants is the α-amylase from barley (*Hordeum vulgare*)[1]. This soluble protein is synthesized during seed germination by the cells of the aleurone layer and converts, after its secretory transport into the endosperm the accumulated starch into sugars as an energy source for the growing embryo. After synthesis and folding in the lumen of the endoplasmic reticulum (ER), the soluble α-amylase is exported from the ER and is transported along the secretory pathway to the apoplast. Secretion of soluble proteins occurs by bulk flow without the presence of sorting signals whilst sorting signals are mandatory for a protein to accumulate in the ER or for its selective targeting to vacuolar compartments[2-9]. Therefore, secretory proteins and sorting signals are ideal building blocks for the generation of reporter proteins for various intracellular locations to elucidate sorting and transport mechanisms in the endomembrane system. The most critical aspects here however are the sensitivity of the detection and the quantification of the reporter transport. A strategy that meets both requirements is the use of reporters that possess intrinsic features like an enzymatic activity. This strategy furthermore assures that only functional reporter molecules are detected and that the interpretation of the results is not compromised by the detection of reporters that have been partially degraded or were erroneously sorted due to quality control mechanisms of the cells.

A reporter that meets all requirements is α-amylase: it is a secretory molecule that is transported without any intrinsic sorting signal and it can be detected by its endogenous enzymatic activity. Over the past decades, various α-amylase-based reporters have been generated and the performed quantitative protein transport assays have significantly shaped our current view on the molecular mechanisms of protein sorting and transport in plants[3, 5, 10-23].

We have recently generated sensor proteins for compartment-specific analysis of the interaction between vacuolar sorting receptors (VSR) and their ligands. These sensors assemble *in vivo* from a compartment-specific transmembrane anchor protein and a soluble ligand binding receptor domain. This assembly is driven by the specific interaction between a green fluorescent protein (GFP)-binding V_HH domain of a heavy-chain antibody, termed GFP nanobody (Nb_G) and its corresponding epitope, the GFP[24]. The development of such experimental strategies requires however systems for testing whether protein-protein interactions between soluble proteins already occurs during their transit through the endomembrane system. For this, we have envisaged a system, in which a protein-protein interaction between a soluble secretory protein and a soluble vacuolar protein triggers the vacuolar rerouting of the

otherwise secreted protein. As a proof of concept, we trigger such a protein-protein interaction with the Nb_G and its GFP-epitope. Heretofore, we have fused GFP to the α-amylase, resulting in the secretory reporter α-amylase-GFP whilst the Nb_G was fused to the soluble vacuolar reporter Aleurain-RFP (Aleu-RFP-Nb_G) that carries a sequence-specific vacuolar sorting signal[25].

Here we exemplify the experimental procedure for such a protein-protein interaction analysis *in vivo*, starting with the generation of protoplasts from tobacco mesophyll and suspension cultured *Arabidopsis* and tobacco BY2 cells, their electrotransfection, the harvesting of the culture medium and the extraction of the cells for the quantitative biochemical transport analyses. We coexpress the secretory reporter α-amylase-GFP with the interacting vacuolar protein Aleu-RFP-Nb_G in a dosage-response experiment to characterize the protein-protein interaction by analyzing dose-dependent alterations of the transport of the secretory reporter (Fig. 2).

2. Materials

All buffer and solutions are prepared with deionized water and stored at room temperature (unless indicated otherwise)

1. Nicotiana tabacum L. SR1 is grown on solid Murashige and Skoog (MS) medium at sterile conditions in 16/8 h light-dark cycles at 22 °C in Weck “Schmuckform” jars (Weck, Wehr, Germany).
2. Solid medium for plant growth: MS medium (2.56 mM 2-(N-morpholino)ethanesulfonic acid (MES), 100 ml/l macro elements stock solution (260 mM NH_4NO_3, 188 mM KNO_3, 29.9 mM $CaCl_2*2H_2O$, 15 mM $MgSO_4*7H_2O$, 12.4 mM KH_2PO_4), 1ml/l micro elements stock solution (29.9 mM $ZnSO_4*7H_2O$, 100 mM H_3BO_3, 10 mM $MnSO_4*H_2O$, 100.12 µM $CuSO_4*5H_2O$, 4.99 mM Kl, 105 µM $CoCl_2*6H_2O$, 1.03 mM $Na_2MoO_4*2H_2O$), 10 ml/l Fe EDTA stock solution (10.02 mM $FeSO_4*7H_2O$, 9.03 mM Na_2EDTA)), supplemented with 58.4 mM sucrose and 8 g/l bacto agar. pH is adjusted with 1 M KOH to 5.7 (see **Note 1**).
3. Incubation buffer (IB): 2.56 mM MES, 400 mM sucrose, 4.3 g/l Murashige and Skoog Medium - Basal Salt Mixture, 5.1 mM $CaCl_2*2H_2O$ and 3.12 mM NH_4NO_3. pH is adjusted with HCl to 5.7, sterilized with a 0.2 µm bottle-top filter and stored at 4 °C.
4. Enzyme stock solution for protoplast isolation: 2 % (w/v) macerozyme R10 and 4 % (w/v) cellulase R10 are dissolved in IB by gentle agitation for 30 min, followed by a centrifugation at 3000 xg to sediment insoluble

particles. The clear supernatant is filter sterilized and 5 ml aliquots are kept at -20 °C.

5. Electrotransfection buffer (EB): 10.1 mM 4-(2-Hydroxyethyl)piperazine-1-ethanesulfonic acid (HEPES), 400 mM sucrose, 80.5 mM KCl, and 5.4 mM $CaCl_2$. The pH is adjusted with HCl to 7.2 and the solution is sterilized with a 0.2 µm bottle-top filter and stored at 4°C.
6. Harvesting solution for protoplasts: 250 mM NaCl.
7. α-amylase extraction buffer (20X stock solution): 1 M $C_4H_6O_5$, 1 M NaCl, 40 mM $CaCl_2$, 0.1 % (w/v) NaN_3. pH is adjusted with NaOH to 5.2 (see **Note 2**).
8. α-amylase substrate solution: α-amylase assay reagent (Megazyme, R-CAAR4) is dissolved in 10 ml deionized water and stored at -20 °C (see **Note 2**).
9. Stopping buffer: 1 % (w/v) Trizma base.

3. Methods

3.1. Isolation of tobacco mesophyll protoplasts for electrotransformation

Isolation of protoplasts is performed at sterile conditions using a lamina-flow cabinet at 22 °C. In this procedure, leaves are treated with digestive enzymes to release protoplasts, which are then purified and recovered in EB for the electrotransfection.

1. Leaves from six-eight week old tobacco plants are harvested and perforated at the lower surface using a derma roller with 1 mm needles (Fig 1a, b). Do not use the three youngest leaves from the plants and do not use leaves that are moistened with condensed water since such material will result in low protoplasts yields.
2. The midvein is removed with a scalpel blade and the two halves of the leaf are transferred to a Petri dish containing 7 ml enzyme solution with the perforated side facing the solution. This strategy allows for optimal penetration of the leaves with enzyme solution (see **Note 3**).
3. Perforate and transfer further leaves to fully cover the surface of the Petri dish but avoid overlap of leaves. Usually, 2-3 leaves are used per Petri dish for the efficient use of the enzyme solution. Do not fully submerse the leaves in the enzyme solution, since this reduces the protoplast yield significantly (see **Note 4**).

4. The leaves are incubated in the dark for 16 h at 25 °C to allow for gentle digestion of the cell walls.
5. Prior to the protoplast purification, shake the Petri dishes gently without submersing the floating leaves to release the protoplasts and incubate for further 30 min as above. This short investment of time will significantly increase the yield. (Fig 1 c).
6. Filter the suspension through a sterile 100 µm nylon mesh which was moistured before with EB to prevent the protoplasts from sticking to the filter.
7. Transfer the filtered protoplasts into a 50 ml centrifugation tube for further purification.
8. Protoplasts are separated from debris by flotation. Here, the protoplasts alive will float on top of the solution, whilst debris remains in the underlying solution or form a sediment. Centrifuge the suspension for 15 minutes at 80 xg at room temperature in a swingout rotor. Allow for minimum deceleration to avoid perturbation of the layer of floating protoplasts and mixing of protoplasts with the debris of the solution below.
9. Remove the sediment and the underlying solution and quickly resuspend the floating protoplasts in a total volume of 40 ml EB.
   This is done with a long Pasteur pipette that is connected to a peristaltic pump. Loss of protoplast can be minimized if the cells are gently pushed to create an opening in the layer of the floating cells in the middle of the tube. This opening is then used to insert the pipette into the underlying solution (see **Note 5**).
10. Centrifuge again as before (8) and repeat step 9 until the underlying solution is clear. If large amounts of protoplasts are needed, the content of multiple centrifugation tubes can be combined to generate a large pool of protoplasts. For this, cells should be resuspended in a smaller volume e.g. 15 ml prior to transfer into one single tube. This case however will require additional washing steps (8,9).
11. After the last washing step, centrifuge the protoplasts again and estimate the volume of the floating cells. Remove the underlying solution as described above and resuspend the protoplasts in a 3-fold volume with EB to obtain 2-5*10^6 protoplasts/ml. This protoplast suspension is used next for electrotransformation.

3.2. Isolation of protoplasts from suspension-cultured *Arabidopsis* and tobacco BY2 cells

Protoplasts are isolated from 50 ml suspension cultures three days after sub-culturing, all steps are carried out at sterile conditions at 22 °C.

1. Transfer the cell suspension to a 50 ml centrifugation tube and sediment the cells at 80 xg for 10 min.
2. Decant the culture medium, resuspend the cells in a total volume of 40 ml with enzyme solution (see **Note 3**) and distribute the suspension to 4 Petri dishes.
3. Incubate the suspension in the dark for 16 h at 25 °C.
4. Gently shake the plates and transfer the cell suspension to a 50 ml centrifugation tube.
5. To purify the protoplasts, continue with step 8 of the protocol given above for the isolation of mesophyll protoplasts.

3.3. Electrotransformation of protoplasts

The electrotransformation of the above described protoplasts is performed at sterile conditions using a lamina-flow cabinet at 22 °C.

1. Transfer 500 µl of the protoplast suspension into a semi-micro disposable cuvette by using a cut-off blue pipette tip to avoid shearing forces which would rapture the protoplasts (Fig 1 d).
2. Dilute the plasmid DNA in a total volume of 100 µl with EB. Usually, 10 - 50 ng of plasmid DNA is used per µl transformation reaction. A mock transfection that lacks plasmid DNA is used as a negative control.
3. Transfer the 100 µl diluted plasmid DNA on top of the protoplast suspension in the cuvette, mix immediately by gentle shaking and incubate for 5 minutes.
4. Sterilize the hand-held electrode by swirling in a small volume of 99 % EtOH and flaming. Cool-down the electrode by gentle dipping in EB prior to the transformation.
5. Gently shake the cuvette again to distribute the floating protoplasts homogeneously in the suspension and insert the hand-held electrode (Fig 1 e).
6. The protoplasts are transformed by applying a high capacitance square-wave pulse with 160 V for 10 ms.
7. Carefully remove the electrode from the cuvette and incubate the protoplasts for 15 min without any agitation.
8. Rinse the electrode by dipping multiple times into deionized water. Sterilize and cool the electrode as described in step 4.

9. Gently pour the cells from the cuvette into a small Petri dish (4.5 cm diameter). Immediately rinse the cuvette twice with 1 ml IB buffer to recover all protoplasts (Fig 1 f).
10. Incubate the cells for the expression of the proteins in the dark at 25°C. Expression time depends on the respective experiment and can vary between 2 h and 48 h.

3.4. Harvesting of the culture medium and cells

Harvesting of medium and cells and all subsequent procedures do not require sterile conditions. Harvesting occurs through centrifugation to separate the living protoplasts from the culture medium by floatation.

1. Prepare 15 ml centrifuge tubes for harvesting by puncturing with a glowing hot cannula in the lower conical part of the tube. Smoothen the surface around the hole with a scalpel blade and seal the tube again with multiple layers of parafilm.
2. Transfer the cells from the Petri dish into the modified tube and centrifuge for 10 minutes at 80 xg at room temperature in a swingout rotor. Allow for minimum deceleration to avoid perturbation of the layer of floating living protoplasts.
3. 500 µl of the underlying medium is harvested with an insulin syringe through the prepared hole (Fig 1 g). Transfer this medium sample to a 1.5 ml reaction tube, keep it on ice and immediately seal the tube again with multiple layers of parafilm.
4. The remaining cell suspension is diluted to a total volume of 10 ml with the harvesting solution for protoplasts and gently resuspended by inverting the centrifugal tube for several times.
5. Sediment the cells for 7 minutes at 80 xg at room temperature in a swingout rotor with moderate deceleration (Fig 1 h).
6. Remove the supernatant with a Pasteur pipette which is connected to a peristaltic pump and freeze the cells at -80 °C.
7. Centrifuge the medium samples at 20,000 xg for 15 min at 4 °C to remove particles and transfer the cleared supernatant into a new reaction tube.
8. Cell samples are defrosted on ice and extracted in a total volume of 250 µg with 1X α-amylase extraction buffer.
9. Cell extracts are homogenized by sonication for 3 seconds.
10. Cell extracts are centrifuged at 20,000 xg for 15 min at 4 °C and the supernatant is transferred into a precooled reaction tube and kept on ice.

3.5. Analysis of the enzymatic α-amylase activity and quantification of protein transport

Enzymatic activity of α-amylase is determined by a single-point spectrophotometric assay that measures the release of *p*-nitrophenolate anions after the metabolization of the α-amylase substrate *p*-nitrophenyl maltoheptaoside (BPNPG7) at alkaline conditions. The activity of the α-amylase is calculated as the amount of metabolized substrate per minute per milliliter sample.
Protein transport is quantified by the comparison of the amounts of α-amylase that was secreted to the culture medium and the α-amylase that remained in the cells. This ratio is defined as the secretion index (SI).

1. Dilute the samples with α-amylase extraction buffer (see **Note 6**).
2. Transfer 30 µl of diluted sample into a 1.5 ml reaction tube (see **Note 7, 8**).
3. Add 30 µl α-amylase substrate solution to the sample, mix carefully by pipetting tree times up and down to start the reaction and immediately incubate the reaction mix at 40 °C (see **Note 9**).
4. The enzymatic reaction is stopped by the addition of 150 µl stopping buffer. This increase of pH immediately inhibits the α-amylase and triggers the dissociation of the *p*-nitrophenol to the yellow colored *p*-nitrophenolate anion.
5. Transfer 200 µl of the reaction into a 96-well plate and read the absorbance (OD) with a plate reader at 405 nm (see **Note 10**).
6. Average the ODs from all duplicates.
7. Subtract the averaged OD of the blank from the averaged OD of the sample to determine the amount of substrate that was metabolized during the reaction ($\boldsymbol{\Delta E}$) (see **Note 11**).
   $$\boldsymbol{\Delta E = \overline{OD}_{sample} - \overline{OD}_{blank}}$$
8. Divide the amount of metabolized substrate by the volume of the undiluted sample that was used in the reaction in µl and multiply by 1000 to calculate the metabolized substrate per milliliter and divide the term by the reaction time in minutes to calculate the activity.
   $$\boldsymbol{activity = \frac{\frac{\Delta E}{sample\ volume\ [\mu l]} * 1000}{reaction\ time\ [min]}}$$
9. In order to compare values from medium and cells, values of cell samples have to be divided by 10 to compensate for the volume change between the expression and extraction.
10. The total activity is calculated as the sum of activity in the medium and the activity in the cells (Fig 2).
    $$\boldsymbol{total\ acivity = activity\ (medium) + activity\ (cells)}$$

11. Divide the calculated α-amylase activity from the culture medium by the calculated α-amylase activity in the cells (Fig 2).

$$\boldsymbol{SI} = \frac{\boldsymbol{activity\ (medium)}}{\boldsymbol{activity\ (cells)}}$$

4. Notes

1. All stock solutions for the MS medium are stored at 4 °C. To prepare the Fe EDTA stock solution, prepare the iron(II) sulfate ($FeSO_4*7H_2O$) solution and the sodium EDTA (Na_2EDTA) solution separately and mix both solution afterwards according to the desired volume.
2. All solutions and reagents for measuring the enzymatic α-amylase activity are also available as α-Amylase Assay Kit (K-CERA) from Megazyme, Ireland (www.megazyme.com).
3. Dilute 5 ml of enzyme stock solution with IB to 50 ml, distribute the content to 7 Petri dishes and shake the dish gently to cover the bottom of the dish.
4. 7 Petri dishes with perforated leaves are sufficient for 10-12 electrotransfections.
5. When removing cell debris and the underlying medium, make sure that the peristaltic pump is not started before the tip of the Pasteur pipette is below the floating cells. Also make sure, to fully turn off the peristaltic pump shorty before the medium is removed completely in order to remove the pipette without losing the protoplasts.
6. Dilute 2.5 ml of 20X α-amylase extraction buffer to a final volume of 50 ml with deionized water.
7. When diluting cell and medium samples with 1X α-amylase extraction buffer make sure that you dilute them at least 1:1 to provide optimal reaction conditions for the α-amylase
8. All transfected samples are analyzed in duplicate samples.
9. The enzymatic reactions are started in 10 to 20 second intervals by the addition of the α-amylase substrate. Reactions are stopped after the respective reaction time in the same intervals by adding the stopping buffer.
10. If extinction values are higher than 1.2, repeat the assay with a more dilute sample or shorten the reaction time.
11. Samples from mock transfected cells are also subjected to the enzymatic assay. These values serve as blanks during the calculation of the α-

amylase activity. This is important, since these blanks account for p-nitrophenol that was released from the substrate due to thermal decay during the incubation time.

Figures

Figure 1

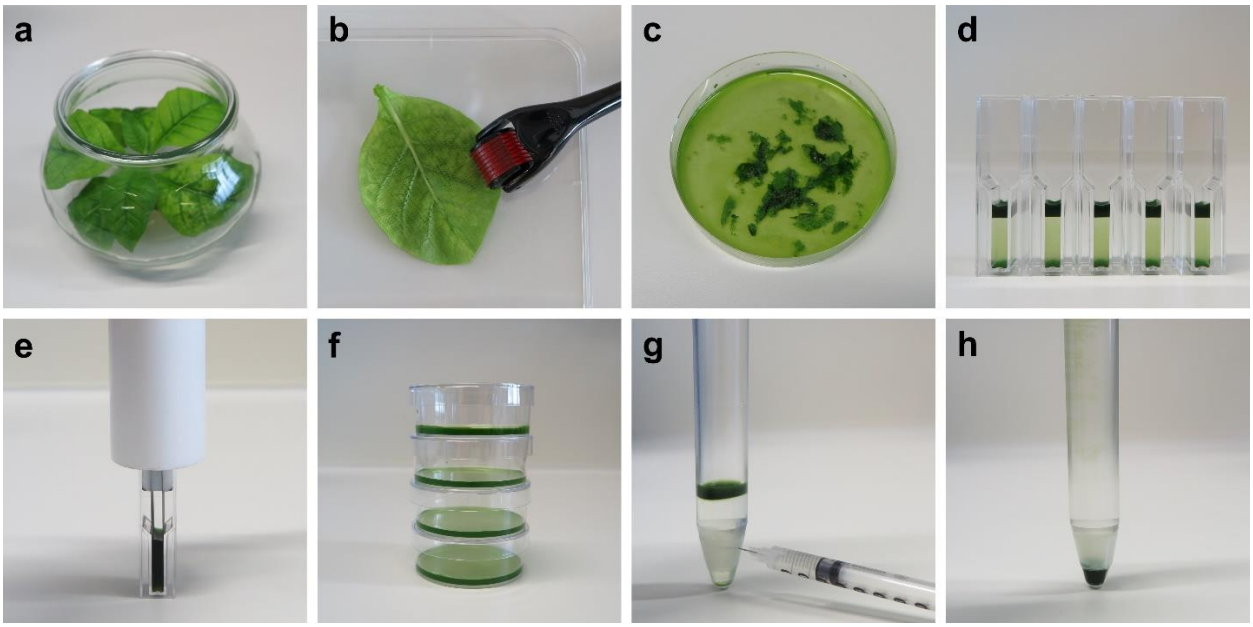

Figure 1 Transient gene expression in Tobacco mesophyll protoplasts. (**a**) Tobacco plant in a Weck jar on solid MS medium. (**b**) Leaves after perforation with a derma roller. (**c**) Leaves after overnight incubation in enzyme solution. (**d**) Aliquots of protoplast suspension in disposable cuvettes for electrotransfection. (**e**) Cuvette with inserted hand-held electrode. (**f**) Electrotransfected protoplasts in small Petri dishes for gene expression. (**g**) Harvesting of culture medium with an insulin syringe through the prepared hole. (**h**) Sedimented cells after harvesting.

Figure 2

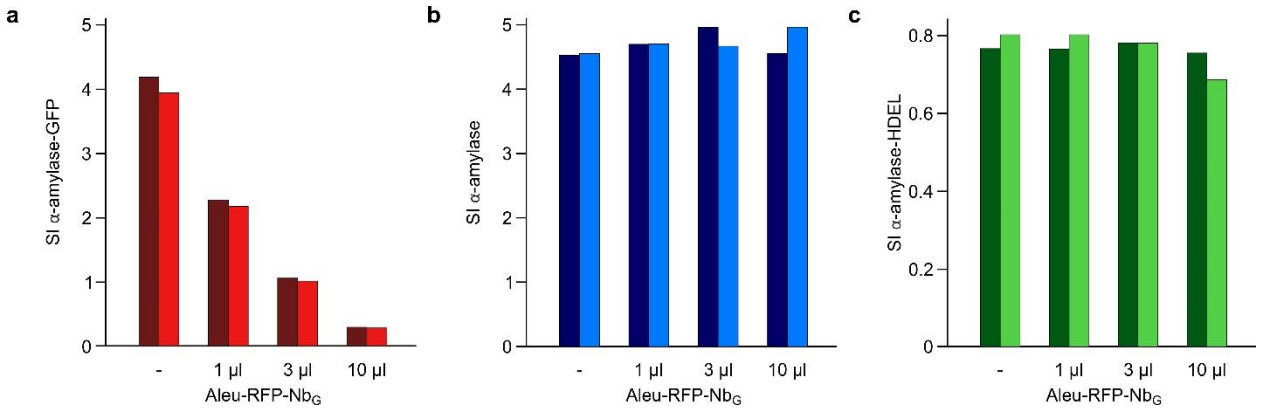

Figure 2 Quantitative analysis of the protein transport.

A large pool of protoplasts was divided in 26 aliquots and electrotransfected with plasmid DNA (see Table 1 below). For each sample condition, two transfections were performed and are given as a dark/bright color pair in the bar chart, whilst two aliquots were mock-transfected.

(**α-c**) Protoplasts were transfected with plasmids coding for (**a**) the epitope-tagged secretory reporter α-amylase-GFP, (**b**) the non-epitope-tagged α-amylase or (**c**), the ER-retained α-amylase-HDEL, either alone (-) or were cotransfected with raising concentration of plasmids coding for the vacuolar targeted Aleu-RFP-Nb$_G$ as indicated. The secretion indices (SI) of two independent experiments were calculated and are given next to each other. (**a**) The SI of α-amylase-GFP (red) is drastically reduced by the coexpressed Aleu-RFP-Nb$_G$. This dose-dependent rerouting of the secretory reporter reveals the interaction-triggered attachment of the vacuolar sorting signal. (**b**) The SI of α-amylase (blue) is not influenced by the coexpressed Aleu-RFP-Nb$_G$ due to the absence of interaction. (**c**) The secretion index SI of α-amylase-HDEL (green) is also not influenced by the coexpressed Aleu-RFP-Nb$_G$, also indicating the specificity of the interaction shown in (**a**).

Table 1

Plasmids used

	Primers	Sequence (5'-3' direction)	Template	Recipient Vector
Aleu-RFP-Nb$_G$ (pDV04)	PLUS: P35S-Aleu (*EcoR*I/*Nhe*I), subcloned from pFF15[24]			pCN [26]; cut *BamH*I/*EcoR*I
	RFP_*Nco*I_S	CTAGCGCCATGGCCTC CTCCGAGGAC	pFK12[26]	
	RFP_*Kpn*I_AS	ATACATGGTACCTGCT CCAGTACTGTGGCGGC		
	PLUS: Nb$_G$ (*Kpn*I/*BamH*I), subcloned from pBL14[24]			
Amy-GFP (pDV05)	Amy_*Nco*I_S	CTATAACCATGGCGAA CAAACACTTGTCCCTC	pCN1[26]	pCN1[26]; cut *BamH*I/*Nco*I
	Amy_*Not*I_AS	ATCAACGCGGCCGCCG ATCTTCTCCCATACGG CAT		
	GFP_*Not*I_S	CCATGAGCGGCCGCAT GAGTAAAGGAGAAGAA CT	GFP-spo[13]	
	GFP-GGGG_*BamH*I_AS	TGCTTCGGATCCCTAT CCTCCTCCTCCTTTGTA TAGTTCATCCATGC		
Amy-HDEL (pCN02)	PLUS: P35S-Amy-HDEL-T35S (*EcoR*I/*Hind*III); subcloned from pAmy-HDEL [3]			pCN1[26]; cut *Hind*III/*EcoR*I
Established plasmids used in this study				
Amy	Secretory reporter[10]			

References

1. Rogers JC (1985) Two barley alpha-amylase gene families are regulated differently in aleurone cells. J. Biol. Chem. 260(6):3731-3738.
2. Denecke J, Botterman J,Deblaere R (1990) Protein secretion in plant cells can occur via a default pathway. Plant Cell 2(1):51-59.
3. Phillipson BA*, et al.* (2001) Secretory bulk flow of soluble proteins is efficient and COPII dependent. Plant Cell 13(9):2005-2020.
4. Denecke J, De Rycke R,Botterman J (1992) Plant and mammalian sorting signals for protein retention in the endoplasmic reticulum contain a conserved epitope. EMBO J. 11(6):2345-2355.
5. Pimpl P*, et al.* (2006) Golgi-mediated vacuolar sorting of the endoplasmic reticulum chaperone BiP may play an active role in quality control within the secretory pathway. Plant Cell 18(1):198-211.
6. Bednarek SY, Wilkins TA, Dombrowski JE,Raikhel NV (1990) A carboxyl-terminal propeptide is necessary for proper sorting of barley lectin to vacuoles of tobacco. Plant Cell 2(12):1145-1155.
7. Holwerda BC, Padgett HS,Rogers JC (1992) Proaleurain vacuolar targeting is mediated by short contiguous peptide interactions. Plant Cell 4(3):307-318.
8. Frigerio L, de Virgilio M, Prada A, Faoro F,Vitale A (1998) Sorting of phaseolin to the vacuole is saturable and requires a short C-terminal peptide. Plant Cell 10(6):1031-1042.
9. Koide Y, Hirano H, Matsuoka K,Nakamura K (1997) The N-terminal propeptide of the precursor to sporamin acts as a vacuole-targeting signal even at the C terminus of the mature part in tobacco cells. Plant Physiol. 114(3):863-870.

10. Pimpl P, Hanton SL, Taylor JP, Pinto-DaSilva LL,Denecke J (2003) The GTPase ARF1p Controls the Sequence-Specific Vacuolar Sorting Route to the Lytic Vacuole. Plant Cell 15(5):1242-1256.
11. Bottanelli F, Foresti O, Hanton S,Denecke J (2011) Vacuolar Transport in Tobacco Leaf Epidermis Cells Involves a Single Route for Soluble Cargo and Multiple Routes for Membrane Cargo. Plant Cell 23(8):3007-3025.
12. daSilva LL*, et al.* (2004) Endoplasmic reticulum export sites and Golgi bodies behave as single mobile secretory units in plant cells. Plant Cell 16(7):1753-1771.
13. daSilva LL*, et al.* (2005) Receptor salvage from the prevacuolar compartment is essential for efficient vacuolar protein targeting. Plant Cell 17(1):132-148.
14. Gershlick DC*, et al.* (2014) Golgi-Dependent Transport of Vacuolar Sorting Receptors Is Regulated by COPII, AP1, and AP4 Protein Complexes in Tobacco. Plant Cell.
15. Langhans M*, et al.* (2008) In vivo Trafficking and Localization of p24 Proteins in Plant Cells. Traffic 9(5):770-785.
16. Langhans M, Niemes S, Pimpl P,Robinson DG (2009) Oryzalin bodies: in addition to its anti-microtubule properties, the dinitroaniline herbicide oryzalin causes nodulation of the endoplasmic reticulum. Protoplasma 236(1-4):73-84.
17. Leborgne-Castel N, Jelitto-Van Dooren EP, Crofts AJ,Denecke J (1999) Overexpression of BiP in tobacco alleviates endoplasmic reticulum stress. Plant Cell 11(3):459-470.
18. Niemes S*, et al.* (2010) Sorting of plant vacuolar proteins is initiated in the ER. Plant J. 62(4):601-614.
19. Niemes S*, et al.* (2010) Retromer recycles vacuolar sorting receptors from the trans-Golgi network. Plant J. 61(1):107-121.
20. Pimpl P*, et al.* (2000) In Situ Localization and in Vitro Induction of Plant COPI-Coated Vesicles. Plant Cell 12(11):2219-2236.
21. daSilva LL, Foresti O,Denecke J (2006) Targeting of the plant vacuolar sorting receptor BP80 is dependent on multiple sorting signals in the cytosolic tail. Plant Cell 18(6):1477-1497.
22. Bubeck J*, et al.* (2008) The syntaxins SYP31 and SYP81 control ER-Golgi trafficking in the plant secretory pathway. Traffic 9(10):1629-1652.
23. Shahriari M*, et al.* (2010) The AAA-type ATPase AtSKD1 contributes to vacuolar maintenance of Arabidopsis thaliana. Plant J. 64(1):71-85.
24. Künzl F, Früholz S, Fäßler F, Li B,Pimpl P (2016) Receptor-mediated sorting of soluble vacuolar proteins ends at the trans-Golgi network/early endosome. Nat Plants:16017.
25. Humair D, Hernandez Felipe D, Neuhaus JM,Paris N (2001) Demonstration in yeast of the function of BP-80, a putative plant vacuolar sorting receptor. Plant Cell 13(4):781-792.
26. Scheuring D*, et al.* (2012) Ubiquitin initiates sorting of Golgi and plasma membrane proteins into the vacuolar degradation pathway. BMC plant biology 12:164.

Acknowledgement

We gratefully acknowledge the financial support of the Deutsche Forschungsgemeinschaft (PI 769/1-2 and the Collaborative Research Centre SFB 1101 “Molecular Encoding of Specificity in Plant Processes”) and of the German Academic Exchange Service (Project 57219822).

9.3 Nanobody mediated lockdown of VSRs reveals ligand reloading in the Golgi

Simone Früholz, Florian Fäßler, Üner Kolukisaoglu and Peter Pimpl

Nature Communications (in press)

Nanobody triggered lockdown of VSRs reveals ligand reloading in the Golgi

Simone Früholz[2], Florian Fäßler[2], Üner Kolukisaoglu[2] and Peter Pimpl[1,2]

[1]SUSTech-PKU Institute of Plant and Food Science (IPFS), Department of Biology, Southern University of Science and Technology (SUSTech), Shenzhen, Guangdong 518055, China.
[2]Center for Plant Molecular Biology (ZMBP), University of Tübingen, Auf der Morgenstelle 32, 72076 Tübingen, Germany.

Correspondence and requests for materials should be addressed to P.P. (email: pimpl@sustc.edu.cn)

Abstract

Protein degradation in lytic compartments is crucial for eukaryotic cells. At the heart of this process, vacuolar sorting receptors (VSRs) bind soluble hydrolases in the secretory pathway and release them into the vacuolar route. Sorting efficiency is suggested to result from receptor recycling. However, how and to where plant VSRs recycle remains controversial. Here we present a nanobody-epitope interaction-based protein labeling and tracking approach to dissect their anterograde and retrograde transport routes *in vivo*. We employ simultaneously two different nanobody-epitope pairs: one for the location-specific post-translational fluorescence labeling of receptors and the other pair to trigger their compartment-specific lockdown via an endocytosed dual epitope linker protein. We demonstrate VSR-recycling from the TGN/EE, thereby identifying the *cis*-Golgi as the recycling target and show that recycled VSRs reload ligands. This is evidence that bidirectional VSR-mediated sorting of vacuolar proteins exists and occurs between the Golgi and the TGN/EE.

Introduction

Degradation in lytic compartments is a hallmark of eukaryotic cells. It allows for rapid modulations of compartmental protein and lipid compositions as responses to cellular communication or environmental cues[1, 2, 3, 4]. This necessitates constant supply of vacuoles/lysosomes with acid hydrolyses by the action of sorting receptors[5]. Despite its significance for viability and development, the core mechanism of vacuolar sorting receptor (VSR)-mediated protein transport and its implementation in the plant endomembrane system is still controversial[5, 6].

The concept of receptor-mediated protein transport dates back to the discovery of the low-density lipoprotein receptor and the cation independent (CI)-mannose 6-phosphate receptor (MPR) for lysosomal sorting in mammals[7, 8, 9]. They bind ligands either at the cell surface or the TGN and transport them to endosomes, where ligands are released due to low compartmental pH[8, 10]. The key to the efficiency of this transport however, is the continuous recycling of receptors after ligand release, allowing receptors to go through hundreds of transport-cycles during their life span[7, 8, 11, 12, 13].

The recycling route of MPRs was most elegantly mapped biochemically, by assaying for Golgi cisternae-specific glycan processing after receptor labeling with [^{3}H]galactose at the cell surface by using exogenous galyctosyltransferases[14]. However, endogenous VSRs do not localize to the cell surface and are thus not amendable to exogenously applied modifying enzymes to decipher their function or to trace their transport route *in vivo*.

VSRs are type I transmembrane proteins and bind ligands via a luminal ligand-binding domain (LBD), whereas their cytosolic tail carries the sorting information for their own transportation[15, 16, 17, 18, 19, 20, 21, 22, 23]. They were originally proposed to transport ligands into prevacuoles, nowadays referred to as multivesicular bodies/late endosomes (MVBs/LEs)[16, 19, 21, 24, 25, 26]. However, we have recently demonstrated that VSRs bind ligands in the early secretory pathway and instead release them in the *trans*-Golgi network (TGN)[27], the early endosome (EE) of plants (TGN/EE)[28, 29]. This raised the fundamental questions as to how to where VSRs recycle after ligand release. To address this, we have devised a strategy that utilizes the *in vivo* interaction of two different antibody-epitope pairs. This allows (a) for the location-specific green fluorescent protein (GFP)-labeling of VSRs in the TGN/EE and (b) for the tracking and lockdown of such labeled VSRs in upstream compartments, upon retrograde recycling. For this, we have translationally fused a variable domain of a lama (*Lama paco*)

heavy chain antibody (V_HH)[27, 30], termed nanobody (Nb), that was raised against GFP (Nb_G)[27, 31] to a VSR (Nb_G-VSR). The other Nb, which was raised against α-synuclein (Nb_S)[32], was fused to compartment-specific membrane marker proteins. Finally, we have designed a dual epitope linker protein, which contains the epitopes of both nanobodies and therefore allows for both, specific GFP-labeling of the Nb_G-tagged VSR via the GFP domain and attachment to Nb_S-tagged compartmental marker proteins via the α-synuclein (SYN) epitope. Labeling of Nb_G-VSR in the lumen of the TGN/EE is achieved by incubation of Nb_G and Nb_S fusion protein-expressing cells with the dual epitope linker protein GFP-SYN, which is endocytosed and delivered to the TGN/EE. Using this approach, we have traced GFP-labeled VSRs from the TGN/EE back to the *cis*-Golgi, where we demonstrate their ligand binding capability. Together, these data demonstrate the cycling of VSRs between the Golgi stack and the TGN/EE.

RESULTS

Post-translational GFP-labeling via endocytosed GFP

The challenge when analyzing bidirectional protein transport of sorting receptors in live-cell imaging studies is to differentiate between anterograde and retrograde transported receptors under steady state conditions. This is particularly true when translational fusions between receptors and fluorescent proteins are used. Here, fluorescent signals become detectable immediately after synthesis and protein folding in the ER and they persist throughout the lifespan of the molecule. Consequently, the localization of the receptor does not provide any information on its transport direction or ligand status (**Fig. 1a**). An analysis of receptor recycling therefore demands strategies that allow for the specific tracing of those VSRs that have released their ligands in the TGN/EE[27] and are about to be recycled. This requirement is fulfilled if a post-translational labeling strategy is used where signals of the labeled VSRs become first detectable in the TGN/EE (**Fig. 1b**). To achieve this, we have devised an approach that accounts for both, the target-specificity of the labeling and the intracellular location where the labeling occurs. For this, we have employed a GFP-binding nanobody (Nb_G)[27, 31] that is translationally fused to the VSR and we deliver its epitope GFP as the fluorescent labeling agent to the TGN/EE via endocytosis. We produced the labeling GFP as a

secretory protein in another population of tobacco mesophyll protoplasts. The resulting GFP-containing culture medium is then used for labeling of the cell population that expresses the Nb_G-tagged VSRs. This strict separation between cells that produce the labeling agent GFP and cells that are used for the labeling ensures that no newly synthesized VSR on its anterograde route is labeled prior to reaching the TGN/EE.

To develop a compartment-specific post-translational GFP-labeling strategy, we firstly decided to employ the established marker proteins α-mannosidase 1 (Man1) for the *cis*-Golgi, sialyltransferase (ST) for the *trans*-Golgi, SYNTAXIN OF PLANTS (SYP) 61 for the TGN/EE, and the luminal ligand binding domain-deprived (ΔLBD) binding protein 80 kDa (BP80) from *Pisum sativum* for MVB/LE in coexpression experiments to discriminate between the various punctate signals (**Supplementary Fig. 1**). Next, we generated and tested red fluorescent protein (RFP)-tagged Nb_G fusion proteins of these markers in tobacco mesophyll protoplasts for post-translational labeling in the TGN/EE (SYP61-RFP-Nb_G), the MVB/LE (Nb_G-RFP-BP80ΔLBD), the *trans*-Golgi (ST-RFP-Nb_G), the *cis*-Golgi (Man1-RFP-Nb_G) and the ER (Nb_G-RFP-Calnexin (CNX). After transfection with the respective marker construct, we incubated the cells in GFP-containing culture medium for the endocytic uptake of GFP (endocyt GFP) (**Fig. 1c-g**). Confocal laser-scanning microscopy (CLSM) demonstrated that the endocytosed GFP was trapped by the Nb_G-tagged markers SYP61-RFP-Nb_G and Nb_G-RFP-BP80ΔLBD in the TGN/EE and downstream in the MVB/LE, respectively (**Fig. 1c,d**). In sharp contrast, labeling of the markers in compartments upstream of the TGN/EE like the *trans*-/*cis*-Golgi (ST-RFP-Nb_G, Man1-RFP-Nb_G) or the ER (Nb_G-RFP-CNX) with endocytosed GFP was never observed (**Fig. 1e-g**). However, post-translational GFP-labeling based on Nb_G-epitope interaction is also possible in these compartments, if the labeling agent GFP is coexpressed as a secretory protein (Sec-GFP) with the respective Nb_G-fusion proteins (**Fig. 1h-j**). This shows that post-translational GFP-labeling via Nb_G-epitope interaction is applicable to Nb_G-tagged proteins in all compartments and furthermore demonstrates that endocytosed GFP alone does not reach locations upstream of the TGN/EE like the *cis*-/*trans*-Golgi and the ER. Consequently, this also demonstrates that none of the Nb_G-tagged markers that reside in the ER or the Golgi apparatus, ever reach or cycle through the TGN/EE in order to reach their respective steady state distribution.

Post-translationally labeled VSRs localize to the TGN/EE

In the next step, we applied this post-translational GFP-labeling protocol to VSRs (**Fig. 2a,b**). To better judge the labeling efficiency, we tagged a fluorescent VSR[33] with the Nb_G (Nb_G-RFP-VSR) and performed post-translational GFP-labeling (**Fig. 2b**). CLSM-based colocalization reveals almost perfectly matching punctate signals of the red Nb_G-RFP-VSR and the green signals from the endocytosed GFP (**Fig. 2c,d**), demonstrating a high degree of labeling efficiency. However, since Nb_G-RFP-VSR can acquire the labeling GFP only in the TGN/EE, this high degree of colocalization furthermore suggests that under steady state conditions almost all of the Nb_G-RFP-VSR molecules had already reached the TGN/EE, at least once.

We have recently demonstrated that VSRs bind their ligands in the ER, in the *cis*- and *trans*-Golgi, but release their ligands in the TGN/EE[27]. Therefore, we hypothesized that the ligand-free receptors that were post-translationally labeled with endocytosed GFP in the TGN/EE would recycle to an upstream compartment for ligand reloading. In such a scenario, we would then expect to detect a population of labeled VSRs in a compartment upstream of the TGN/EE. To precisely define the VSR localizations we next post-translationally labeled non-fluorescent Nb_G-tagged VSRs (Nb_G-VSR) with endocytosed GFP and tested for colocalization with established red fluorescent compartmental markers (**Fig. 2e,f**) for the TGN/EE (RFP-SYP61), the MVB/LE and vacuole (Aleu-RFP), *trans*- and *cis*-Golgi (ST-RFP and Man1-RFP, respectively) and for the ER (RFP-CNX) in coexpression experiments (**Fig. 2g-m**). The post-translationally labeled Nb_G-VSRs colocalized with the TGN/EE marker (**Fig. 2g**). Surprisingly, the post-translationally labeled Nb_G-VSRs neither colocalized with the MVB/LE and vacuole marker Aleu-RFP (**Fig. 2h,i**) nor with markers for upstream compartments like the *trans*- and *cis*-Golgi or the ER (**Fig. 2j-m**). This steady state localization of Nb_G-VSR at the TGN/EE rather than at the MVB/LE, as is commonly assumed, is not restricted to post-translationally labeled Nb_G-VSRs, it is also seen in control experiments using the fluorescent full-length receptor fusion protein Nb_G-RFP-VSR (**Supplementary Fig. 2**). The differential localization of these full-length VSRs and LBD-lacking MVB/LE markers of the RFP/GFP-BP80ΔLBD type, therefore suggests that the presence of the LBD is required for both, the ligand binding capability and for the correct transport of the receptor.

Nanobody triggered lockdown of recycled VSRs

One possible explanation for the TGN/EE-localization of VSRs under steady state conditions is that VSRs do not recycle to reload ligands. Such a one-way transport mode was suggested for members of the receptor homology region-transmembrane domain-RING-H2 (RMR) receptor family, which sort proteins to the protein storage vacuole[34]. However, considering that the TGN/EE is expected to be the recycling point of a bidirectional transport system[27, 35], the TGN/EE-localization of cycling VSRs may indicate that anterograde transport is faster than the subsequent recycling step. To test for his hypothesis, we have devised a strategy that allows for the specific detection of recycled receptors in compartments upstream of the TGN/EE by blocking their further export and onward forwarding upon completion of recycling. For this, we have combined the nanobody-mediated post-translational labeling of recycling VSRs in the TGN/EE with an approach for compartment-specific lockdown of these labeled VSRs via an antibody-epitope interaction that is triggered by a second nanobody-epitope pair (**Fig. 3a-c**).

Hereto, we translationally fused a nanobody that is directed against the mammalian α-synuclein (Nb_S) to red fluorescent compartment-specific membrane markers (CM-RFP-Nb_S) and we fused its corresponding epitope termed SYN, which is a sequence of 23 amino acids, to GFP (GFP-SYN). Endocytic uptake of this dual epitope linker as the labeling agent by cells coexpressing Nb_G-VSRs and Nb_S-tagged compartmental markers was then expected to firstly label Nb_G-VSRs in the TGN/EE and then to trigger an *in vivo* crosslink between the SYN-epitope of the GFP-SYN-labeled VSR and the Nb_S-tagged compartmental marker in the compartmental lumen.

This complex strategy required that we first test whether Nb_S interacts with the SYN-epitope in the lumen of secretory pathway compartments. To this end, we developed an assay for analyzing protein-protein interaction *in vivo*. This assay is based on the simultaneous use of a quantifiable soluble secretory reporter with a soluble vacuolar protein, each of which carries either the nanobody or the epitope, respectively. In this approach, the interaction occurring between the Nb_S and the epitope triggers the attachment of the vacuolar sorting signal to the secretory reporter and consequently, its transport to the lytic vacuole via the vacuolar sorting machinery (**Fig. 3d,e**).

We therefore tagged the secretory reporter α-amylase from barley (*Hordeum vulgare*)[36] with the SYN-epitope (amylase-SYN) and employed the vacuolar reporter Aleu-RFP as a Nb_S-

fusion protein (Aleu-RFP-Nb$_S$). Quantitative transport analysis of the secretory amylase-SYN in tobacco mesophyll protoplasts shows that its secretion is drastically reduced by the coexpressed vacuolar Aleu-RFP-Nb$_S$ (**Fig. 3f**), suggesting an interaction between the Nb$_S$ and the SYN-epitope. In the next step, we tested the functionality of Nb$_S$ in the context of the compartment-specific membrane anchors for the ER, *cis*- and *trans*-Golgi and the TGN/EE. For this, we fused the Nb$_S$ to RFP-CNX (Nb$_S$-RFP-CNX), Man1-RFP (Man1-RFP-Nb$_S$), ST-RFP (ST-RFP-Nb$_S$) and SYP61-RFP (SYP61-RFP-Nb$_S$) and verified firstly their correct location in colocalization experiments with their respective GFP-tagged counterpart (**Supplementary Fig. 3**). Second, we tested their ability to bind the dual epitope linker GFP-SYN (**Fig. 3g-j)**. To do this, we immunoprecipitated the above-mentioned marker proteins and their Nb$_S$-tagged pendants, the anchors, with RFP antibodies in bead-binding assays and subjected all of them to the GFP-SYN-containing culture medium from GFP-SYN-secreting protoplasts. The immunoblot analysis of the precipitates revealed that all of the Nb$_S$-tagged anchors coprecipitated the SYN-epitope-tagged GFP, whilst this molecule was absent in precipitates from markers lacking the Nb$_S$. To rule out that on the other side the SYN-epitope from GFP-SYN perturbs the interaction between the GFP-epitope and Nb$_G$, we performed comparative coimmunprecipitation experiments using bead-bound Nb$_G$-VSR with either secreted GFP or secreted GFP-SYN, to show that the Nb$_G$-VSR binds GFP and GFP-SYN to comparable levels (**Fig. 3k**).

Finally, we performed colocalization experiments of GFP-SYN-labeled Nb$_G$-VSRs with the markers for the TGN/EE, *trans*- and *cis*-Golgi and the ER, showing that the labeling of Nb$_G$-VSR with GFP-SYN does not alter the localization of the labeled VSR (**Supplementary Fig. 4,** compare to **Fig. 2**).

Together, these results show that this second Nb$_S$-SYN nanobody-epitope pair is suitable for triggering a stable linkage between proteins, both *in vitro* and *in vivo*. The results also demonstrate that each epitope of GFP-SYN is accessible for Nb$_G$ or Nb$_S$ interaction.

The *cis*-Golgi is the target of the VSR-recycling route

To apply the strategy for nanobody triggered lockdown to the analysis of VSR recycling, we have subjected cells that coexpress Nb$_G$-tagged VSRs with the above-mentioned Nb$_S$-tagged anchors to post-translational VSR-labeling using the endocytosed dual epitope linker GFP-SYN (**Fig. 4**). First labeling of Nb$_G$-VSRs in cells coexpressing the TGN/EE anchor SYP61-

RFP-Nb$_S$ resulted in almost perfect colocalization of both signals (**Fig. 4a**), as was seen before when the non-tagged TGN/EE marker was used (**Fig. 4b**). This suggested that the endocytosed Nb$_G$-VSR-labeling agent GFP-SYN does not generally perturb membrane trafficking events in the presence of the Nb$_S$-tagged membrane anchor. In the next step, we subjected cells that coexpressed the anchors for the upstream compartments to this procedure. Here, the localization of the GFP-SYN-labeled Nb$_G$-VSRs shifted drastically and now colocalized with the *trans*-Golgi anchor ST-RFP-Nb$_S$ (**Fig. 4c,d,** compare to **4b**). Likewise, localization of GFP-SYN-labeled Nb$_G$-VSRs shifted strongly towards the *cis*-Golgi when the anchor Man1-RFP-Nb$_S$ was used for the lockdown of the labeled Nb$_G$-VSR (**Fig. 4e,f,** compare to **4b**). The colocalization of GFP-SYN-labeled VSRs and the Nb$_S$-tagged anchors for the *trans*- and *cis*-Golgi strictly depends on the presence of the second nanobody-epitope pair and was never observed when marker pendants without the Nb$_S$-tag were used (**Fig. 4d,f,** compare to **Supplementary Figs 4 and 5**). This suggests, that the VSRs did indeed recycle from the TGN/EE to the Golgi stack. To rule out that the GFP-SYN triggered crosslink between Nb$_G$-VSR and ST-RFP-Nb$_S$ or Man1-RFP-Nb$_S$ altered the Golgi-localization of the anchors in these experiments, we used the fungal toxin brefeldin A (BFA) as a diagnostic tool to confirm the Golgi localization of both anchors. In tobacco, BFA causes a fusion between Golgi stacks and the ER[37] thereby triggering a shift of signals from Golgi anchors to the ER. After BFA-treatment, the punctate signals from crosslinked GFP-SYN-labeled VSR-*cis*- and *trans*-Golgi cisternal anchors became detectable in the nuclear envelope (**Fig. 4g,h**). This demonstrated that the lockdown did not alter the localization of the Golgi anchors. In sharp contrast, a colocalization between GFP-SYN-labeled Nb$_G$-VSRs and the ER anchor Nb$_S$-RFP-CNX was never observed (**Fig. 4i**). This, however, indicates that the VSRs do not recycle to upstream compartments further than the *cis*-Golgi.

Recycled VSRs reload ligands in the *cis*-Golgi

We have previously used the soluble model ligand Aleu-RFP together with a soluble Nb$_G$-tagged LBD of a VSR that was anchored to a GFP-tagged membrane marker by nanobody-epitope interaction. There, ligand binding to the anchored LBD in a given compartment was visualized through coaccummulation/colocalization of the otherwise passing ligands[27]. We have now extended this visualization concept to the analysis of the ligand-binding capabilities of recycled full-length VSRs in the Golgi (**Fig. 5a-d**).

Hereto, we performed a *cis*-Golgi-specific dual-epitope triggered VSR-lockdown in cells, coexpressing the vacuolar reporter Aleu-RFP, Nb_G-VSR, Man1-Nb_S, which is used for the lockdown and Man1-blue fluorescent protein (BFP)2, which serves as neutral marker to verify the localization (**Fig. 5e**). The analysis clearly shows the triple-overlap of the fluorescence signals from the vacuolar reporter Aleu-RFP with the recycled GFP-SYN-labeled Nb_G-tagged VSR and the *cis*-Golgi marker Man1-BFP2, demonstrating the interaction between the recycled VSRs and the ligand in the *cis*-Golgi. The same was also seen when the VSR lockdown was performed in the *trans*-Golgi by using ST-Nb_S (**Supplementary Fig. 6a**). In sharp contrast, no colocalization between VSRs and ligands are seen in controls without the Nb_S-SYN triggered VSR lockdown: neither in the absence of the Nb_S-tagged anchor (**Fig. 5f, Supplementary Fig. 6b**) nor in the absence of the SYN-epitope, when GFP is used for the labeling instead of GFP-SYN (**Fig. 5g, Supplementary Fig. 6c**). This was to be expected, since "free" labeled VSRs localize to the TGN/EE in these controls (compare to **Fig. 2g,i and Supplementary Fig. 4a**), a compartment that does not provide ligand-binding conditions[27].

Discussion

Being only about 125 amino acids long, nanobodies are the smallest entities, capable of specific antigen recognition and binding[38]. Nanobodies are therefore ideally suited for the generation of genetically encoded molecular tools for the identification, localization and manipulation of protein function in living cells for basic research and applied sciences[39, 40]. We have previously generated VSR-sensors for a compartment-specific analysis of VSR-ligand interactions[27]. They self-assemble from soluble VSR_LBD-Nb_G fusion proteins and GFP-tagged compartment-specific membrane anchors. Using this approach, we have demonstrated that VSRs bind ligands in the ER, the *cis*- and the *trans*-Golgi and ultimately release ligands in the TGN/EE[27], thereby opening the question about the fate of VSRs after this step. The analysis of bidirectional receptor transport and receptor recycling in particular, however, is technically most challenging in living cells. It requires molecular tools that permit the strict differentiation between VSRs from the anterograde and the retrograde trafficking route.

To overcome these constraints, we have taken advantage of the TGN as also being the EE by incubating Nb_G-VSR-expressing cells with exogenously applied protoplast-secreted GFP to

trigger compartment-specific labeling of VSRs in the TGN/EE by its endocytic uptake. This ensures labeling of only those VSRs that have reached the recycling point, whereas newly synthesized VSRs from the anterograde route remain invisible. Most interesting for future application however is, the simultaneous use of two different Nb-epitope pairs *in vivo*. This allows for triggering a protein-specific lockdown of recycled Nb_G-VSRs at Nb_S-tagged membrane proteins by the exogenously applied dual epitope linker peptide GFP-SYN. Using this strategy, we demonstrated retrograde VSR recycling to the *cis*-Golgi as being the most distant compartment upstream of the TGN/EE. Together with the fact that VSRs reload ligands after recycling, this supports the concept of bidirectional VSR transport.

Based on our investigations we now present the following concept for the operation of VSR-mediated vacuolar sorting in the plant endomembrane system (**Fig. 6**). Newly synthesized VSRs bind ligands in the early secretory pathway[23, 27, 41, 42] at neutral pH[21, 26, 43] and transport them to the TGN/EE, where they ultimately release their ligands[27], due to a shift in compartmental pH. The TGN/EE is the most acidic compartment en route to the vacuole[26, 43, 44], since it harbors characteristic V-ATPases[28] that are absent from the MVBs/LEs[45], thus preventing further acidification. Therefore, the locations for binding and release of ligands are in agreement with the initially recorded pH dependency for VSR-ligand interactions *in vitro*[21]. After release in the TGN/EE, ligands progress without further involvement of VSRs onwards to the lytic vacuole by default[27]. This occurs due to a maturation event of the TGN/EE that results in the biogenesis of a MVB/LE[46, 47]. While fusion of the MVB/LE with the vacuole represents the final step in the vacuolar delivery of ligands[46] it is unrelated to VSR function. VSRs, however, recycle from the TGN/EE back to the *cis*-Golgi, for ligand reloading and renewed rounds of ligand delivery to the TGN/EE. Considering the life span of VSRs greatly exceeding the time it takes for a round of transport, it is plausible to assume that cycling VSRs bear the brunt of the ligand transport from the Golgi to the TGN/EE with only a minor contribution of *de novo* synthesized VSRs, binding their ligands in the ER.

Methods

Plant materials

Nicotiana tabacum L. SR1 was grown on Murashige and Skoog medium supplemented with 2 % (w/v) sucrose, 0.5 g L^{-1} MES and 0.8 % (w/v) Agar at pH 5.7 in 16/8 h light–dark cycles at 22 °C.

Plasmid constructs

All constructs are given in Supplementary Table 1. DNA manipulations were performed according to established procedures, using pGreenII[48]-based vectors and *Escherichia coli* MC1061. An anti-SYN nanobody sequence was generated by reverse-translation of the amino acid sequence NbSyn87 without the C-terminal 6xHis tag[32], optimized for *Arabidopsis*-specific codon usage (EMBOSS Backtranseq), modified with an N-terminal HA-tag and chemically synthesized (GeneArt Gene Synthesis). The blue fluorescent protein mTagBFP2 (GenBank AIQ82697.1) was also generated by reverse translation of the amino acid sequence, optimized for *Arabidopsis*-specific codon usage (EMBOSS Backtranseq) and chemically synthesized (GeneArt Gene Synthesis).

All VSR constructs were assembled from AtVSR4 (GenBank accession no. NM_127036) and fused to the GFP nanobody[27]. The red fluorescent compartment specific anchors carry a monomeric RFP[48]. The correct localization of all generated VSR-/marker-fluorophore fusions was verified.

Protoplast isolation and gene expression

Protoplasts were isolated from perforated leafs by over-night incubation in incubation buffer (3,05 g L^{-1} Gamborg B5 Medium, 500 mg L^{-1} MES, 750 mg L^{-1} $CaCl_2 \cdot 2H_2O$, 250 mg L^{-1} NH_4NO_3 adjusted to pH 5.7 with KOH) supplemented with 0.2 % w/v macerozyme and 0.4 % w/v cellulase) at 25 °C in the dark. They were rebuffered by washing them three times in 50 mL electrotransfection-buffer (137 g L^{-1} sucrose, 2.4 g L^{-1} HEPES, 6 g L^{-1} KCl, 600 mg L^{-1} $CaCl_2 \cdot 2H_2O$ adjusted to pH 7.2 with KOH). 150 µL protoplasts in a total volume of 600 µL electrotransfection-buffer were electrotransfected with 1–10 µg plasmid DNA using the square-wave pulse generator EPI-2,500 (Fischer) applying a pulse at 130 V for 10 ms. After transfection, each sample was supplemented with 2 ml incubation buffer and incubated for 18–24 h at 25 °C in the dark.

Biosynthesis of fluorescent reporters

Protoplast-secreted reporters (GFP/GFP-SYN) for endocytic uptake experiments were obtained from cell-free culture medium after expression, harvesting, sonication and clearance, ruling out contaminations with reporter-synthesizing cells during uptake experiments. For the endocytic uptake, populations of protoplasts expressing Nb_G/Nb_S-tagged constructs were supplemented with cleared reporter-containing medium for 20 h.

Confocal microscopy and statistical analysis

Image acquisition was performed using a Leica TCS-SP8 confocal laser-scanning microscope, equipped with a ×63 (1.2 numerical aperture) water immersion objective. Fluorophores were excited (ex) and emission (em) was detected in sequential line scanning mode using HyD detectors: mTagBFP2 (ex/em, 405 nm/407-452 nm), GFP (ex/em, 488 nm/496–525 nm) and RFP (ex/em, 561 nm/569–636 nm). Pinholes were adjusted to 1 Airy unit for each wavelength. Post-acquisition image processing and assembly of figures was performed using Adobe Photoshop CS3 and CorelDraw X8.

The linear Pearson's correlation coefficient (r_P) and the nonlinear Spearman's rank coefficient (r_S) of green and red fluorescent signals was calculated with the PSC colocalization plug-in (http://www.cpib.ac.uk/~afrench/coloc.html) for ImageJ[48]. The threshold levels were set to 10. For the statistics, 10 individual cells were analyzed and the correlation coefficients are shown as mean values with standard errors of the mean. Statistical significance was calculated with R using an unpaired, two tailed *t-test*[49].

Analysis of the SYN-nanobody epitope interaction

Cell-free culture medium was harvested after flotation of electrotransfected tobacco protoplasts for 5 min at 80 g in sealed pre-punctured tubes, using insulin syringes. Afterwards, cells were harvested by addition of 7.5 mL of 250 mM NaCl, sedimentation for 7 min at 80 g, followed by removal of the supernatant. The culture medium was cleared by centrifugation at 20,000 g for 15 min at 4 °C and diluted with α-amylase extraction buffer (50 mM acid malic, 50 mM sodium chloride, 2 mM calcium chloride, 0.02% (w/v) sodium azide). Cell samples were extracted in a total volume of 250 µg with α-amylase extraction buffer, sonicated and

centrifuged at 20,000 g for 15 min at 4 °C. The supernatant was recovered and employed for the reporter assay and SDS-PAGE/Western blot (SDS-PAGE/WB).

The quantitative reporter transport analysis was performed in samples from the cell extracts and the culture medium, using the α-amylase reagent kit (Megazyme R-CAAR4). Individual enzymatic assays were started by addition of 30 µl of substrate solution to 30 µl of extracted and diluted sample. After incubation at 40 °C, the reaction was stopped by the addition of 150 µL of 1% w/v Trizma base. 200 µL of the reaction was transferred into a well of a microtitre plate to measure absorbance at 405 nm[50].

For SDS-PAGE/WB, samples were mixed 1:1 with freshly prepared 2× Xtreme loading dye (900 µL of sample buffer (0.1 % (w/v) bromophenol blue, 5 mM EDTA, 200 mM Tris-HCl, pH 8.8, 1 M sucrose) supplemented with 300 µL 10 % w/v SDS and 20 µL of 1 M DTT), incubated for 5 min at 95 °C and loaded onto 10 % (w/v) SDS-polyacrylamide gels. After electrophoretic separation at 40 mA, proteins were electroblotted onto nitrocellulose membranes at 200 mA. For immunodetection, membranes were incubated in blocking solution (TBS-T (6.06 g L^{-1} Trizma base, 8.88 g L^{-1} NaCl, 0.05 % (v/v) Tween-20), supplemented with 5 % (w/v) BSA) for 30 min and then probed with the following antibodies diluted in blocking solution: rabbit polyclonal anti-GFP (Life Technologies A6455, 1:10,000), rat monoclonal anti-RFP (ChromoTek 5F8, 1:1,000) and rat monoclonal anti-HA–Peroxidase (Roche 12013819001, 1:2,500). Uncropped immunoblots are given in Supplementary Fig.7.

Immunoprecipitation

For anchor-epitope and VSR-epitope interaction anchors/VSRs were expressed *in vivo* and extracted 1:1 in 2× binding buffer (40 mM HEPES, 300 mM NaCl, 2 mM $CaCl_2$, 2 mM $MgCl_2$, pH 7.1) with 2% (v/v) CHAPS[27]. Immunoprecipitation was performed for 1 h with RFP-Trap®_MA (ChromoTek, rxns-20) for the anchors and with Pierce™ Anti-HA Magnetic Beads (Life Technologies, 88836) for the VSRs at 4°C. Beads were washed three times with binding buffer containing 0.4% (v/v) CHAPS and afterwards incubated with GFP-SYN/GFP, which were in parallel samples transiently expressed and recovered from the medium, overnight at 4 °C. SDS-PAGE/WB was performed as described above.

Data availability

Data will be available to readers on request

References

1. Paez Valencia J, Goodman K, Otegui MS. Endocytosis and Endosomal Trafficking in Plants. *Annual review of plant biology* **67**, 309-335 (2016).

2. Carmona-Gutierrez D, Hughes AL, Madeo F, Ruckenstuhl C. The crucial impact of lysosomes in aging and longevity. *Ageing Res Rev* **32**, 2-12 (2016).

3. Jackson MP, Hewitt EW. Cellular proteostasis: degradation of misfolded proteins by lysosomes. *Essays Biochem* **60**, 173-180 (2016).

4. Schroder B, Saftig P. Intramembrane proteolysis within lysosomes. *Ageing Res Rev* **32**, 51-64 (2016).

5. Robinson DG, Neuhaus JM. Receptor-mediated sorting of soluble vacuolar proteins: myths, facts, and a new model. *J Exp Bot* **67**, 4435-4449 (2016).

6. Robinson DG, Pimpl P. Receptor-mediated transport of vacuolar proteins: a critical analysis and a new model. *Protoplasma* **251**, 247-264 (2014).

7. Goldstein JL, Brown MS. Binding and degradation of low density lipoproteins by cultured human fibroblasts. Comparison of cells from a normal subject and from a patient with homozygous familial hypercholesterolemia. *J Biol Chem* **249**, 5153-5162 (1974).

8. Gonzalez-Noriega A, Grubb JH, Talkad V, Sly WS. Chloroquine inhibits lysosomal enzyme pinocytosis and enhances lysosomal enzyme secretion by impairing receptor recycling. *J Cell Biol* **85**, 839-852 (1980).

9. Hoflack B, Kornfeld S. Purification and characterization of a cation-dependent mannose 6-phosphate receptor from murine P388D1 macrophages and bovine liver. *J Biol Chem* **260**, 12008-12014 (1985).

10. Mellman I, Fuchs R, Helenius A. Acidification of the endocytic and exocytic pathways. *Annu Rev Biochem* **55**, 663-700 (1986).

11. Rome LH, Weissmann B, Neufeld EF. Direct demonstration of binding of a lysosomal enzyme, alpha-L-iduronidase, to receptors on cultured fibroblasts. *Proc Natl Acad Sci USA* **76**, 2331-2334 (1979).

12. Sahagian GG, Neufeld EF. Biosynthesis and turnover of the mannose 6-phosphate receptor in cultured Chinese hamster ovary cells. *J Biol Chem* **258**, 7121-7128 (1983).

13. Brown MS, Anderson RG, Basu SK, Goldstein JL. Recycling of cell-surface receptors: observations from the LDL receptor system. *Cold Spring Harb Symp Quant Biol* **46 Pt 2**, 713-721 (1982).

14. Duncan JR, Kornfeld S. Intracellular movement of two mannose 6-phosphate receptors: return to the Golgi apparatus. *J Cell Biol* **106**, 617-628 (1988).

15. Ahmed SU, Bar-Peled M, Raikhel NV. Cloning and subcellular location of an Arabidopsis receptor-like protein that shares common features with protein-sorting receptors of eukaryotic cells. *Plant Physiol* **114**, 325-336 (1997).

16. Paris N*, et al.* Molecular cloning and further characterization of a probable plant vacuolar sorting receptor. *Plant Physiol* **115**, 29-39 (1997).

17. Cao X, Rogers SW, Butler J, Beevers L, Rogers JC. Structural requirements for ligand binding by a probable plant vacuolar sorting receptor. *Plant Cell* **12**, 493-506 (2000).

18. Luo F, Fong YH, Zeng Y, Shen J, Jiang L, Wong KB. How vacuolar sorting receptor proteins interact with their cargo proteins: crystal structures of apo and cargo-bound forms of the protease-associated domain from an Arabidopsis vacuolar sorting receptor. *Plant Cell* **26**, 3693-3708 (2014).

19. daSilva LL, Foresti O, Denecke J. Targeting of the plant vacuolar sorting receptor BP80 is dependent on multiple sorting signals in the cytosolic tail. *Plant Cell* **18**, 1477-1497 (2006).

20. Happel N, Honing S, Neuhaus JM, Paris N, Robinson DG, Holstein SE. Arabidopsis micro A-adaptin interacts with the tyrosine motif of the vacuolar sorting receptor VSR-PS1. *Plant J* **37**, 678-693 (2004).

21. Kirsch T, Paris N, Butler JM, Beevers L, Rogers JC. Purification and initial characterization of a potential plant vacuolar targeting receptor. *Proc Natl Acad Sci USA* **91**, 3403-3407 (1994).

22. Shen J, Ding Y, Gao C, Rojo E, Jiang L. N-linked glycosylation of AtVSR1 is important for vacuolar protein sorting in Arabidopsis. *Plant J* **80**, 977-992 (2014).

23. Watanabe E*, et al.* An ER-Localized Form of PV72, a Seed-Specific Vacuolar Sorting Receptor, Interferes the Transport of an NPIR-Containing Proteinase in Arabidopsis Leaves. *Plant Cell Physiol* **45**, 9-17 (2004).

24. Li YB*, et al.* BP-80 and Homologs are Concentrated on Post-Golgi, Probable Lytic Prevacuolar Compartments. *Plant Cell Physiol* **43**, 726-742 (2002).

25. Tse YC*, et al.* Identification of multivesicular bodies as prevacuolar compartments in Nicotiana tabacum BY-2 cells. *Plant Cell* **16**, 672-693 (2004).

26. Martiniere A*, et al.* In Vivo Intracellular pH Measurements in Tobacco and Arabidopsis Reveal an Unexpected pH Gradient in the Endomembrane System. *Plant Cell* **25**, 4028-4043 (2013).

27. Künzl F, Früholz S, Fäßler F, Li B, Pimpl P. Receptor-mediated sorting of soluble vacuolar proteins ends at the trans-Golgi network/early endosome. *Nature Plants* **2**, 16017 (2016).

28. Dettmer J, Hong-Hermesdorf A, Stierhof YD, Schumacher K. Vacuolar H+-ATPase activity is required for endocytic and secretory trafficking in Arabidopsis. *Plant Cell* **18**, 715-730 (2006).

29. Lam SK*, et al.* Rice SCAMP1 defines clathrin-coated, trans-golgi-located tubular-vesicular structures as an early endosome in tobacco BY-2 cells. *Plant Cell* **19**, 296-319 (2007).

30. Rothbauer U*, et al.* Targeting and tracing antigens in live cells with fluorescent nanobodies. *Nature methods* **3**, 887-889 (2006).

31. Kubala MH, Kovtun O, Alexandrov K, Collins BM. Structural and thermodynamic analysis of the GFP:GFP-nanobody complex. *Protein Sci* **19**, 2389-2401 (2010).

32. Guilliams T*, et al.* Nanobodies raised against monomeric alpha-synuclein distinguish between fibrils at different maturation stages. *J Mol Biol* **425**, 2397-2411 (2013).

33. Saint-Jean B, Seveno-Carpentier E, Alcon C, Neuhaus JM, Paris N. The cytosolic tail dipeptide Ile-Met of the pea receptor BP80 is required for recycling from the prevacuole and for endocytosis. *Plant Cell* **22**, 2825-2837 (2010).

34. Shen Y*, et al.* The Rice RMR1 Associates with a Distinct Prevacuolar Compartment for the Protein Storage Vacuole Pathway. *Mol Plant* **4**, 854-868 (2011).

35. Niemes S*, et al.* Retromer recycles vacuolar sorting receptors from the trans-Golgi network. *Plant J* **61**, 107-121 (2010).

36. Rogers JC. Two barley alpha-amylase gene families are regulated differently in aleurone cells. *J Biol Chem* **260**, 3731-3738 (1985).

37. Ritzenthaler C*, et al.* Reevaluation of the effects of brefeldin A on plant cells using tobacco Bright Yellow 2 cells expressing Golgi-targeted green fluorescent protein and COPI antisera. *Plant Cell* **14**, 237-261 (2002).

38. Hamers-Casterman C*, et al.* Naturally occurring antibodies devoid of light chains. *Nature* **363**, 446-448 (1993).

39. Steeland S, Vandenbroucke RE, Libert C. Nanobodies as therapeutics: big opportunities for small antibodies. *Drug Discov Today* **21**, 1076-1113 (2016).

40. Dmitriev OY, Lutsenko S, Muyldermans S. Nanobodies as Probes for Protein Dynamics in Vitro and in Cells. *J Biol Chem* **291**, 3767-3775 (2016).

41. Niemes S*, et al.* Sorting of plant vacuolar proteins is initiated in the ER. *Plant J* **62**, 601-614 (2010).

42. Gershlick DC*, et al.* Golgi-Dependent Transport of Vacuolar Sorting Receptors Is Regulated by COPII, AP1, and AP4 Protein Complexes in Tobacco. *Plant Cell* **26**, 1308-1329 (2014).

43. Shen J*, et al.* Organelle pH in the *Arabidopsis* Endomembrane System. *Mol Plant* **6**, 1419-1437 (2013).

44. Luo Y*, et al.* V-ATPase activity in the TGN/EE is required for exocytosis and recycling in Arabidopsis. *Nature Plants* **1**, 15094 (2015).

45. Viotti C*, et al.* The Endoplasmic Reticulum Is the Main Membrane Source for Biogenesis of the Lytic Vacuole in Arabidopsis. *Plant Cell* **25**, 3434-3449 (2013).

46. Scheuring D*, et al.* Multivesicular bodies mature from the trans-Golgi network/early endosome in Arabidopsis. *Plant Cell* **23**, 3463-3481 (2011).

47. Singh MK*, et al.* Protein delivery to vacuole requires SAND protein-dependent Rab GTPase conversion for MVB-vacuole fusion. *Curr Biol* **24**, 1383-1389 (2014).

48. Scheuring D*, et al.* Ubiquitin initiates sorting of Golgi and plasma membrane proteins into the vacuolar degradation pathway. *BMC plant biology* **12**, 164 (2012).

49. Team RDC. R: A Language and Environment for Statistical Computing. http://wwwR-projectorg, (2008).

50. Foresti O, daSilva LL, Denecke J. Overexpression of the Arabidopsis syntaxin PEP12/SYP21 inhibits transport from the prevacuolar compartment to the lytic vacuole in vivo. *Plant Cell* **18**, 2275-2293 (2006).

Acknowledgments

We thank Diana Vranjkovic for technical help. The financial support of the Deutsche Forschungsgemeinschaft (PI 769/1-2 and the Collaborative Research Centre SFB 1101 "Molecular Encoding of Specificity in Plant Processes" and TP A03) and the Deutscher

Akademischer Austauschdienst (Project 57057314 & 57219822) and the Southern University of Science and Technology (SUSTech)/SUSTech-PKU Institute of Plant and Food Science (IPFS) Start-up fund is gratefully acknowledged. P.P. is indebted to L. Kilmister for inspirations and support ♠.

Author contributions

S.F., F.F., Ü.K. and P.P. designed and analysed the experiments. S.F. performed experiments. S.F. and P.P. wrote the manuscript, P.P. conceived the study.

Competing interests

The authors declare no competing financial interests.

Figure Legends

Figure 1. Post-translational GFP-labeling via nanobody-epitope interaction. (**a**) Translational GFP-labeling of VSRs. (**b**) Post-translational GFP-labeling of a Nb_G-tagged VSR in the TGN/EE by endocytosed GFP. (**c-g**) Post-translational GFP-labeling of compartment-specific Nb_G-tagged red fluorescent membrane anchors (red) by endocytosed GFP (green) in (**c**) the TGN/EE and (**d**) the MVB/LE. Endocytosed GFP does not reach (**e**) the *trans*-Golgi, (**f**) the *cis*-Golgi nor (**g**) the ER. (**h-j**) Post-translational GFP-labeling by coexpression of secreted (Sec)-GFP (green) and Nb_G-tagged red fluorescent membrane anchors (red) for (**h**) the *trans*-Golgi, (**i**) the *cis*-Golgi and (**j**) the ER. Insets in (**g**,**j**) show cortical sections, others show magnifications. Scale bars 10µm, insets 5µm.

Figure 2. Localization of post-translationally labeled Nb_G-tagged VSRs. (**a**) Cycling Nb_G-tagged red fluorescent VSRs are (**b**) post-translationally labeled by endocytosed GFP. (**c)** GFP-labeled red fluorescent Nb_G-tagged VSRs. (**d**) Pearson's (r_P) and Spearman's (r_S) correlation (PSC) coefficients of Nb_G-RFP-VSRs and labeling GFP. Data are presented as average ± s.e.m. of 10 individual cells. The graph shows a representative sample of two independent experiments.

(**e,f**) Colocalization of post-translationally GFP-labeled non-fluorescent cycling Nb_G-tagged VSRs (Nb_G-VSR) with red fluorescent compartmental markers (CM) for (**g,i**) the TGN/EE, (**h,i)** MVBs/LEs and vacuole, (**j,l**) the *trans*-/ and (**k,l**) *cis*-Golgi and (**m**) the ER. (**i,l**) PSC coefficients of the labeled Nb_G-VSR and coexpressed markers RFP-SYP61, Aleu-RFP, Man1-RFP and ST-RFP are calculated and presented as in (**d**). Graphs show a representative sample of two independent experiments. Labeled Nb_G-VSRs colocalize with the TGN/EE marker but not with markers for MVB/LE and vacuole and the *cis*-/*trans*-Golgi. (**i)** Significance was calculated using unpaired, two tailed *t-test* (n=10, P<0.001, ***, highly significant). Scale bars 10µm, insets 5µm. Insets show magnifications.

Figure 3. Nanobody triggered lockdown of recycled VSRs. (**a**) Coexpression of Nb_G-VSRs with red fluorescent Nb_S-tagged compartmental markers (anchors) and (**b**) post-translational labeling with the dual-epitope GFP-SYN in the TGN/EE to (**c**) anchor VSRs upon recycling. (**d,e**) Nb_S-SYN epitope interaction occurs in the endomembrane system. (**d**) SYN epitope-tagged secreted amylase (amy-SYN) is (**e**) rerouted to the lytic vacuole (LV) upon Aleu-RFP-Nb_S triggers attachment of the vacuolar sorting signal (Aleu). (**f**) Coexpression of amy-SYN with different amounts of Aleu-RFP-Nb_S. Upper panel: secretion index (SI); lower panel: corresponding immunoblot (α-RFP). (**g-j**) Co-immunoprecipitations revealing Nb_S-SYN epitope interaction. RFP-tagged markers and anchors for (**g**) ER, (**h**) *cis*-Golgi, (**i**) *trans*-Golgi and (**j**) TGN/EE were immunoprecipitated (IP, α-RFP), incubated with GFP-SYN and immunoblotted (IB). Total extracts (T) and immunoprecipitates (IP) were probed to detect markers, anchors (α-RFP) and co-precipitated GFP-SYN (α-GFP). (**k**) Co-immunoprecipitation revealing Nb_G-GFP epitope interaction. Expressed Nb_G-VSRs or samples from mock-transfected cells were immunoprecipitated (IP, α-HA), incubated with GFP or GFP-SYN and immunoblotted (IB). Total extracts (T) and immunoprecipitates (IP) were probed to detect VSRs (α-HA) and co-precipitated GFP (white arrowhead) or GFP-SYN (black arrowhead) (α-GFP), respectively.

Figure 4 The *cis*-Golgi stack is the target of VSR recycling. GFP-SYN labeled Nb_G-VSR is locked to the anchors in (**a**) the TGN/EE (SYP61-RFP-Nb_S), and after recycling to (**c**) *trans*-Golgi (ST-RFP-Nb_S) and (**e**) *cis*-Golgi (Man1-RFP-Nb_S) anchors but does not reach (**i**) the ER anchor Nb_S-GFP-CNX. PSC coefficients of the labeled Nb_G-VSR with (**b**) the marker Syp61-

RFP or the anchor Syp61-RFP-Nb_S, presented/calculated as in (**2g**) with n=10, P≥0.05, n.s., not significant, (**d**) the marker ST-RFP or the anchor ST-RFP-Nb_S, presented/calculated as above with n=10, P<0.001, ***, highly significant and (**f**) the marker Man1-RFP or the anchor Man1-RFP-Nb_S, presented/calculated as in (**d**). Graphs show a representative sample of two independent experiments. (**g,h**) BFA-treatment of samples from (**c,e**) for 1 h at 20 µM triggers fusion of Golgi with ER, verifying Golgi-localization of locked VSRs from (**c,e**). Scale bars 10µm, insets 5µm, showing magnifications.

Figure 5. VSRs bind ligands after recycling. (**a**) Targeted VSR sensors (Nb_G-LDB) were shown to bind Aleu-RFP ligands in the Golgi[27] (**b**) GFP-SYN labeled Nb_G-VSRs are locked to the anchor Man1-Nb_S in the *cis*-Golgi, positively identified by the marker Man1-BFP2. Ligand-binding of recycled full-length VSRs is assessed by colocalization with ligands (Aleu-RFP). Controls with cycling VSRs that lack (**c**) the anchor or (**d**) the SYN epitope at the labeling GFP for the VSR lockdown, result in VSR localization at the TGN/EE, which does not promote ligand binding. (**e**) GFP-SYN labeled Nb_G-VSRs are locked after recycling in the *cis*-Golgi and colocalize with the Golgi marker Man1-BFP2 and bind the ligand Aleu-RFP, as shown by the overlapping signal peaks in the line intensity plot (see **b**). (**f,g**) Not locked VSRs (see **c** and **d**) do not localize to the Golgi and thus do not bind the ligand Aleu-RFP as judged by the separated peaks in the line intensity plots. Scale bars 10µm, insets 5µm, showing magnifications.

Figure 6. Model for receptor mediated vacuolar sorting in plants. VSRs bind ligands in the early secretory pathway and transport them to the TGN/EE. There, the ligands are released from the VSR. Next, VSRs are recycled back to the *cis*-Golgi stack for further rounds of ligand transport. Post-TGN/EE transport of released vacuolar cargo ligands but also endocytosed proteins occurs independent of VSRs and travel to the lytic vacuole per default. Transport in this route is mediated by multivesicular bodies, the late endosomes (MVBs/LEs). They bud off the TGN/EE in a maturation-based step and confer cargo delivery by their ultimate fusion with the lytic vacuole (LV).

Figure 1

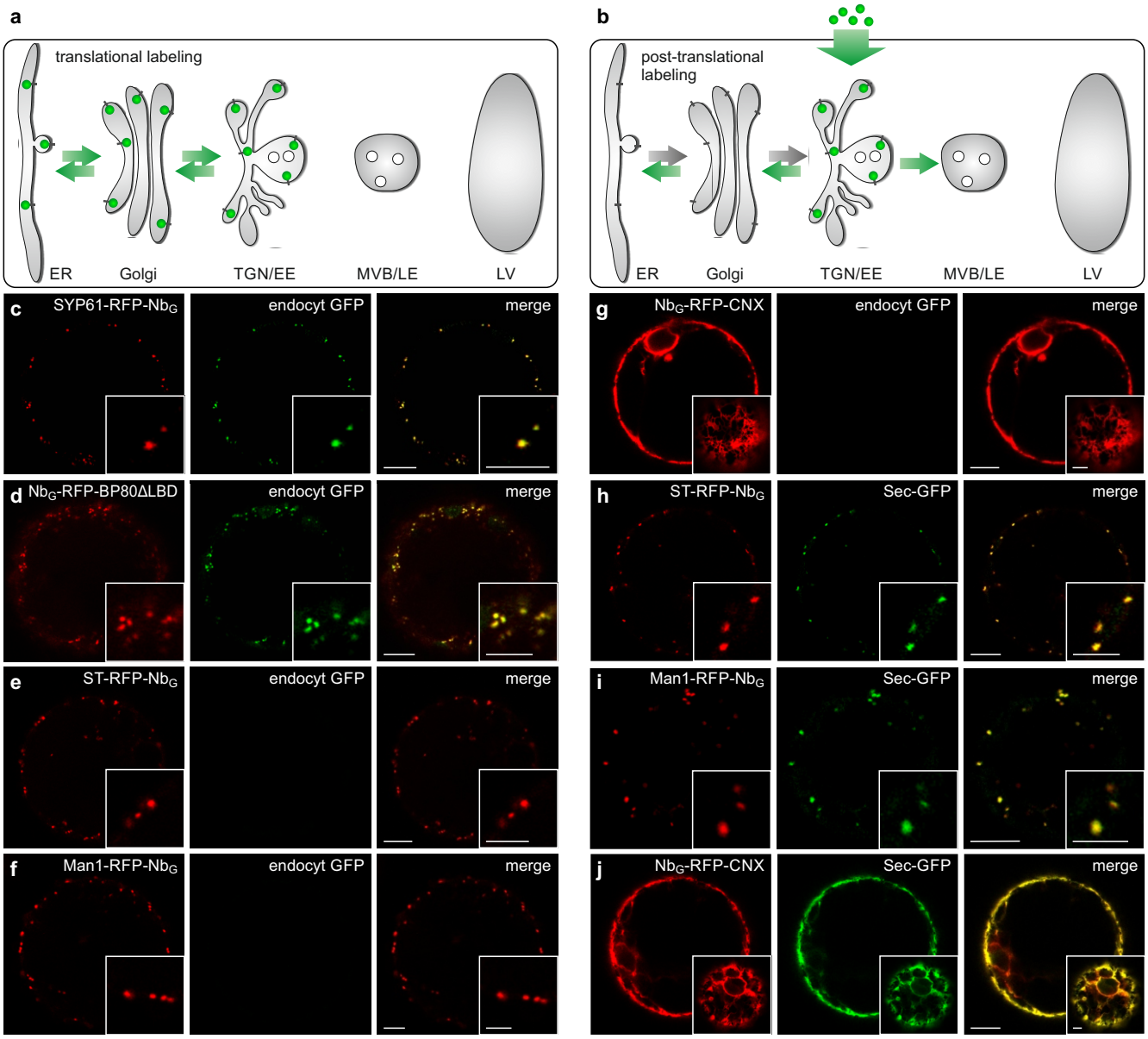

Figure 1. Post-translational GFP-labeling via nanobody-epitope interaction. (**a**) Translational GFP-labeling of VSRs. (**b**) Post-translational GFP-labeling of a Nb_G-tagged VSR in the TGN/EE by endocytosed GFP. (**c-g**) Post-translational GFP-labeling of compartment-specific Nb_G-tagged red fluorescent membrane anchors (red) by endocytosed GFP (green) in (**c**) the TGN/EE and (**d**) the MVB/LE. Endocytosed GFP does not reach (**e**) the *trans*-Golgi, (**f**) the *cis*-Golgi nor (**g**) the ER. (**h-j**) Post-translational GFP-labeling by coexpression of secreted (Sec)-GFP (green) and Nb_G-tagged red fluorescent membrane anchors (red) for (**h**) the *trans*-Golgi, (**i**) the *cis*-Golgi and (**j**) the ER. Insets in (**g**,**j**) show cortical sections, others show magnifications. Scale bars 10µm, insets 5µm.

Figure 2

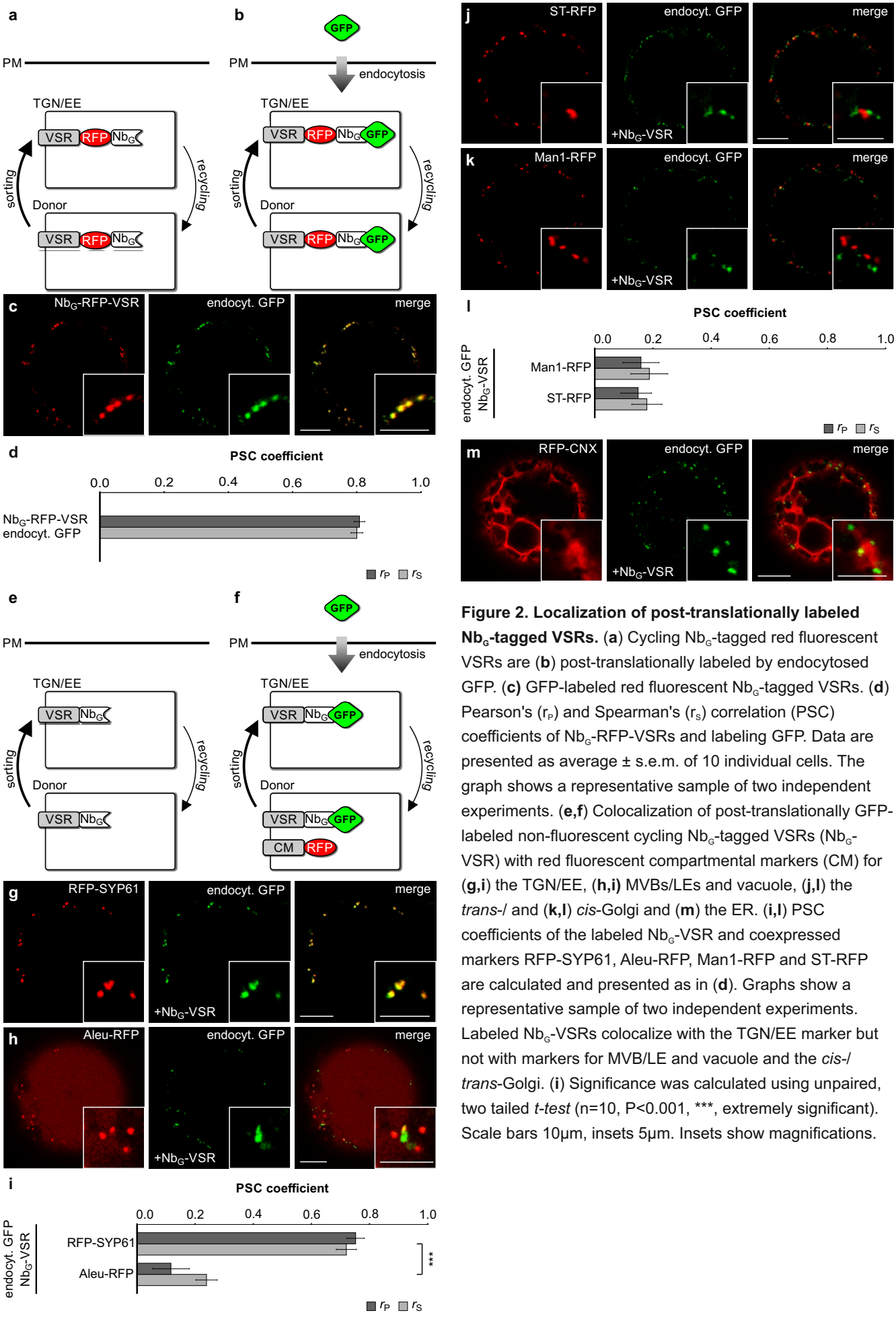

Figure 2. Localization of post-translationally labeled Nb_G-tagged VSRs. (**a**) Cycling Nb_G-tagged red fluorescent VSRs are (**b**) post-translationally labeled by endocytosed GFP. (**c**) GFP-labeled red fluorescent Nb_G-tagged VSRs. (**d**) Pearson's (r_P) and Spearman's (r_S) correlation (PSC) coefficients of Nb_G-RFP-VSRs and labeling GFP. Data are presented as average ± s.e.m. of 10 individual cells. The graph shows a representative sample of two independent experiments. (**e,f**) Colocalization of post-translationally GFP-labeled non-fluorescent cycling Nb_G-tagged VSRs (Nb_G-VSR) with red fluorescent compartmental markers (CM) for (**g,i**) the TGN/EE, (**h,i**) MVBs/LEs and vacuole, (**j,l**) the *trans*-/ and (**k,l**) *cis*-Golgi and (**m**) the ER. (**i,l**) PSC coefficients of the labeled Nb_G-VSR and coexpressed markers RFP-SYP61, Aleu-RFP, Man1-RFP and ST-RFP are calculated and presented as in (**d**). Graphs show a representative sample of two independent experiments. Labeled Nb_G-VSRs colocalize with the TGN/EE marker but not with markers for MVB/LE and vacuole and the *cis*-/*trans*-Golgi. (**i**) Significance was calculated using unpaired, two tailed *t-test* (n=10, P<0.001, ***, extremely significant). Scale bars 10µm, insets 5µm. Insets show magnifications.

Figure 3

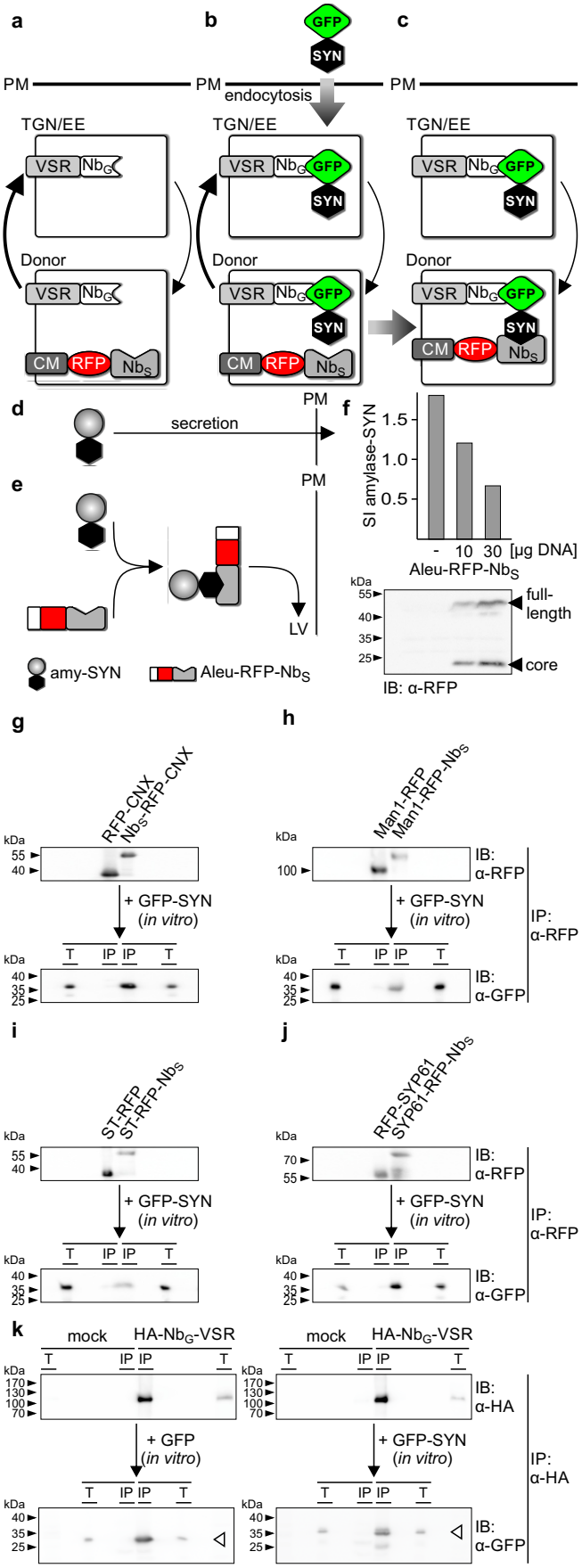

Figure 3. Nanobody-triggered lockdown of recycled VSRs. (**a**) Coexpression of Nb$_G$-VSRs with red fluorescent Nb$_S$-tagged compartmental markers (anchor) and (**b**) post-translational labeling with the dual-epitope GFP-SYN in the TGN/EE to (**c**) anchor VSRs upon recycling. (**d**,**e**) Nb$_S$-SYN epitope interaction occurs in the endomembrane system. (**d**) SYN epitope-tagged secreted amylase (amy-SYN) is (**e**) rerouted to the LV upon Aleu-RFP-Nb$_S$ triggers attachment of the vacuolar sorting signal (Aleu). (**f**) Coexpression of amy-SYN with different amounts of Aleu-RFP-Nb$_S$. Upper panel: secretion index (SI); lower panel: corresponding immunoblot (α-RFP). (**g-j**) Co-immunoprecipitations revealing Nb$_S$-SYN epitope interaction. RFP-tagged markers and anchors for (**g**) ER, (**h**) *cis*-Golgi, (**i**) *trans*-Golgi and (**j**) TGN/EE were immunoprecipitated (IP, α-RFP), incubated with GFP-SYN and immunoblotted (IB). Total extracts (T) and immunoprecipitates (IP) were probed to detect markers, anchors (α-RFP) and co-precipitated GFP-SYN (α-GFP). (**k**) Co-immunoprecipitation revealing Nb$_G$-GFP epitope interaction. Expressed Nb$_G$-VSRs or samples from mock-transfected cells were immunoprecipitated (IP, α-HA), incubated with GFP or GFP-SYN and immunoblotted (IB). Total extracts (T) and immunoprecipitates (IP) were probed to detect VSRs (α-HA) and co-precipitated GFP (white arrowhead) or GFP-SYN (black arrowhead) (α-GFP), respectively.

Figure 4

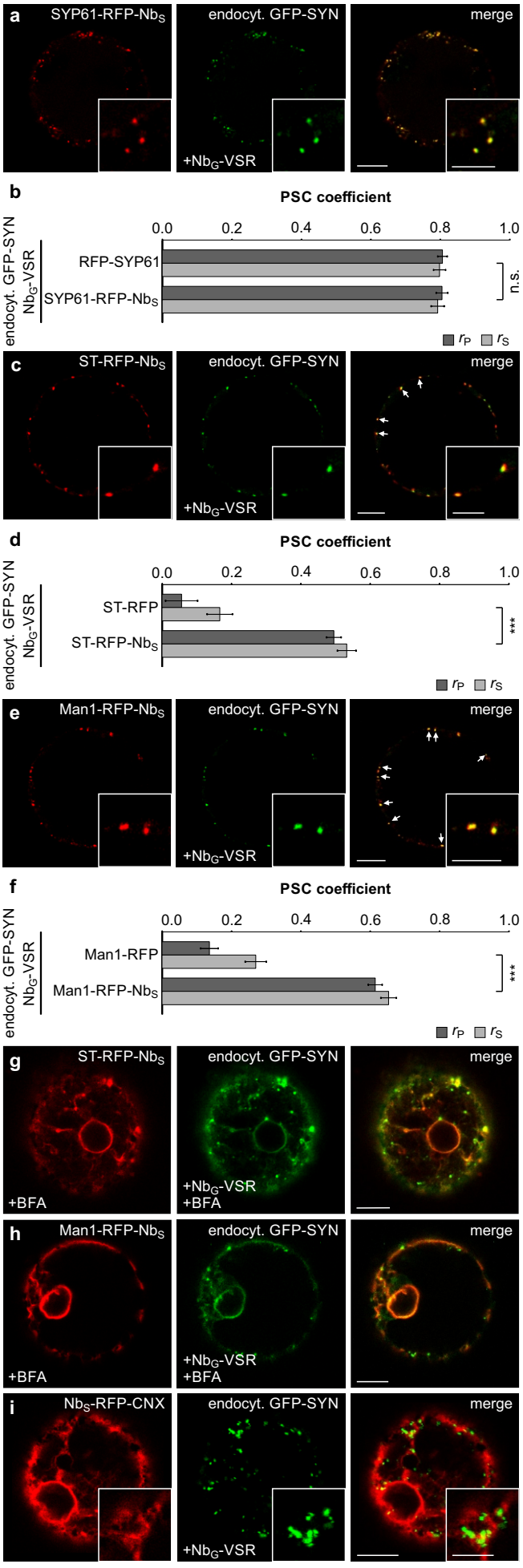

Figure 4 The *cis*-Golgi stack is the target of VSR recycling. GFP-SYN labeled Nb_G-VSR is locked to the anchors in (**a**) the TGN/EE (SYP61-RFP-Nb_S), and after recycling to (**c**) *trans*-Golgi (ST-RFP-Nb_S) and (**e**) *cis*-Golgi (Man1-RFP-Nb_S) but does not reach (**i**) the ER anchor Nb_S-GFP-CNX. PSC coefficients of the labeled Nb_G-VSR with (**b**) the marker Syp61-RFP or the anchor Syp61-RFP-Nb_S, presented/calculated as in (**2i**) with n=10, P≥0.05, n.s., not significant, (**d**) the marker ST-RFP or the anchor ST-RFP-Nb_S, presented/calculated as above with n=10, P<0.001, ***, extremely significant and (**f**) the marker Man1-RFP or the anchor Man1-RFP-Nb_S, presented/ calculated as in (**d**). Graphs show a representative sample of two independent experiments. (**g,h**) BFA-treatment of samples from (**c,e**) for 1 h at 20 µM triggers fusion of Golgi with ER, verifying Golgi-localization of locked VSRs from (**c,e**). Scale bars 10µm, insets 5µm, showing magnifications.

Figure 5

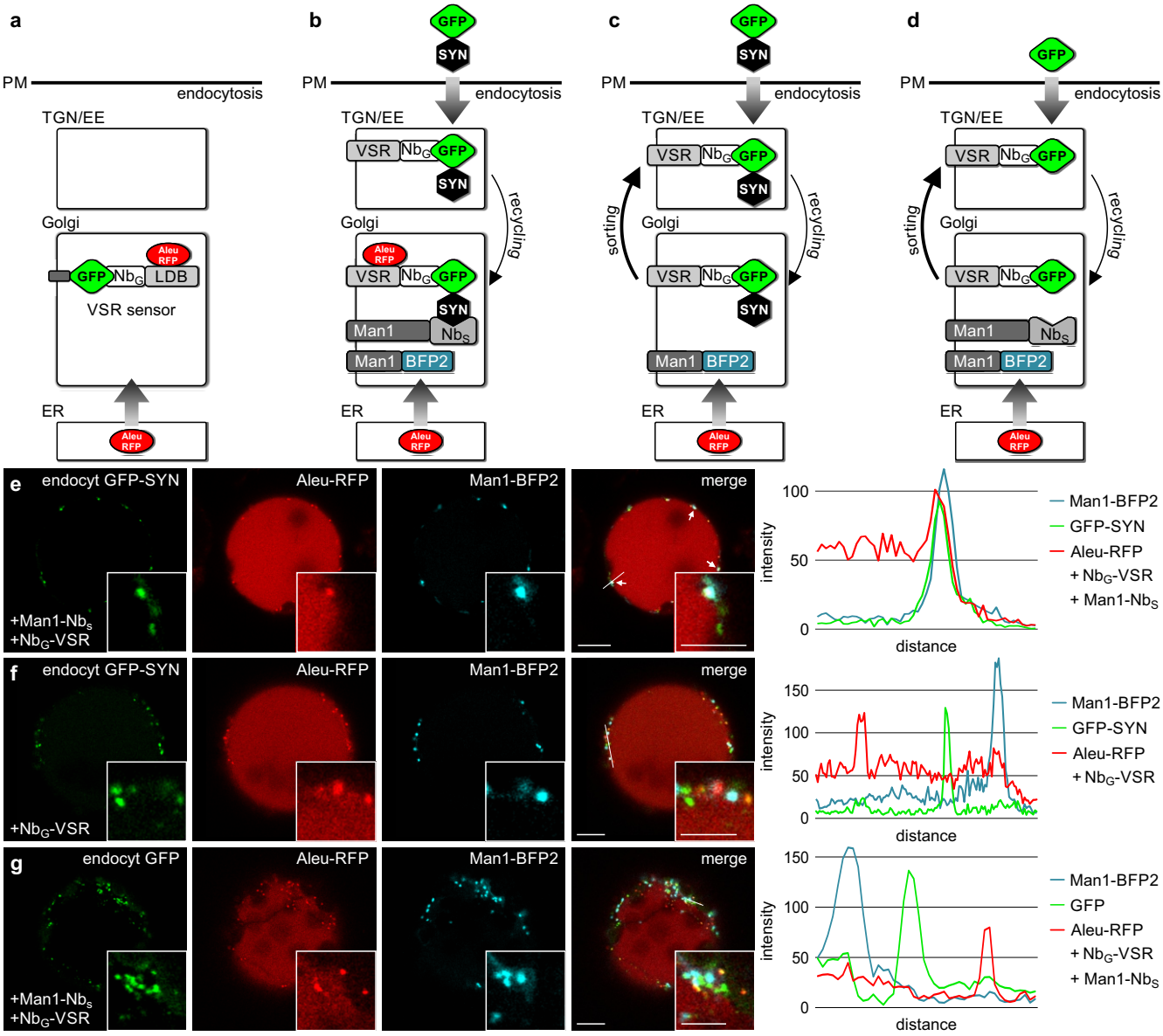

Figure 5. VSRs bind ligands after recycling. (**a**) Targeted VSR sensors (Nb_G-LDB) were shown to bind Aleu-RFP ligands in the Golgi (**b**) GFP-SYN labeled Nb_G-VSRs are locked to the anchor Man1-Nb_S in the *cis*-Golgi, positively identified by the marker ManI-BFP2. Ligand-binding of recycled full-length VSRs is assessed by colocalization with ligands (Aleu-RFP). Controls with cycling VSRs that lack (**c**) the anchor or (**d**) the SYN epitope at the labeling GFP for the VSR lockdown, result in VSR localization at the TGN/EE, which does not promote ligand binding. (**e**) GFP-SYN labeled Nb_G-VSRs are locked after recycling in the *cis*-Golgi and colocalize with the Golgi marker Man1-BFP2 and bind the ligand Aleu-RFP, as shown by the overlapping signal peaks in the line intensity plot (see **b**). (**f**,**g**) Not locked VSRs (see **c** and **d**) do not localize to the Golgi and thus do not bind the ligand Aleu-RFP as judged by the separated peaks in the line intensity plots. Scale bars 10µm, insets 5µm, showing magnifications.

Figure 6

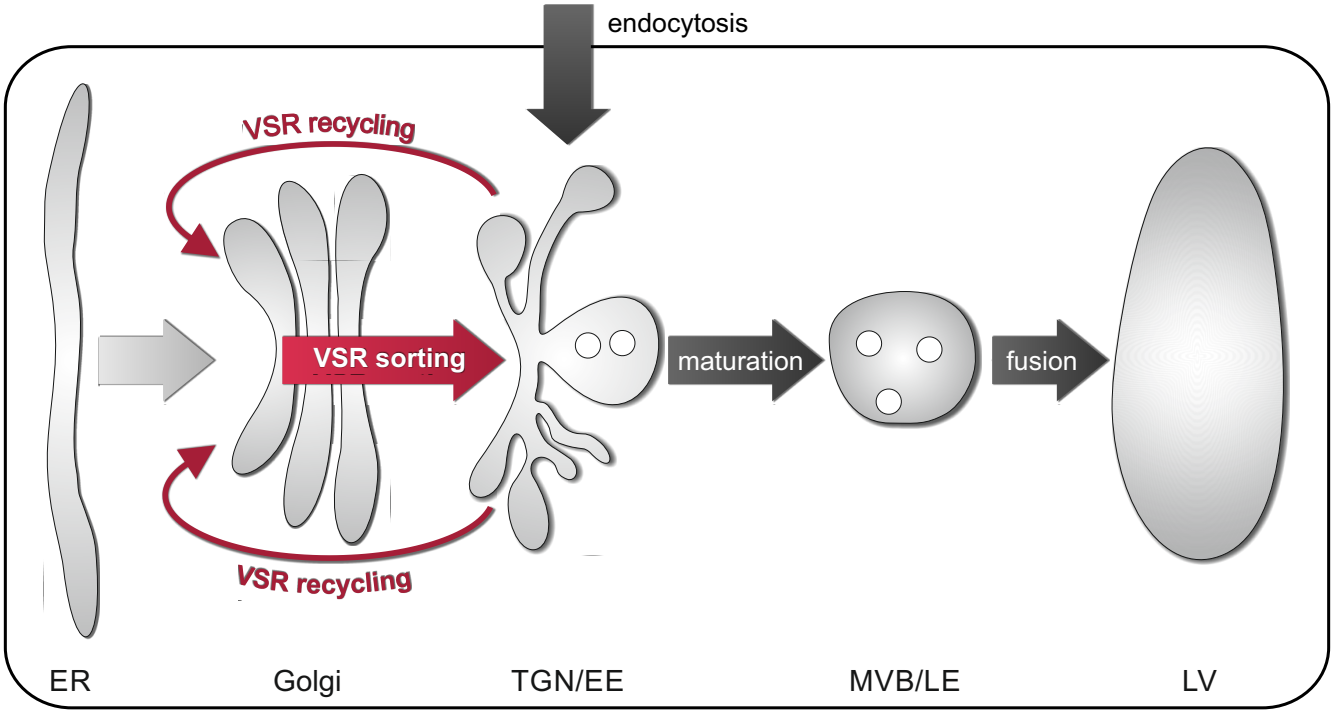

Figure 6. Model for receptor mediated vacuolar sorting in plants. VSRs bind ligands in the early secretory pathway and transport them to the TGN/EE. There, the ligands are released from the VSR. Next, VSRs are recycled back to the *cis*-Golgi stack for further rounds of ligand transport. Post-TGN/EE transport of released vacuolar cargo ligands but also endocytosed proteins occurs independent of VSRs and travel to the lytic vacuole per default. Transport in this route is mediated by multivesicular bodies, the late endosomes (MVBs/LEs). They bud off the TGN/EE in a maturation-based step and confer cargo delivery by their ultimate fusion with the lytic vacuole (LV).

Supplementary Figure 1

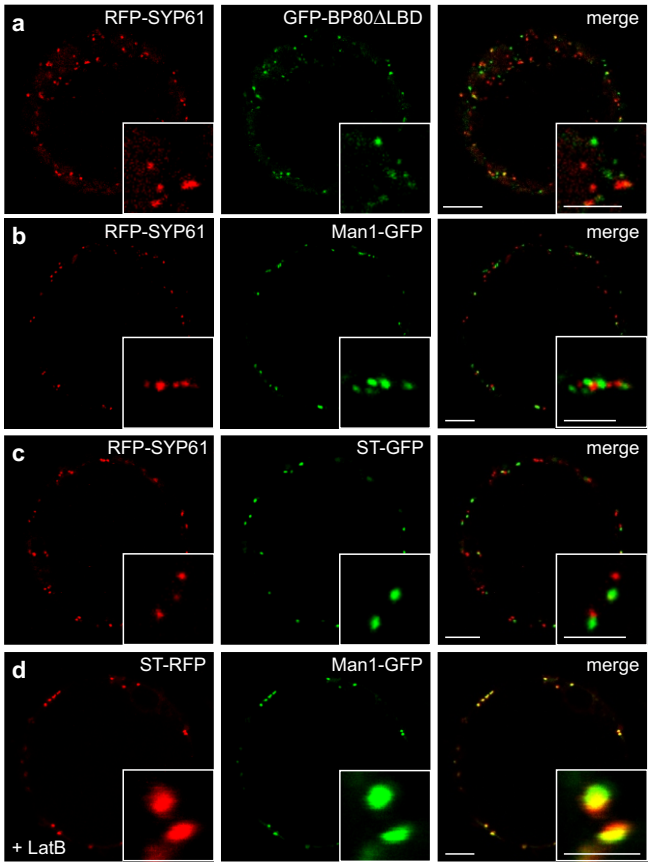

Supplementary Figure 1. Membrane marker proteins to discriminate punctate signals in the MVB/LE, the TGN/EE and the *cis*-/*trans*-Golgi in colocalization experiments. Comparison of signals for TGN/EE, MVB/LE and *cis*-/*trans*-Golgi in coexpression experiments. Coexpression of: (**a**) RFP-SYP61 with GFP-BP80ΔLBD to discriminate TGN/EE from MVB/LE, (**b**) RFP-SYP61 with Man1-GFP to discriminate TGN/EE from the *trans*-Golgi, (**c**) RFP-SYP61 with ST-GFP to discriminate TGN/EE from the *trans*-Golgi and (**d**) ST-RFP with Man1-GFP to discriminate between *cis*- and *trans*-Golgi. Performed in the presence of 4 µM latrunculin B (LatB) to avoid Golgi movement during image acquisition. Scale bars 10µm, insets 5µm, showing magnifications.

Supplementary Figure 2

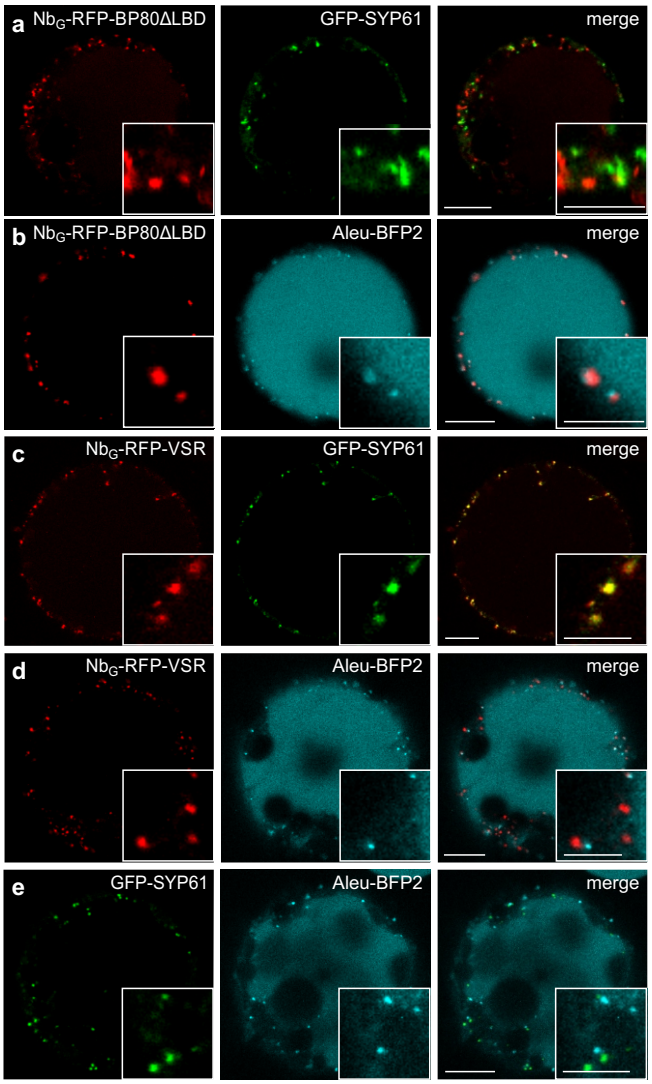

Supplementary Figure 2. Differential localization of the fluorescent full-length VSR Nb_G-RFP-VSR and the LBD-lacking MVB/LE marker Nb_G-RFP-BP80ΔLBD. (**a**) Coexpression of Nb_G-RFP-BP80ΔLBD with the N-terminal GFP fusion of SYP61, GFP-SYP61, as marker for the TGN/EE, and (**b**) with the MVB/LE and vacuolar marker Aleu- blue fluorescent (BFP)2 confirms the unaltered MVB/LE localization of the marker Nb_G-RFP-BP80ΔLBD. (**c**) In sharp contrast, coexpression of Nb_G-RFP-VSR with GFP-SYP61, and with (**d**) Aleu-BFP2 confirms the unaltered TGN/EE localization of the receptor Nb_G-RFP-VSR. (**e**) GFP-SYP61-labeled TGN/EE are clearly distinguishable from Aleu-BFP2-labeled MVB/LE in co-expression experiments **(compare to Suppl. Fig. 1a)**.

Supplementary Figure 3

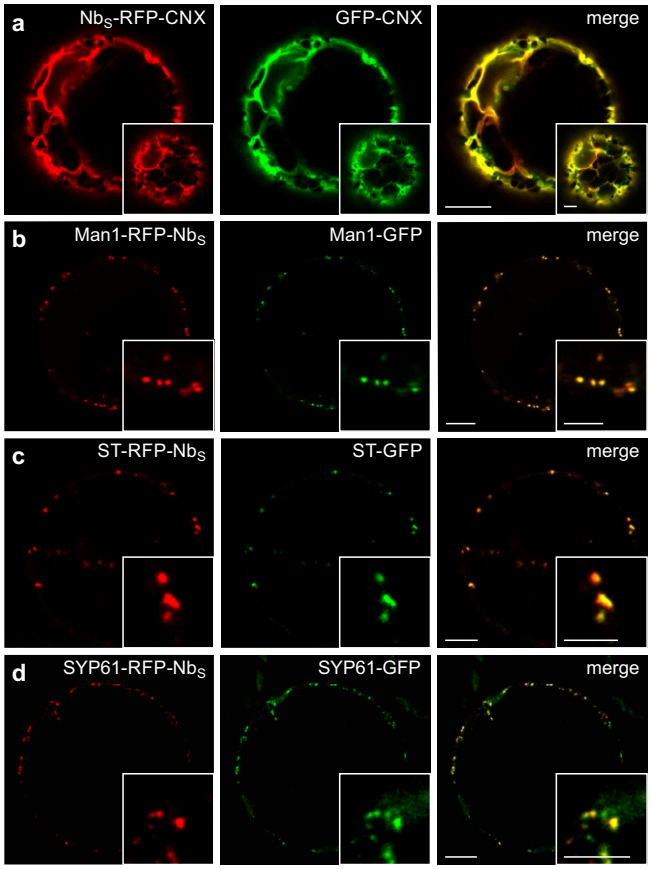

Supplementary Figure 3. Fusion of the Nb_s to compartment-specific marker proteins does not alter their compartment-specific localization. The localization of red fluorescent Nb_s-tagged marker proteins is compared to their GFP-tagged counterparts. Colocalization of (**a**) Nb_s-RFP-CNX with GFP-CNX in the ER, (**b**) Man1-RFP-Nb_s with Man1-GFP in the *cis*-Golgi stack, (**c**) ST-RFP-Nb_s with ST-GFP in the *trans*-Golgi stack and (**d**) SYP61-RFP-Nb_s with Syp61-GFP in the TGN/EE. Scale bars 10µm, insets 5µm, showing magnifications.

Supplementary Figure 4

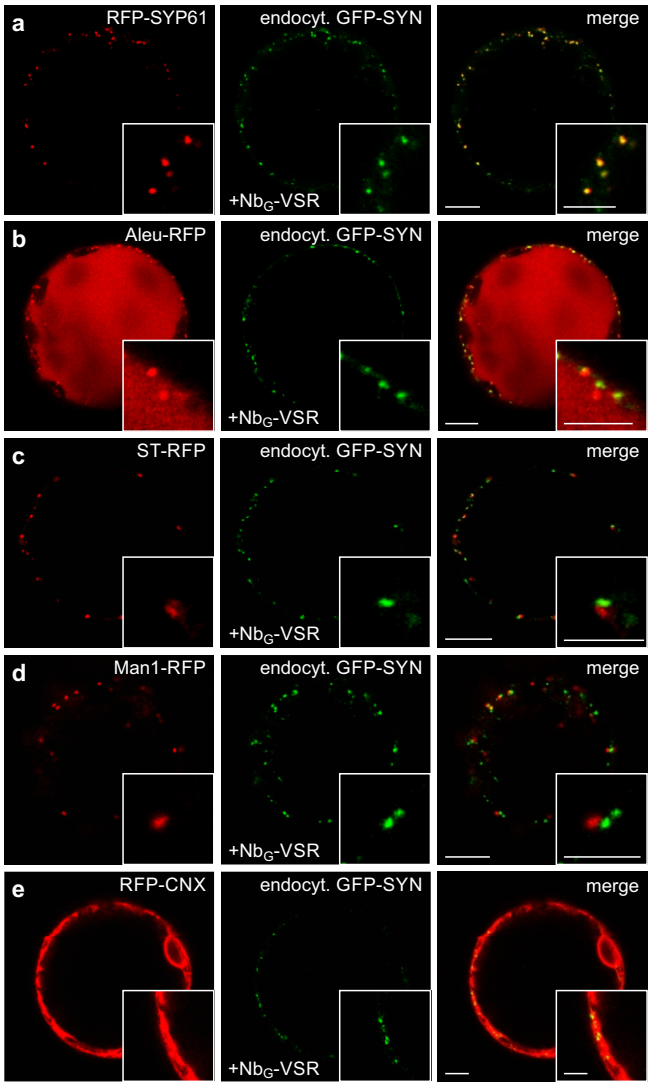

Supplementary Figure 4. The GFP-SYN labeled Nb$_G$-VSR localizes to the TGN/EE under steady state conditions. Colocalization of post-translationally GFP-SYN labeled non fluorescent Nb$_G$-tagged VSRs with red fluorescent compartmental markers for (**a**) the TGN/EE, (**b**) the MVB/LE and the vacuole, (**c**) the *trans*-Golgi, (**d**) the *cis*-Golgi and (**e**) the ER. Scale bars 10µm, insets 5µm, showing magnifications.

Supplementary Figure 5

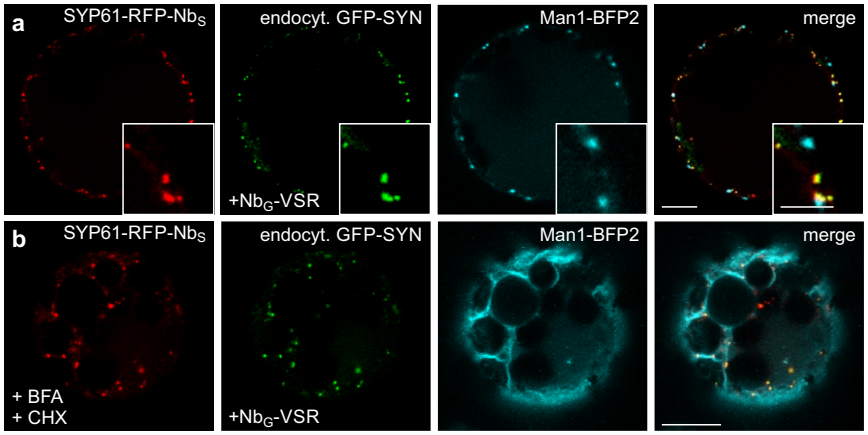

Supplementary Figure 5. The TGN/EE-locked VSR does not colocalize with the coexpressed marker for the *cis*-Golgi. (**a**,**b**) Colocalization of post-translationally GFP-SYN labeled non fluorescent Nb$_G$-tagged VSRs with the TGN/EE membrane anchor SYP61-RFP-Nb$_S$ and the marker for the *cis*-Golgi Man1-BFP2 upon GFP-SYN-triggered lockdown. (**a**) The overlapping signals of the labeled VSR and the TGN/EE membrane anchor (yellow) do not colocalize with the signals of the Golgi marker (cyan). (**b**) The colocalizing signals of TGN/EE anchored and the locked VSR persist after BFA treatment, whilst the Golgi signal redistributes to the ER, due to the BFA-triggered fusion of these compartments. Cells were treated with 20 µM BFA and 50 µM cycloheximide (CHX) for 1 h prior to imaging analysis. Scale bars 10µm, insets 5µm, showing magnifications.

Supplementary Figure 6

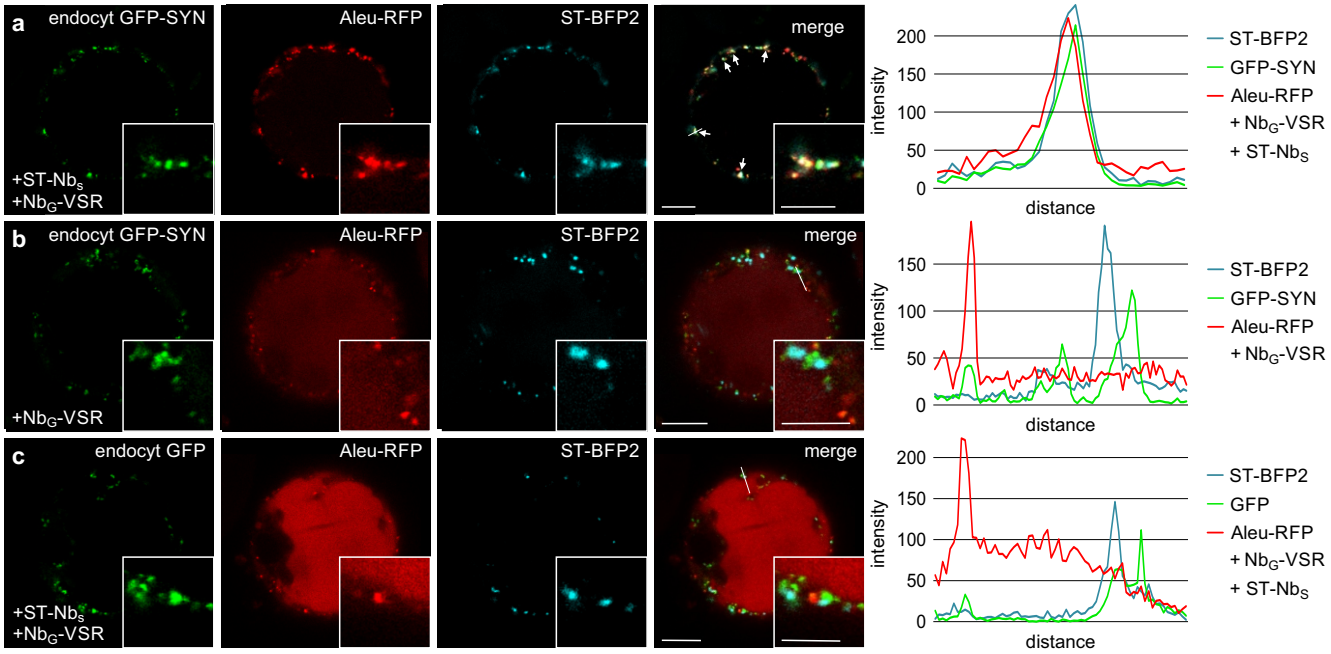

Supplementary Figure 6. VSRs bind ligands in the *trans*-Golgi after recycling. (**a**) GFP-SYN labeled Nb$_G$-VSRs are locked after recycling in the *trans*-Golgi and colocalize with the *trans*-Golgi marker ST-BFP2 and bind the ligand Aleu-RFP, as shown by the overlapping signal peaks in the line intensity plot (compare to Figure **5b**). (**b,c**) Not locked VSRs (compare to Figure **5c**,**d**) do not localize to the Golgi and thus do not bind the ligand Aleu-RFP as judged by the separated peaks in the line intensity plots. Scale bars 10µm, insets 5µm, showing magnifications.

Supplementary Figure 7

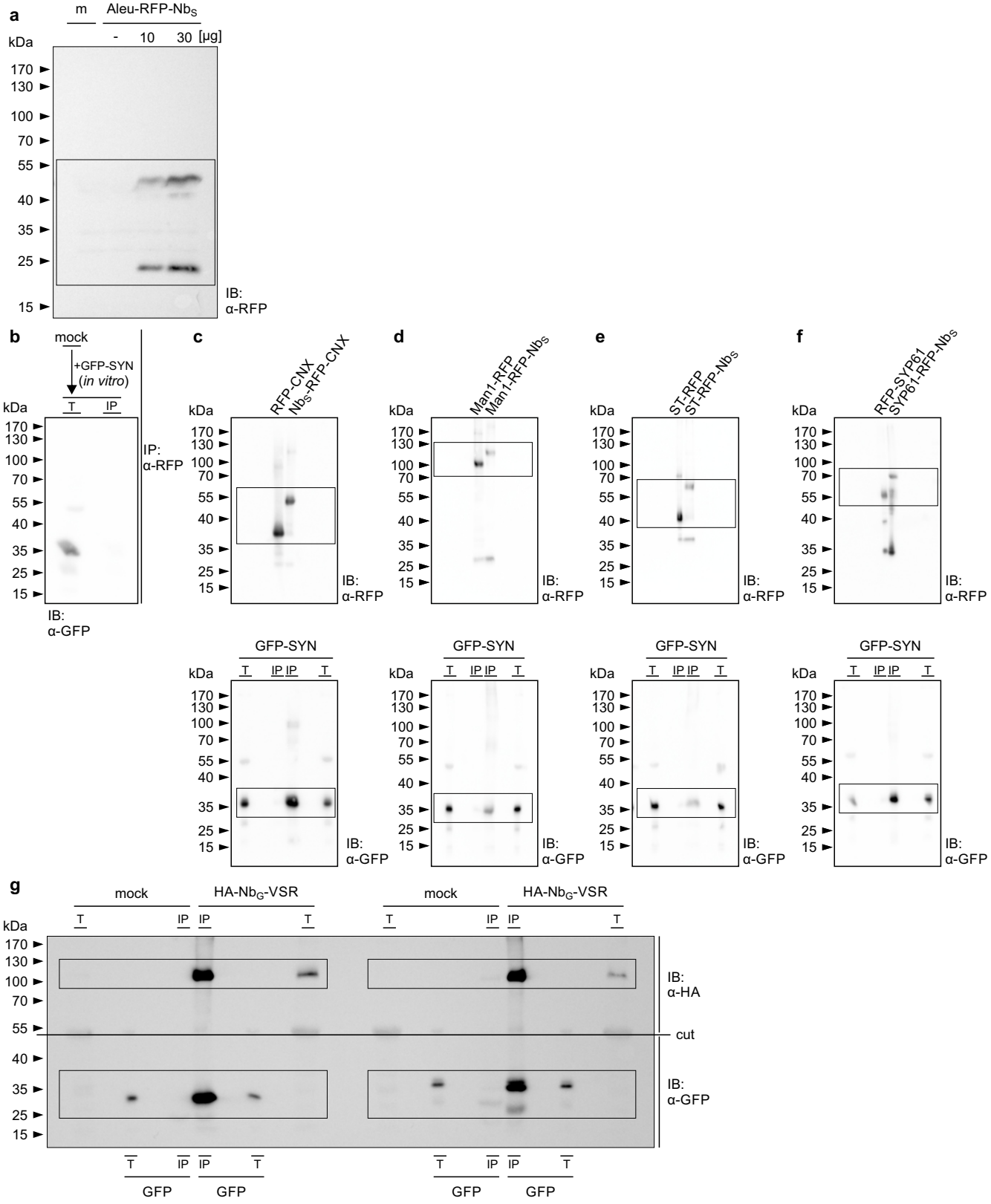

Supplementary Figure 7. Uncropped immunoblots. (**a**) Detection of Aleu-RFP-Nb$_S$ as illustrated in Figure **3f**. Section shown in Figure **3f** is highlighted with a black rectangle. The immunoblot (IB) was probed with α-RFP. (**b-f**) Detection of the markers/anchors and the dual epitope GFP-SYN as shown in Figure **3g-j**. (**b**) Control using mock transfected protoplasts for the immunoprecipitation (IP, α-RFP). Beads were incubated with GFP-SYN and immunoblotted (IB). The total extract (T) and the immunoprecipitate (IP) was probed with α-GFP to detect GFP-SYN. (**c-f**) Sections shown in Figure **3g-j** are highlighted with black rectangles. The immunoblots (IB) were probed to detect markers/anchors (α-RFP) and GFP-SYN (α-GFP). (**g**) Detection of VSRs and epitopes (GFP/GFP-SYN) as shown in Figure **3k**. Sections shown in Figure **3k** are highlighted with black rectangles. The immunoblots (IB) are probed to detect VSRs (α-HA) and GFP/GFP-SYN (α-GFP).

Supplementary Table 1

	Primers	Sequence (5'-3' direction)	Template	Recipient Vector
Nb_G-RFP-CNX (pDV01)	Nb_G_*Nhe*I_S	GCTCAGGCTAGCGCTAT GGACTATAAAGACGACGA CGACAAAATGGGATCTG GAGGAATGGCTCA	pBL14 [1]	pFF04 [1]; cut *Not*I/*Nhe*I to keep the N-terminal signal peptide of pFF04
	Nb_G_*Nco*I_AS	GGCCATCCATGGATGAT GATGATGATGATGAG		
	RFP_*Nco*I_S	CATCATCCATGGATGGCC TCCTCCGAGGACGT	pFK12 [2]	
	RFP_*Not*I_AS	GTCACTGCGGCCGCGTG CTCCAGTACTGTGGCGG C		
Man1-RFP-Nb_G (pSF65)	RFP_*Not*I_S	GAGGATGCGGCCGCATG GCCTCCTCCGAGGACGT	pFK12 [2]	pFF06 [1]; cut *BamH*I/ *Not*I
	RFP_*Cla*I_AS	CATCATATCGATTGCTCC AGTACTGTGGCGGC		
	FLAG_*Cla*I_S	GAGGACATCGATATGGA CTATAAAGACGACGA	pDV01 (see above)	
	Nb_G_*BamH*I_AS	GCATGAGGATCCCTAATG ATGATGATGATGATGAG		
ST-RFP-Nb_G (pSF128)	PLUS: ST (*Nhe*I/*Not*I), subcloned from pSF83 [1]			pSF65 (see above); cut *Not*I/*Nhe*I
Syp61-RFP-Nb_G (pSF129)	PLUS: Syp61 (*Nhe*I/*Not*I), subcloned from pFF25 [1]			pSF65 (see above); cut *Not*I/*Nhe*I
Nb_G-RFP-BP80ΔLBD (pSF130)	PLUS: BP80 (*Not*I/*BamH*I), subcloned from pFF03 [1]			pDV01 (see above); cut *BamH*I/*Not*I
Sec-GFP (pFK68)	GFP_*Sal*I_S	CATGACGTCGACTATGAG TAAAGGAGAAGAAC	GFP-spo [3]	pFF14 [1]; cut *Spe*I/*Sal*I to keep the N-terminal signal peptide of pFF14
	GFP-GGGG_*Spe*I_AS	TGCTTCACTAGTCTATCC TCCTCCTCCTTTGTATAG TTCATCCATGC		
Nb_G-RFP-VSR (pSF75)	Nb_G_*Nhe*I_S	GCTCAGGCTAGCGCTAT GGACTATAAAGACGACGA CGACAAAATGGGATCTG GAGGAATGGCTCA	pBL14 [1]	pFF04 [1]; cut *BamH*I/*Nhe*I to keep the N-terminal signal peptide of pFF04
	Nb_G_*Nco*I_AS	GGCCATCCATGGATGAT GATGATGATGATGAG		
	RFP_*Nco*I_S	CATCATCCATGGATGGCC TCCTCCGAGGACGT	pFK12 [2]	
	RFP_*Nde*I_AS	TTCGGCCATATGTGCTCC AGTACTGTGGCGGC		
	VSR_*Nde*I_S	GTGGTTCATATGTTTAAC GAGGCTCGATTCGT	first strand cDNA from 3-day-old *A. thaliana* seedlings	
	VSR_*BamH*I_AS	CTAGTCGGATCCCTAGG CACGTTCATCATTCGT		
Nb_G-VSR (pSF76)	Nb_G_*Nhe*I_S	GCTCAGGCTAGCGCTAT GGACTATAAAGACGACGA CGACAAAATGGGATCTG GAGGAATGGCTCA	pBL14 [1]	pSF75 (see above); cut *Nde*I/*Nhe*I to keep the N-terminal signal peptide of pSF75
	Nb_G_*Nde*I_AS	GTCCTCCATATGATGATG ATGATGATGATGAG		
ST-RFP (pSF84)	RFP_*Not*I_S	TGGCCCGCGGCCGCATG GCCTCCTCCGAGGACGT	pFK44 [2]	pSF83 [1]; cut *BamH*I/*Not*I
	RFP_*BamH*I_AS	TGCTTCGGATCCTTATGC TCCAGTACTGTGGC		
Amy-SYN (pSF57)	Amy_*Nco*I_S	CTATAACCATGGCGAACA AACACTTGTCCCTC	pCN1 [2]	pCN1 [2]; cut *BamH*I/*Nco*I
	Amy_*Not*I_AS	ATCAACGCGGCCGCCGA TCTTCTCCCATACGGCAT		
	SYN_*Not*I/*BamH*I_S	GGCCGCGTTGATCCTGA TAATGAAGCATACGAAAT GCCTTCTGAAGAAGGCTA TCAAGATTATGAACCGGA GGCTTAGG	Complementary oligonucleotides to assemble the coding sequence of the SYN-tag [4]	
	SYN_*Not*I/*BamH*I_AS	GATCCCTAAGCCTCCGGT TCATAATCTTGATAGCCT TCTTCAGAAGGCATTTCG TATGCTTCATTATCAGGA TCAACG		
Aleu-RFP-Nb_S (pDV02)	PLUS: P35S-Aleu (*EcoR*I/*Nhe*I), subcloned from pFF15 [1]			pCN1 [2]; cut *BamH*I/*EcoR*I
	RFP_*Nco*I_S	CTAGCGCCATGGCCTCC TCCGAGGAC	pFK12 [2]	
	RFP_*Kpn*I_AS	ATACATGGTACCTGCTCC AGTACTGTGGCGGC		
	PLUS: Nb_S (*Kpn*I/*BamH*I); chemically synthesized			

GFP-SYN (pSF74)	GFP_*Nhe*I_S	GCATGAGCTAGCGCCAT GGTGAGCAAGGGCGAGG	pFF04 [1]	pFF04 [1]; cut *BamH*I/*Nhe*I to keep the N-terminal signal peptide of pFF04
	mEGFP_*Hind*III_AS	GTTGGGGTCTTTGCTAAG CTTGGACTGGGTGCTCA G		
	mEGFP_*Hind*III_S	CTGAGCACCCAGTCCAA GCTTAGCAAAGACCCCAA C	pFF04 [1]	
	GFP_*Not*I_AS	ATCAACGCGGCCGCCCT TGTACAGCTCGTCCATGC		
	PLUS: SYN (*Not*I/*BamH*I), subcloned from pSF57 (see above)			
HA-Nb$_G$-VSR (pSF88)	HA_Nb$_G$_*Nhe*I_S	CTTTCTGCTAGCGCTATG TATCCGTATGATGTTCCA GATTATGCTATGGGATCT GGAGGAATGGCT	pBL14 [1]	pFK120 [1]; cut *BamH*I/*Nhe*I to keep the N-terminal signal peptide of pFK120
	Nb$_G$_*Nde*I_AS	GTCCTCCATATGATGATG ATGATGATGATGAG		
	PLUS: VSR4 (*Nde*I/*BamH*I), subcloned from pSF56 (see above)			
Nb$_S$-RFP-CNX (pDV03)	Nb$_S$_*Nhe*I_S	CGATACGCTAGCGCTATG GACTATAAAGACGACGAC GACAAAATGCAGGTGCA GCTGCAGGA	pDV02, see above	pFF04 [1]; cut *Not*I/*Nhe*I to keep the N-terminal signal peptide of pFF04
	Nb$_S$_*Nco*I_AS	CGATGACCATGGGCTGC TCACGGTCACCTGGG		
	RFP_*Nco*I_S	AGTCTACCATGGATGGCC TCCTCCGAGGACGT	pFK12 [2]	
	RFP_*Not*I_AS	AGTCTAGCGGCCGCCGG GTGCTCCAGTACTGTG		
Man1-RFP-Nb$_S$ (pSF78)	RFP_*Not*I_S	GAGGATGCGGCCGCATG GCCTCCTCCGAGGACGT	pFK12 [2]	pFF06 [1]; cut *BamH*I/*Not*I
	RFP_*Kpn*I_AS	TCCTTAGGTACCTGCTCC AGTGCTGTGGCGGC		
	PLUS: Nb$_S$ (*Kpn*I/*BamH*I), subcloned from pDV02 (see above)			
ST-RFP-Nb$_S$ (pSF82)	PLUS: ST (*Nhe*I/*Not*I), subcloned from pSF83 [1]			pSF78 (see above); *Not*I/*Nhe*I
Syp61-RFP-Nb$_S$ (pSF80)	PLUS: RFP-Nb$_S$ (*Not*I/*BamH*I), subcloned from pSF78 (see above)			pFF25 [1]; cut *BamH*I/*Not*I
Man1-Nb$_S$ (pSF85)	HA_*Not*I_S	CATGTAGCGGCCGCTAT CCTTATGATGTTCCTGA	pDV02, see above	pSF78 (see above); cut *BamH*I/*Not*I
	Nb$_S$_*BamH*I_AS	TGCTTCGGATCCCTAGCT GCTCACGGTCACCTGGG		
Man1-mTagBFP2 (pSF143)	PLUS: mTagBFP2 (*Not*I/*BamH*I); chemically synthesized			pFF06 [1]; cut *BamH*I/*Not*I
Aleu-mTagBFP2 (pFK106)	PLUS: P35S-Aleu (*EcoR*I/*Nhe*I), subcloned from pFF15 [1]			pDS13 [5], cut *BamH*I/*EcoR*I
	mTagBFP2_*Nhe*I_S	GAAAGCGCTAGCATGTCT GAACTTATTAAGGA	pSF143, see above	
	mTagBFP2_*BamH*I_AS	TGCTTCGGATCCTTAATT CAACTTATGTCCCA		
ST-Nb$_S$ (pSF86)	HA_*Not*I_S	CATGTAGCGGCCGCTAT CCTTATGATGTTCCTGA	pDV02, see above	pSF82 (see above); cut *BamH*I/*Not*I
	Nb$_S$_*BamH*I_AS	TGCTTCGGATCCCTAGCT GCTCACGGTCACCTGGG		
ST-mTagBFP2 (pSF142)	PLUS: mTagBFP2 (*Not*I/*BamH*I); chemically synthesized			pSF83 [1]; cut *BamH*I/*Not*I

Established plasmids used in this study	
RFP-Syp61 [1]	TGN marker
Aleu-RFP [1]	MVB/LE and vacuolar marker, VSR ligand
Man1-RFP [6]	*cis*-Golgi marker
RFP-CNX [1]	ER marker
GFP-CNX [1]	ER marker
Man1-GFP [1]	*cis*-Golgi marker
ST-GFP [1]	*trans*-Golgi marker
GFP-Syp61 [1]	TGN marker
GFP-BP80ΔLBD [1]	MBV/LE marker

References

1. Künzl F, Früholz S, Fäßler F, Li B, Pimpl P. Receptor-mediated sorting of soluble vacuolar proteins ends at the trans-Golgi network/early endosome. *Nat Plants*, 16017 (2016).
2. Scheuring D*, et al.* Ubiquitin initiates sorting of Golgi and plasma membrane proteins into the vacuolar degradation pathway. *BMC plant biology* **12**, 164 (2012).
3. daSilva LL*, et al.* Receptor salvage from the prevacuolar compartment is essential for efficient vacuolar protein targeting. *The Plant cell* **17**, 132-148 (2005).

4. Guilliams T*, et al.* Nanobodies raised against monomeric alpha-synuclein distinguish between fibrils at different maturation stages. *Journal of molecular biology* **425**, 2397-2411 (2013).
5. Niemes S*, et al.* Retromer recycles vacuolar sorting receptors from the trans-Golgi network. *The Plant journal : for cell and molecular biology* **61**, 107-121 (2010).
6. Nebenfuhr A*, et al.* Stop-and-go movements of plant Golgi stacks are mediated by the acto-myosin system. *Plant physiology* **121**, 1127-1142 (1999).